LIQUID CHROMATOGRAPHY - MASS SPECTROMETRY FOR THE STUDY OF ARACHIDONIC ACID METABOLITES

Xiaojing Liu

A DISSERTATION

in

Chemistry

Presented to the Faculties of the University of Pennsylvania

in

Partial Fulfillment of the Requirements for the

Degree of Doctor of Philosophy

2012

Supervisor of Dissertation

_____

Ian A. Blair, PhD, A.N. Richards Professor of Pharmacology

Graduate Group Chairperson

_____

Tobias Baumgart, PhD, Associate Professor of Chemistry

Dissertation Committee

E. James Petersson, PhD, Assistant Professor of Chemistry

Alexander S. Whitehead, PhD, Professor of Pharmacology

Tobias Baumgart, PhD, Associate Professor of Chemistry

ACKNOWLEDGMENTS

When I reach this part of my dissertation, the first person comes to my mind is my advisor Dr. Ian A. Blair. I still remember that day, when I went to his office, shyness and low self-confidence on my face, speaking inept English, and a background far away from this lab. I didn't expect I would be accepted by Dr. Blair as his Ph.D. Student. However, what I heard from Dr. Blair was not denial, instead, he told me "To be a good scientist, three characters are required, enthusiasm, hardworking and carefulness." During the past four years, I kept these words in my mind and kept asking myself whether I retained these characters or not. In this period, Dr. Blair also continuously provided me with valuable instructions and great encouragement to keep my research moving forward. One thing I really appreciate is that he always gives us much freedom, and encourages us to do whatever we like to. Even though under the funding pressure, he never transfers this pressure to the lab members, and always creates a nice working environment in the lab. Without Dr. Blair's guidance, without his trustfulness, without his encouragement, I would never be able to finish my thesis. It is my good luck to have such a great advisor.

Secondly, I also want to thank my parents and my boyfriend. They always point me in the right direction whenever I get lost in life, which prevents me from being driven towards frame, money, and self-aggrandizement. I also feel lucky having my boyfriend who is more like my soul mate. His appearance makes the science more interesting to me and also makes my

life full of fun. Thus, even though they are not physically living with me, we are always together in spirit and dependent on each other. Without their unconditional support, I would never be able to reach this step.

Moreover, I want to thank my lab mates and my friends at Penn. Due to Christine's effort, Blair lab is able to run in good order. Due to other lab members' selfless help and close collaboration, I am able to gain valuable knowledge and skills within these four years in Blair lab. I want to specially thank Clementina, Suhong, Sumit, Kannan, Nate, and Bobby for their guidance and helpful discussions. My lab mates and my other friends at Penn, especially Yu, Wan-Ting, Katie, Jasmina, Meng, Li, Zinan, and others are just like my close family members. They physically walk me through my five-year Ph.D. life, leaving lots of good memories, which I will cherish for my whole life. Without their company, I would lose so much of the fun in life.

Finally, I also want to thank my committee members, Professor Petersson, Professor Whitehead, and Professor Baumgart, for their time and great guidance.

Abstract

LIQUID CHROMATOGRAPHY-MASS SPECTROMETRY FOR THE STUDY OF ARACHIDONIC ACID METABOLITES

Xiaojing Liu

Ian A. Blair, PhD

Arachidonic acid (AA) oxidation metabolism has been an important research topic for decades, and numerous oxidation products as well as enzymes involved in AA metabolism together with their downstream metabolites have been identified, although unknown pathways still remain to be characterized. In the present a study a new AA metabolite, 11-oxo-eicosatetraenoic acid (ETE), generated from a major product of cyclooxygenase (COX-2), 11(*R*)-hydroxyeicosatetraenoic acid (HETE), through 15-hydroxyprostaglandine dehydrogenase (15-PGDH)-mediated oxidation. 11-Oxo-ETE was found to have an anti-proliferative effect on human umbilical vein endothelial cells (HUVECs), with a similar IC_{50} to a well- known anti-inflammatory mediator, 15-deoxy-$\Delta^{12,14}$-prostaglandin J_2 (15d-PGJ_2). It was also found that 11-oxo-ETE could be inactivated through the glutathione-*S*-transferase (GST)/glutathione (GSH) pathway by forming a GSH adduct, or by undergoing reduction to 11(*S*)-HETE through metabolism by unknown reductases.

AA is also subject to non-enzymatic oxidation due to its *bis*-allylic hydrogen atoms and four double bonds. Chiral LC-MS methods were used to distinguish the enzymatic and non-enzymatic products by monitoring the relevant products that were formed. Non-enzymatic pathways generate racemic mixtures, while enzymatic pathways are normally highly stereoselective. It is known that both enzymatic and non-enzymatic oxidation of AA followed by decomposition of the resulting oxidized intermediates, can generates short-chain aldehydes such as 4-hydroperoxy-2(*E*)-nonenal (HPNE), 4-hydroxy-2(*E*) nonenal (HNE), and 4-oxo-2(*E*)-nonenal (ONE). However, it was discovered that the endoperoxide product of COX-2, PGG_2, is a major contributor to the formation of these aldehydes. Moreover, PGG_2 and other hydroperoxides generate HPNE or HNE with different chiral characteristics. From COX-2 expressing human colorectal adenocarcinoma epithelial cell line (LoVo) cell lysate, 4(*S*)-HNE was detected with high enantiomeric purity indicating that the primary source was prostaglandin G_2 (PGG_2) and not 15-hydroperoxyeicosatetraenoic acid (HPETE) as had been previously suggested.

Finally, through studies of 11(*R*)-HPETE and 15-HPETE decomposition, a new carboxylate-containing aldehyde, 11-oxoundeca-5,8-dienoic acid (OUDE) was identified. OUDE contains the α–terminus of the lipid hydroperoxide precursor and is analogous to HNE, which is derived from the ω–terminus. Nuclear magnetic resonance spectroscopy (NMR) together with chiral liquid chromatography-mass spectrometry (LC-MS) analysis showed that OUDE was a mixture of two double bond isomers. It has been proposed that the two isomers are generated as a result of a rearrangement reaction

subsequent to the formation of OUDE. In addition, , by monitoring the chirality of the HNE that was formed from 11(*R*)-HPETE and 15-HPETE decomposition, a homolytic mechanism for HNE formation has been proposed.

Table of Contents

List of Tables

List of Figures

ABBREVIATIONS

(5*Z*,8*Z*)-11-oxoundeca-5,8-dienoic acid	OUDE1
(5*Z*,9*E*)-11-oxoundeca-5,9-dienoic acid	OUDE2
11(*R*)-hydroxy-5,8,12,14-(*Z*,*Z*,*E*,*Z*)-eicosatetraenoic acid	11(*R*)-HETE
11-oxo-5,8,12,14-(*Z*,*Z*,*E*,*Z*)-eicosatetraenoic acid	11-oxo-ETE
12S-hydroperoxy-5*Z*,8*E*,10*E*-heptadecatrienoic acid	12-HPTrE
12S-hydroxy-5*Z*,8*E*,10*E*-heptadecatrienoic acid	12-HHT
15-deoxy-$\Delta^{12,14}$-prostaglandin J_2	15d-PGJ_2
15-hydroxy prostaglandin dehydrogenase	15-PGDH
2'-deoxyadenine	dAdo
2'-deoxycytidine	dCyd
2'-deoxyguanosine	dGuo
4-hydroperoxy-2(*E*)-nonenal	HPNE
4-hydroxy-2(*E*)-nonenal	HNE
4-oxo-2(*E*)-nonenal	ONE
acetonitrile	ACN
aldo-keto reductase	AKR
arachidonic acid	AA
arachidonylethanolamide	AEA
atmospheric pressure chemical ionization	APCI
base excision repair	BER
bromodeoxyuridine	BrdU
collision energy	CE
collision-induced dissociation	CID
cyclooxygenase	COX
diabetic nephropathy	DN

diacylglycerol	DAG
electrospray ionization	ESI
ethyl acetate	EtOAc
fatty acid amide hydrolase	FAAH
fetal bovine serum	FBS
glutathione	GSH
glutathione-*S*-transferase	GST
G-protein coupled receptor	GPCR
heptano-etheno-2'-deoxyguanosine	H-εdGuo
human colonic adenocarcinoma HCA-7 Colony 29 cells	HCA-7
human colorectal adenocarcinoma epithelial cell line	LoVo
human umbilical vein endothelial cells	HUVEC
hydroperoxyeicosatetraenoic acid	HPETE
hydroperoxyoctadecadienoic acid	HPODE
linear ion trap	LTQ
lipoxygenase	LOX
liquid chromatography	LC
low-serum growth supplement	LSGS
malondialdehyde	MDA
mass spectrometry	MS
methanol	MeOH
nuclear magnetic resonance	NMR
nucleotide excision repair	NER
organic anion transporter polypeptide	OATP
pentafluorobenzyl bromide	PFB
peroxisome proliferator-activated receptor gamma	PPARγ
phosphatidylinositol	PI
phospholipase A2	PLA_2

polyunsaturated fatty acid	PUFAs
prostaglandin E_2	PGE_2
prostaglandin G_2	PGG_2
selected reaction monitoring	SRM
solid phase extraction	SPE
trans-4,5-epoxy-2(*E*)-decenal	EDE
triple stage quadrupole	TSQ
tyrosine	Tyr
vitamin C	Vit C

Chapter 1 General Introduction

1.1 Lipid classification

1.1.1 Lipid classification by function

Lipids can be classified by their functions into storage lipids, structural lipids (membrane lipids), hormones, and vitamins. Storage lipids exist in the form of triacylglycerols, while structural lipids usually contain a polar head and a long carbon chain tail. Based on the polar head and carbon chain compositions, membrane lipids can be further classified into different categories. Hormones and vitamins represent only a small component of cellular lipids when compared with storage and structural lipids, but they play important roles in regulating biological process. Fatty acids which are major components of lipids, can be classified as saturated and unsaturated based on the presence or absence of double bonds. Polyunsaturated fatty acids (PUFAs) are subject to oxidation by chemical oxidants or enzymes and the resulting oxidation products can function as "hormone-like" signaling molecules.

1.1.2 Phospholipids

Phospholipids are major components of all cell membranes where they form lipid bilayers. Most phospholipids contain a diglyceride, a phosphate group, and a polar head group such as choline. However, sphingolipids, which represent a major class of phospholipid, contain a sphingosine moiety instead of glycerol. The structure of a typical glycerophospholipid, sn1-stearoyl-2-arachidonoyl-phosphatidylinositol is shown in Figure 1.1. Glycerol forms an

ester bond with the carboxylic acid group of stearic acid at the sn-1 position, and the other ester bond at the sn-2 position is formed with arachidonic acid. At-the sn-3 position, there is a polar phosphoinositol head group. As illustrated in Figure 1.1, the arachidonyl substituent has 4 double bonds, while the stearoyl substituent is fully saturated. In addition to arachidonic acid, there are numerous other unsaturated and polyunsaturated fatty acids. These fatty acids are classified as ω-9, ω-6 or ω-3, depending on the position of the last double bond. For example, arachidonic acid (AA) has a double bond at C14-C15, and the terminal carbon is at C-20, which is designated as ω-1. Therefore, the first double bond is at ω-6.

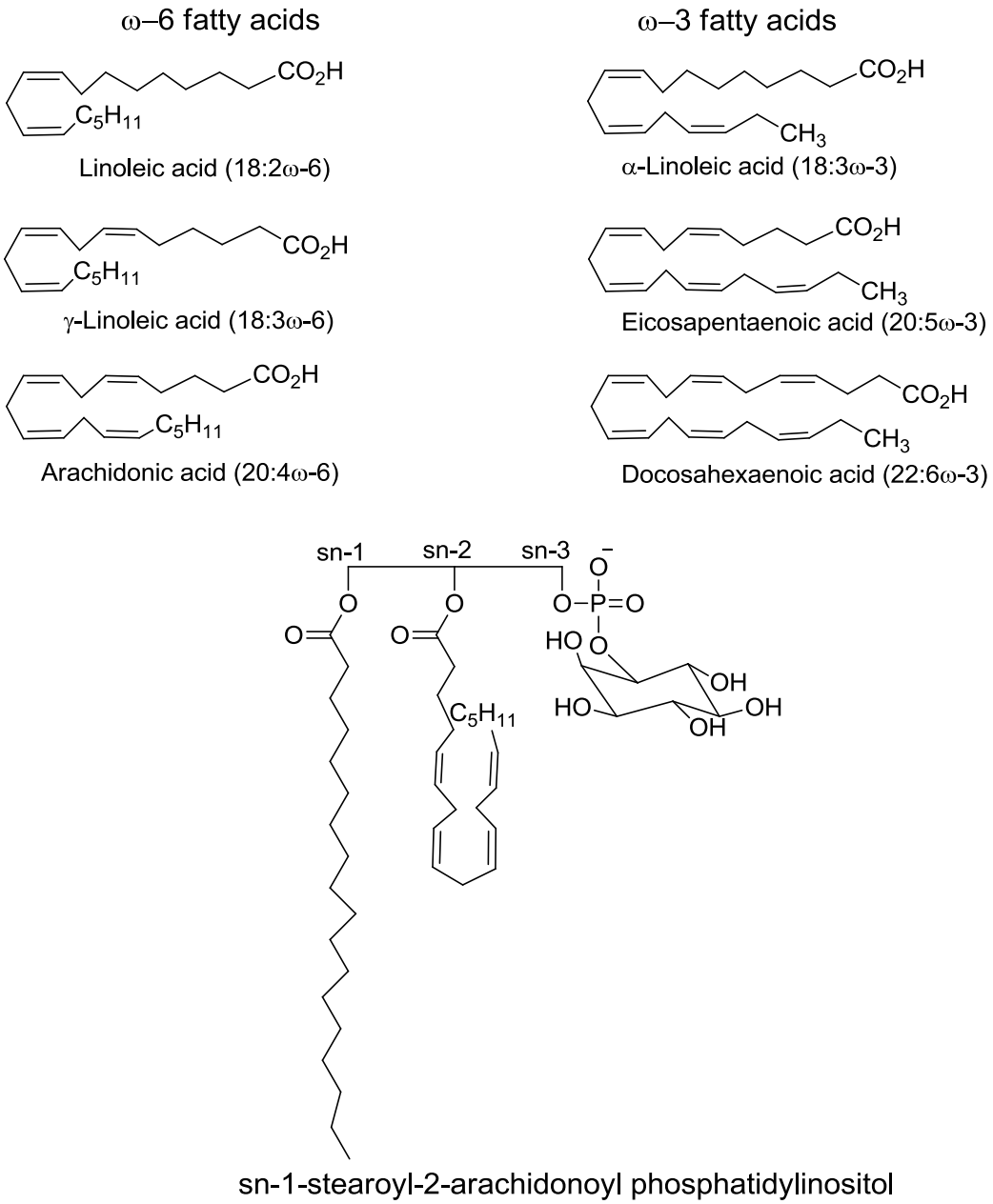

Figure 1.1. Structures of unsaturated fatty acids and sn-1-stearoyl-2-arachidonoyl phosphatidylinositol.

AA has 20 carbon atoms and 4 double bonds, so it can also be abbreviated as 20:4ω-6 or 20:4n-6. Similarly, docosahexaenoic acid (common name: DHA)

has 22 carbons and 6 double bonds, and the last double bond is at C19-C20, so it's abbreviated as 22:6ω-3 or 22:6n-3.

Unsaturated fatty acids with more than three double bonds are frequently seen in animals, while in plants there are usually less than three. The trans-double bonds allow them to be less tightly packed than saturated fatty acids, so membranes containing unsaturated fatty acids have some degree of fluidity. Moreover, compared to saturated fatty acids, the unsaturated fatty acids are much more readily oxidized, and the corresponding oxidation products are important biological signal mediators. When there is more than one double bond, there is usually a methylene group connecting the two double bonds, which is also known as a *bis*-allylic configuration. The abstraction of a *bis*-allylic hydrogen atom is an important step in lipid peroxidation and in enzymatic oxidation.

1.2 Arachidonic acid metabolism

1.2.1 The importance of arachidonic acid

There have been numerous studies on AA metabolism because it is the precursor of a diverse biologically active family of biologically active lipid mediators known as eicosanoids (*1*). They have multiple functions in inflammation, cancer or immunity through modulating signaling pathways, transcription factor activity and gene expression. The eicosanoids derived from arachidonic acid are called ω-6 eicosanoids and are often pro-inflammatory either as G-protein coupled receptor (GPCR) agonists or as nuclear transcription factor ligands (*2,3,4,5*).

1.2.2 Overview of AA metabolism

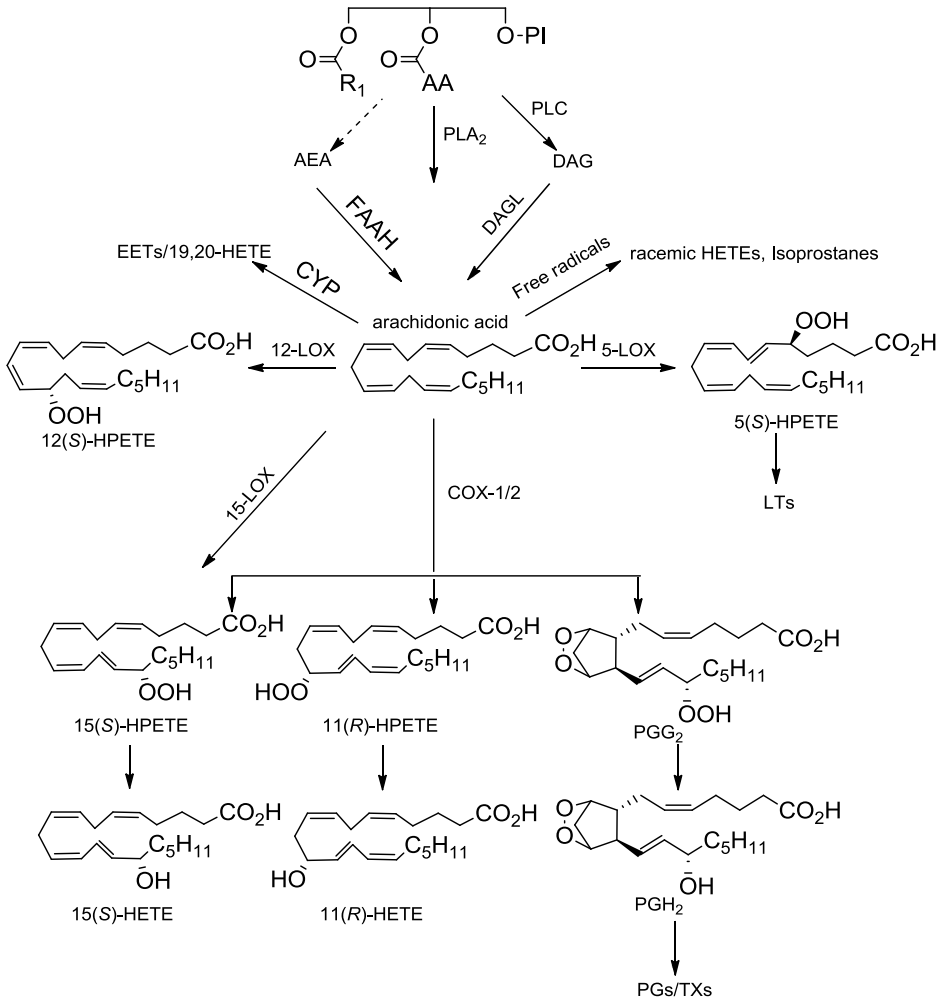

Figure 1.2: Simplified scheme of AA metabolism. R1: stearoyl (18:0); DAG: Diacylglycerol; DAGL: DAG lipase; PI: Phosphatidylinositol; PLA_2: phospholipase A2; PLC: Phospholipase C; AEA: Arachidonoylethanolamide (anandamide); FAAH: Fatty acid amide hydrolase; AA: arachidonic acid

AA in mammals mainly exists as an esterified form in acylglycerides, and phospholipids. Generally, before esterified AA can be converted to eicosanoids, it has to be released as a free fatty acid. For example, as shown in Figure 1.2, esterified arachidonic acid at the sn-2 position on phosphatidylinosotol can be directly released by the phospholipase A_2 (PLA_2)

enzyme (*6*). Alternatively, Phospholipase C (PLC)-mediated hydrolysis of phospholipids can first occur at the sn-3 position, in which case the polar phosphoinositol head group is removed, forming a diacylglycerol (DAG). Then DAG is further metabolized by DAG lipase (DAGL) to release free arachidonic acid. There are also additional sources of free arachidonic acid (*7,8*). For example, arachidonylethanolamide (anandamide, AEA) is an endogenous cannabinoid neurotransmitter. It is the substrate for enzyme fatty acid amide hydrolase (FAAH), which converts AEA into ethanolamine and arachidonic acid. In most of the tissues, the PLA_2 and PLC pathways play the major role, while recent research has shown that in brain, the FAAH pathway are more important than the other two (*8*).

Besides enzymatic pathways, AA is also subject to autoxidation both *in vitro* and *in vivo*. Since arachidonic acid has four double bonds, and three *bis*-allylic hydrogen atoms, when it is exposed to air or free radicals, or when it is heated, it is readily oxidized (*9*). Although the intracellular environment is mostly reducing, within mitochondria there is a pool of free radicals, which could attack AA, and initiate autoxidation. Autoxidation products are different from enzymatic products in that they are racemic rather than enantiomerically pure metabolites observed from enzymatic reactions. Thus, although hydroperoxyeicosatetraenoic acids (HPETEs) can be generated both from enzymatic and non-enzymatic arachidonic acid oxidation, a chiral analysis can distinguish the two pathways. Furthermore, autoxidation occurs with little regioselectivity, which leads to a myriad of products. Thus, the initially formed HPETEs undergo further oxidation to generate a family of

eicosanoids known as isoprostanes (*10*). Several of the isoprostanes have been widely used as biomarkers of oxidative stress (*11,12*). AA-derived ω-6 eicosanoids are mostly pro-inflammatory, while ω-3-derived eicosanoids are much less inflammatory. It has been proposed that ω-3 eicosapentaenoic acid has some health benefits because it can compete with AA as the substrate of related enzymes to lower the formation of inflammatory eicosanoids (*13,14*).

1.3 COX-2 pathway

1.3.1 COX structure and catalytic mechanism

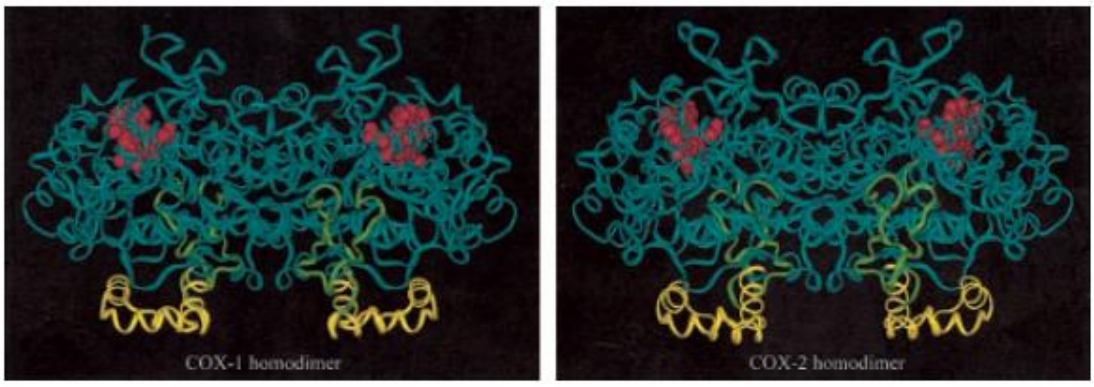

Figure 1.3 Crystal structures of ovine COX-1 (left) and murine COX-2 (right) homodimers by Browner and Kurumbail. The red color represents the catalytic cofactor, heme, the blue area is the dimerization domain, and the yellow color is membrane binding domain. The peroxidase active site is on the top cleft of each monomer. This figure is modified from (*15*).

Cyclooxygenase (COX) is a membrane protein located on the inner and outer membrane of nuclear envelope, and the surface of the endoplasmic reticulum

lumen. It has dual catalytic functions. There are both cyclooxygenase and peroxidase (POX) active sites in one enzyme. The cyclooxygenase site converts AA into PGG_2 and HPETEs, while the peroxidase site reduces the hydroperoxide groups in PGG_2 or HPETEs to the corresponding hydroxyl groups. As shown in Figure 1.3, the red color represents the cofactor heme, while the open cleft on top of each monomer is the POX site. The COX and POX activities are functionally interdependent. As shown in Figure 1.4, it has been generally accepted that there is a protein radical formed during the catalytic process. Alkyl hydroperoxides bind to heme in the POX site, and are reduced to the corresponding alkyl hydroxyl, and meanwhile the resting heme is oxidized to the oxyferryl form and a protoporphyrin radical cation ($Fe^{4+}=O^{\cdot}$) is formed. This intermediate is so unstable that it attacks the neighboring tyrosine residue (^{385}Tyr), and abstracts hydrogen from the ^{385}Tyr side chain, resulting in the formation of ^{385}Tyr radical and oxyferryl $Fe^{4+}=O$. The ^{385}Tyr radical then abstracts pro-S hydrogen at C13 of arachidonic acid, which binds to COX active site. Then ^{385}Tyr is recycled, while the radical is transferred to AA. The C11-C12 double bond then relocates to C12-C13 and forms a conjugate double bond with C14-C15, the C13 radical is also transferred to C11. Then oxygen is inserted at the C11 position and the radical is transferred to oxygen, which rapidly attacks C8-C9 double bond, and form a dioxygen (endoperoxide) bridge between C11 and C9, together with a C8 radical. This is then followed by a C8 radical attraction of C12-C13 double bond and formation of C8-C12 single bond, together with a C13 radical. After translocation of C13 radical and C14-C15 double bond, C15 is

formed and followed by oxygen attachment. Finally this PGG_2 precursor abstracts a hydrogen atom from neighboring reducing environment and forms the final PGG_2. PGG_2 will function as alkyl hydroperoxide and enter the peroxidase site, where it is reduced to PGH_2. Usually after several cycles, the COX will lose it is activity, which is called COX suicide. The exact mechanism is not clear yet, but there are reports showing it may be related with the quench of tyrosine radicals or damage to COX protein by free radicals, and the addition of phenol slows the inactivation process (*16,17*).

1.3.2 COX isoenzymes and diseases

Before 1991, only one COX was identified, and then after that, an inducible COX isoenzyme was described by three independent groups (*18,19,20*). Simmons and Herschman (*19, 20*) together with their colleagues found mRNAs whose expression was induced in chicken and mouse fibroblasts in response to src and tumor-promoting phorbol esters. Later, they found these mRNAs encoded proteins shared 60% amino acid sequence with the earlier COX mRNA, but their expression and their biological activity were quite different. Thus, it is concluded that COX has two isoenzymes, COX-1 and COX-2. COX-1 is constitutively expressed in many cells, while COX-2 is induced in response to cytokines, hormones, growth factors, bacteria endotoxin, and certain other stimuli. Thus, COX-2 is usually over-expressed in inflammatory tissues or tumors. COX-1 functions as a house-keeping enzyme and its products help to maintain normal biological processes. However, COX-2 is related with many diseases, including inflammatory disorders, cancer, diabetes, and so on. Over-expression of COX-2 contributes

to accumulation of prostaglandins, which are usually pro-inflammatory, as described previously, although it was also reported that certain COX-2 mediated ω-3 fatty acids metabolites are anti-inflammatory (*21*).

1.3.3 COX inhibitors

COX is a target for developing anti-inflammatory drugs, known as non-steroidal anti-inflammatory drugs (NSAIDs). Within the NSAIDs, aspirin was the earliest developed. It also differs from other NSAIDs, in that it converts COX-2 into a 15(*R*)-lipoxygenase (LOX), instead of completely inhibiting COX-2 activity. It is also the only NSAID which covalently modifies COX-1 and COX-2, while other NSAIDs are usually competitive substrates of COX. Aspirin completely inhibits both COX-1 activity, and switches COX-2 to a 15(*R*)-LOX, so PG synthesis is inhibited, and it has many side effects, such as a pro-aggregatory effect due to inhibition of platelet COX-1-mediated thromboxane A_2 biosynthesis. Aspirin also causes irritation of the gastric mucosa due to inhibition of PG synthesis. In order to overcome this effect, COX-2 specific inhibitors have been developed, although they have significant adverse cardiovascular effects (*22*).

It is known that among the NSAIDs, aspirin is the most effective anti-platelet drug, because it can covalently modify COX-1, and more efficiently inhibit the biosynthesis of pro-aggregatory thromboxane A_2 (*23*). Moreover, there are studies showing that daily doses of aspirin might help to reduce cancer risk (*24,25*) .

The mechanism through which aspirin functions as a chemoprevention agent is still not quite clear yet, and no evidence shows whether a COX is involved or not. Thus, more studies are needed to address these issues and to develop safer chemoprevention candidates.

Cyclooxygenase activity:

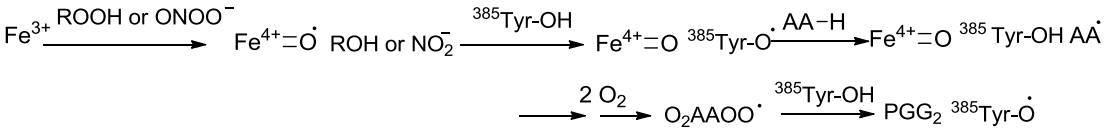

Peroxidase activity:

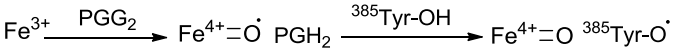

Recycle of Fe^{3+}:

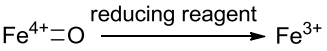

enzyme suicide:

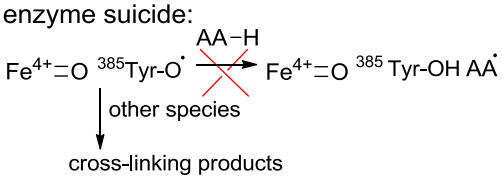

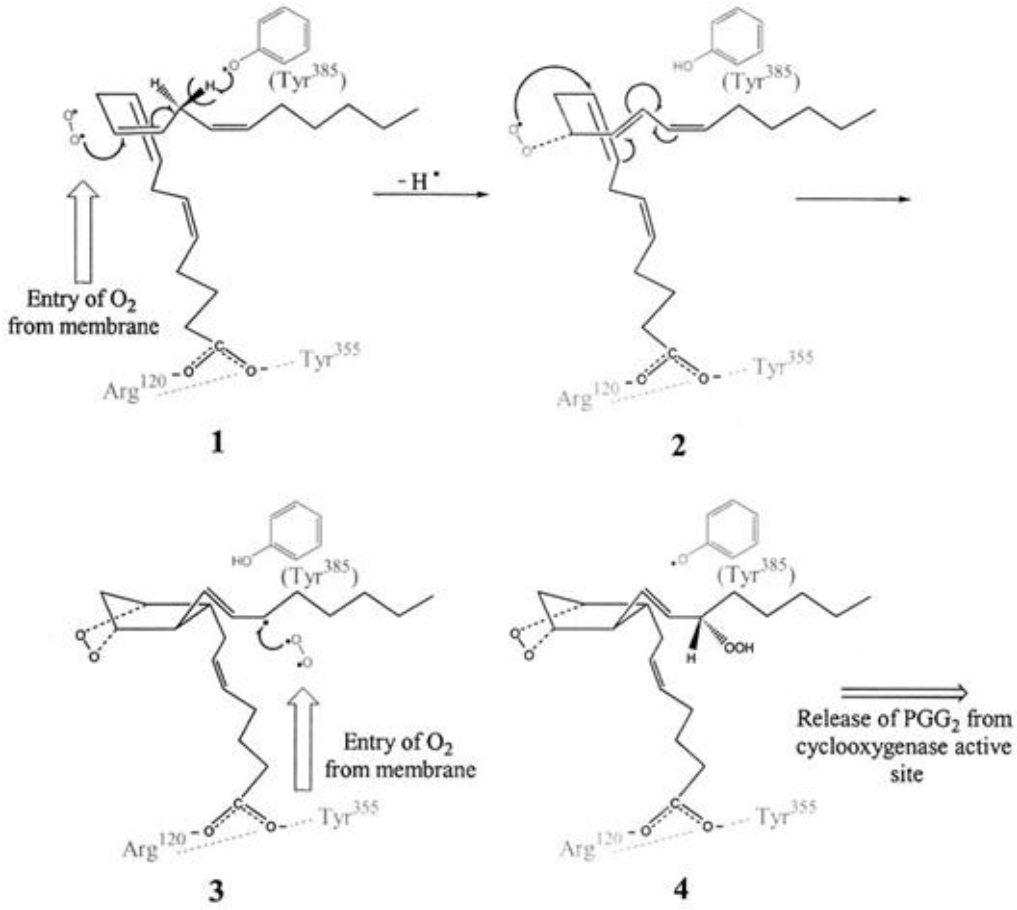

Figure 1.4. The mechanism of cyclooxygenase and peroxidase activity of COX. This figure is modified from (*15*).

1.4 15-PGDH pathway

1.4.1 15-PGDH structure and function

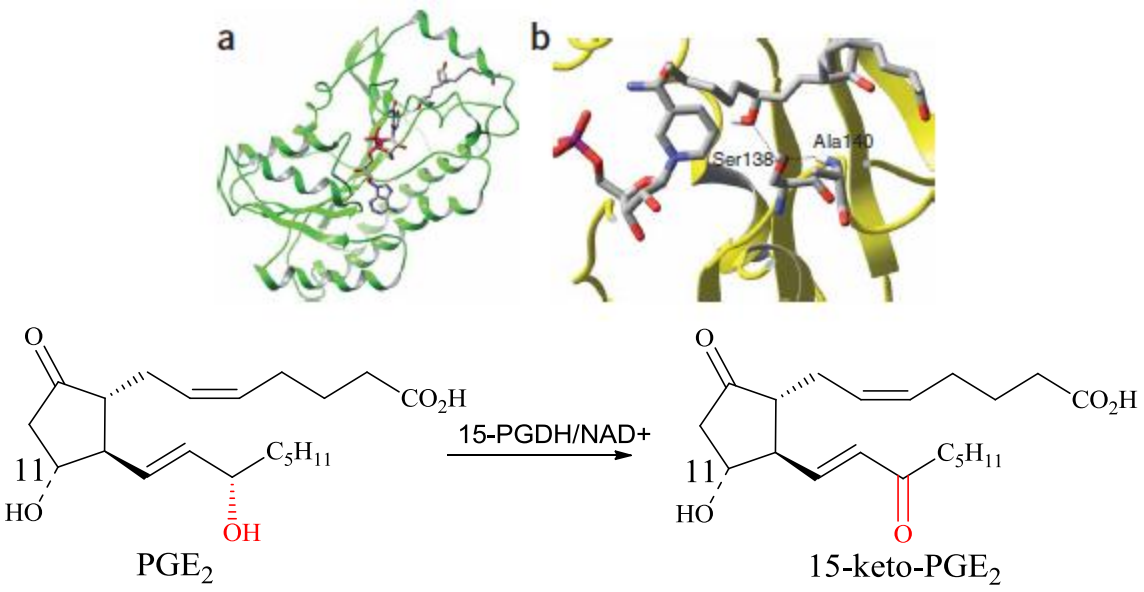

Figure 1.5: Crystal structure of 15-PGDH. Figure 1.5a. the crystal structure of 15-PGDH with NAD+ and PGE_2 complex. Figure 1.5b. the catalytic sites. Bottom, the chemical structures of PGE_2 and dehydrated product 15-keto-PGE_2. Figure 1.5a and 1.5b are modified from ref (*26*)

The eicosanoids generated from COXs are not metabolically stable. Thus, the overall eicosanoid levels are controlled both by COXs and by eicosanoid catabolism enzymes. Among the eicosanoid catabolism enzymes, 15-hydroxyprostaglandin dehydrogenase (15-PGDH) has been studied intensively. 15-PGDH is an enzyme which converts the (*S*)-hydroxyl group at carbon 15 on eicosanoids to a keto group. For example, PGE_2 undergoes 15-PGDH-mediated conversion to the biologically inactive 15-keto-PGE_2 (Figure 1.5, which can be further metabolized to 13,14-dihydro-15-keto-PGE_2 by a specific reductase. 15-PGDH primarily uses NAD^+ as its cofactor. Although there is a type II 15-PGDH which uses $NADP^+$ as its cofactor, type II 15-PGDH has a K_m value toward PGE_2 which is two orders of magnitude higher than NAD^+ dependent 15-PGDH (*27*). In addition to being reduced, 15-keto-

PGE_2 can undergo glutathione *S*-transferase (GST)-mediated conjugation with glutathione (GSH). Other eicosanoids containing a 15(*S*)-hydroxyl group can undergo a similar route of catabolism. The GSH conjugates have higher polarity than their precursors, and they can be excreted out of cells through relevant transporters.

1.4.2 15-PGDH substrates

Although 15-PGDH was first identified as an enzyme which degraded PGs, subsequent studies revealed that LOX-type products, such as 15(*S*)-HETE, 12-HHT, and 12-HETE were also the substrates of 15-PGDH isolated from human IL-60 leukemia cells (*28*). However, based on the data obtained (Table 1.1), it was concluded that substrates containing ω-6 hydroxyl group were more readily degraded by 15-PGDH. This suggests that 15-PGDH could play an important role in the metabolism of many different eicosanoids.

1.4.3 15-PGDH and diseases

It has been reported that in many tumors and cancer cell lines, 15-PGDH is down-regulated so that pro-proliferative PGs can accumulate (*29*). Eruslanov *et al*. showed that delivery of 15-PGDH genes to mouse tumors greatly reduces tumor development through increasing 15-PGDH expression and removing accumulated PGE_2 (*30*). Moreover, decreased PGE_2 levels not only decreased tumor growth rate, but also inhibited the release of immunosuppressive cytokines from CD11b cells associated with tumor cells. Thus, besides COX-2, 15-PGDH is also a chemotherapy target. Another group showed that COX-2 inhibitor therapy fails in some patients who are 15-PGDH

deficient, suggesting that a combination of COX-2 inhibitors and 15-PGDH stimulators provide a better chemoprevention approach (*31*).

Substrate specificity of 15-prostaglandin dehydrogenase obtained from HL-60 cells[a].

Substrate	Relative activity
Prostaglandins	
PGE_2	100%[b]
$PGF_{2\alpha}$	97
PGA_2	80
6-KETO-$PGF_{1\alpha}$	51
PGB_2	–
Hydroxy – fatty acids	
12-HHT[c] (C17 : w6)[d]	85
13-HODD (C18 : w6)	93
15-HETE (C20 : w6)	92
12-HETE (C20 : w9)	21
5-HETE (C20 : w16)	–

Table 1.1. Substrate specificity of 15-prostaglandin dehydrogenase obtained from HL-60 cells. hydroxyl-heptadecatrienoic acid (HHT); hydroxyl-octadecadienoic acid (HODD); hydroxyl-eicosatetraenoic acid (HETE). Activity with PGE_2 was 5.4 nmol/min/mg protein. (Modified from Table 1.1 in Metabolism of cyclooxygenase and LOX products by 15-PGDH from human HL-60 leukemia cells (*28*)

1.5 Lipid hydroperoxide Non-enzymatic decomposition pathway

1.5.1 Hock rearrangement

For many years, it has been known that unsaturated lipids can generate aldehydes, and compared to the lipid precursor, these aldehydes are much

more reactive to cellular macromolecules and thiols. It was reported that these aldehydes can modify proteins, DNA, and induce oxidative stress by conjugating to GSH. Among these aldehydes, the formation of malondialdehyde (MDA), 4-hydroxy-2(*E*)-nonenal (HNE), and 4-oxo-2(*E*)-nonenal (ONE) are the most widely studied (*32*). However, the mechanism by which the aldehydes are formed is still controversial. The Figures 1.6 to1.10 show some of the mechanisms proposed by different research groups.

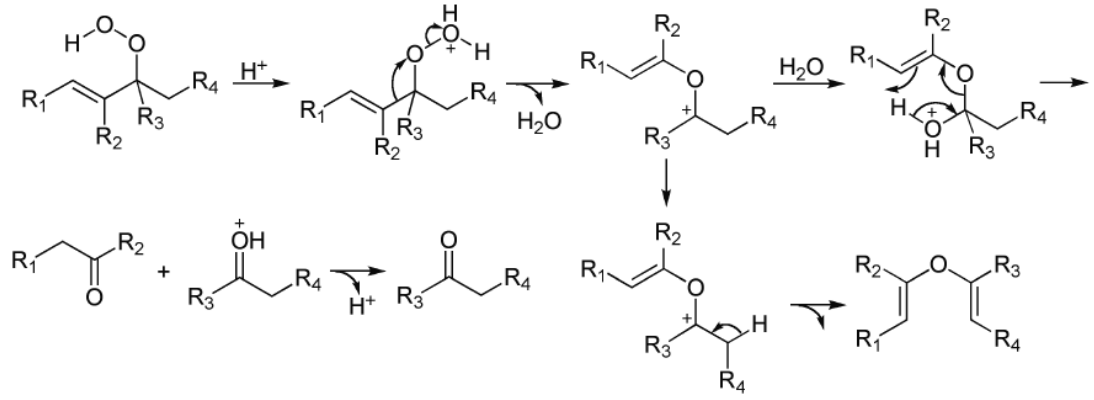

Figure 1.6: Hock rearrangement, modified from the book *Comprehensive Organic Name Reactions and Reagents,* by Zerong Wang, (*34*)

The Hock rearrangement (or Hock cleavage) was first studied by Hock and Schrader in 1936 (*33*). This reaction is initiated by protic or Lewis acid, which promotes the rearrangement of hydroperoxides which have unsaturated group (aryl or vinyl) attached to the carbon bearing the hydroperoxide group, followed by the formation a oxycarbonium ion, which is further attacked by water, initiating another rearrangement. This whole process can convert long chain unsaturated fatty acid into shorter chain carbonyl compounds. This

mechanism is still often used to explain the conversion of lipid hydroperoxides to reactive aldehydes.

1.5.2 Beta scission

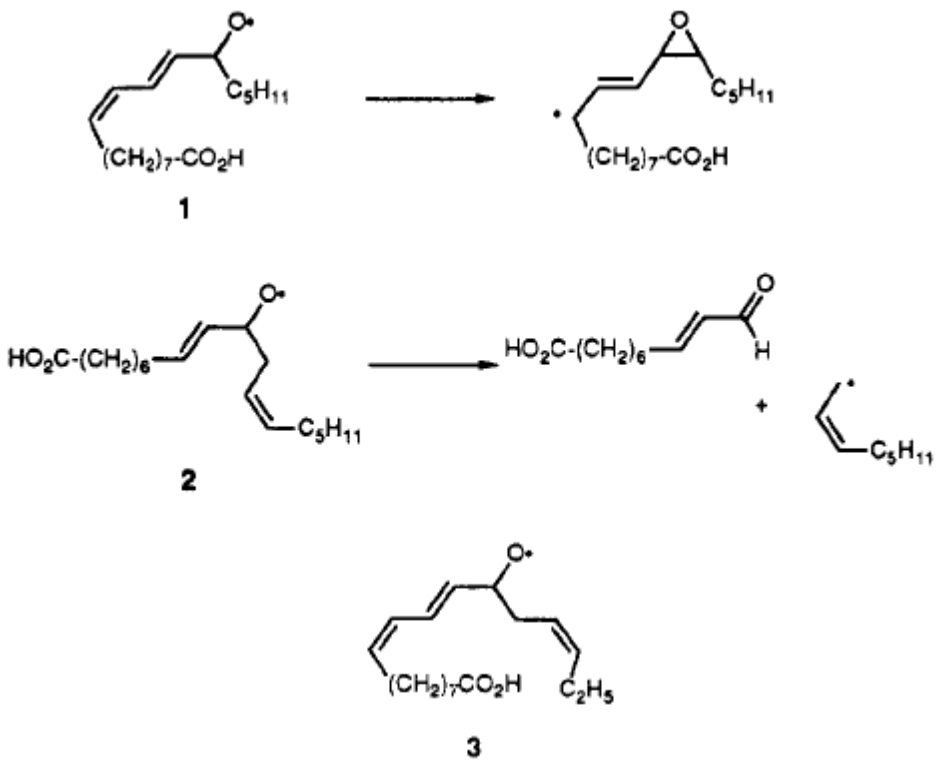

Figure 1.7. Decomposition mechanism via formation of allylic radicals

This mechanism was originally proposed by the Marnett group (*35*). The hydroperoxide group is reduced by iron, forming alkoxyl radical, which either attacks the neighboring unsaturated carbon to form epoxide containing an allylic radical (epoxyallylic radical), or undergo β-scission to break a carbon bond and form an aldehyde together with an allylic radical, although the former pathway is favored. The beta-scission products account for less than

5% of the products. Another observation from the same group is that very little alcohol is formed, which means most of the alkoxyl radicals don't stay long enough to abstract hydrogen from other molecules, instead, they tend to form epoxyallylic radicals, which are much more stable than the alkoxyl radicals.

1.5.3 Dihydroperoxide formation

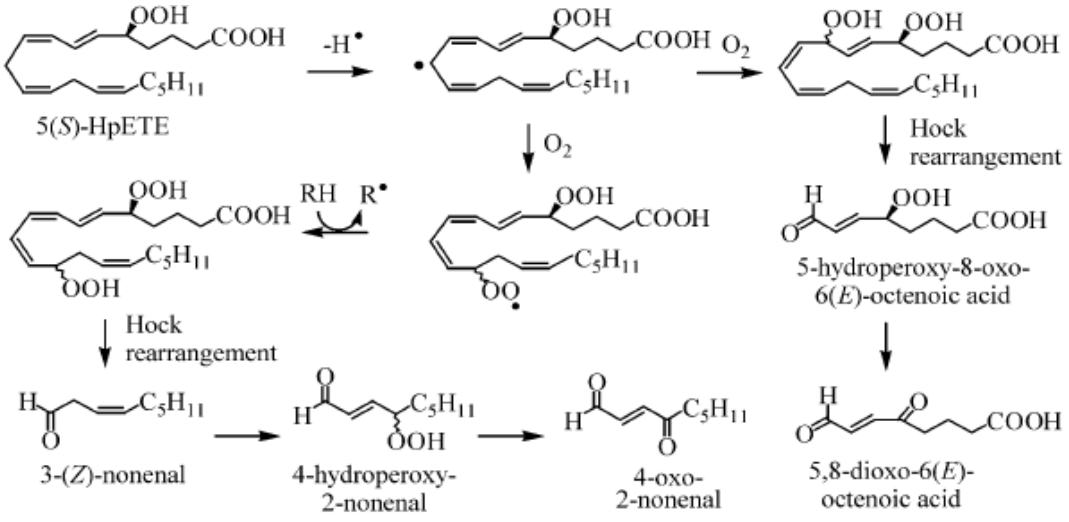

Figure 1.8. Hock rearrangement via dihydroperoxide formation from 5(*S*)-HPETE

The scheme shown in Figure 1.8 was originally proposed by the Blair group (*36*). There is no direct evidence for the formation of the dihydroperoxide, but there was one indirect piece of evidence to support this mechanism. Three products, 4-hydroperoxy-2-nonenal (HPNE), ONE and 5,8-dioxo-6(*E*)-

octenoic acid were detected as their corresponding 2'-deoxyguanosine adducts.

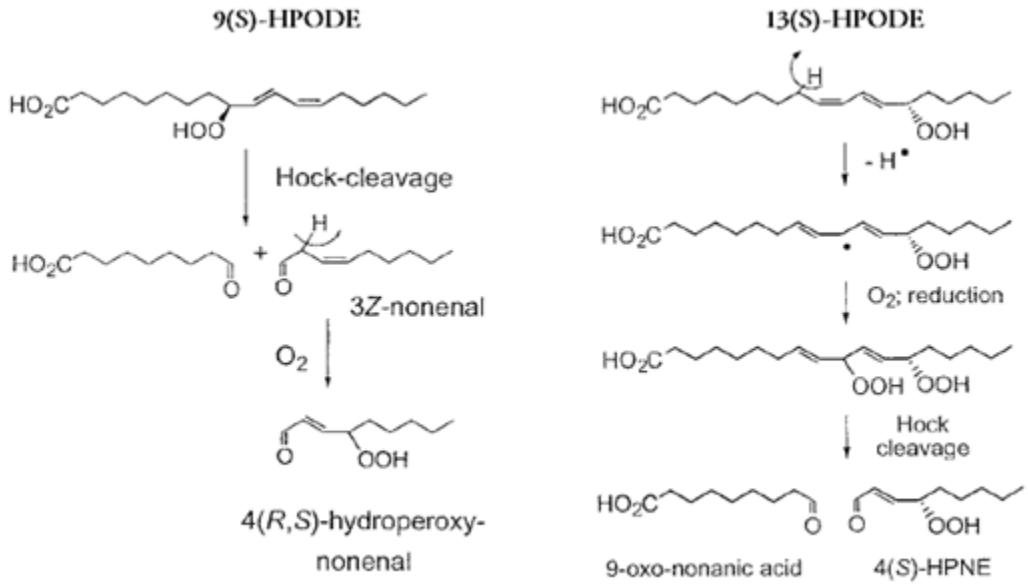

Figure 1.9: Direct hock-cleavage from 9(*S*)-HPODE and 2-step dihydroperoxide formations from 13(*S*)-HPODE. This figure is modified from (*37*)

The mechanism shown in Figure 9 was originally proposed by the Brash group to explain why 9(*S*)-hydroperoxyoctadecadienoic acid (HPODE) generated racemic 4-HPNE, whereas 13(*S*)-HPODE generated enantiomerically pure 4(*S*)-HPNE (*37*). The 9(*S*)-HPODE has a hydroperoxide attached to C9 and also a conjugate double bond next to this C9 carbon, which facilitates the vinyl migration during the Hock-rearrangement. In the case of 13(*S*)-HPODE, the direct Hock-rearrangement product was also observed, but to generate HPNE, another hydroperoxide group must be first formed at C10. However, the Brash group subsequently

synthesized the dihydroperoxide intermediate, 10,13-dihydroperoxy-HPODE, and showed that no HPNE could be detected from this intermediate under autoxidation condition. In contrast, under acidic conditions, HPNE formation could be observed. This indicated that conjugated diene group was a better migratory group compared to vinyl group during the Hock-rearrangement. In order to explain these finding, the Brash group proposed an alternative mechanism (*37,38*). This involved the formation of trimers or oligomers derived from 15(*S*)-HPETE (Figure 1.10).

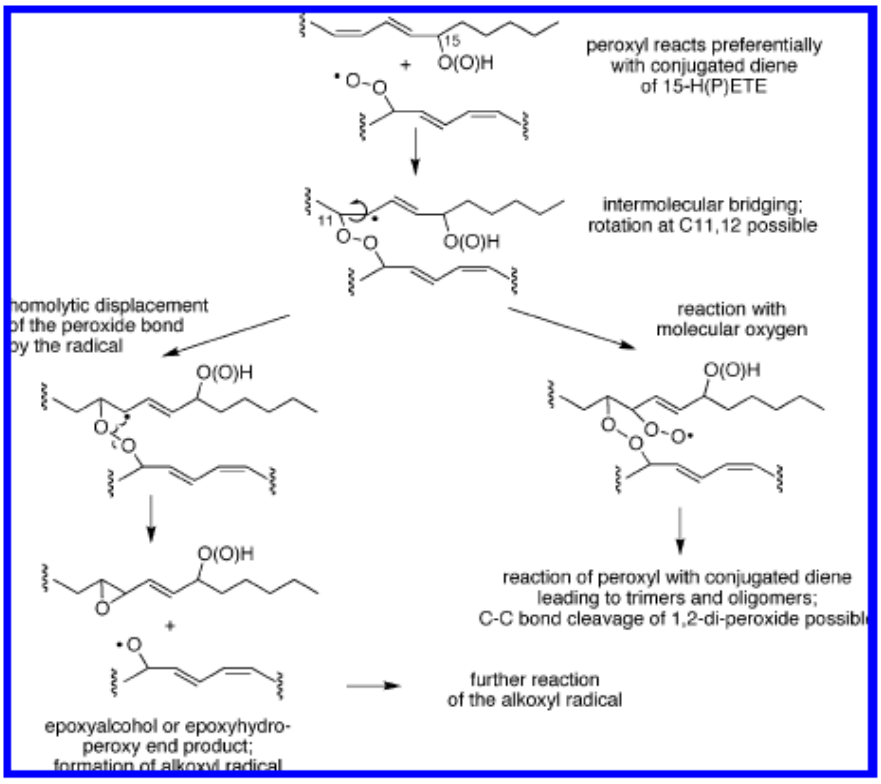

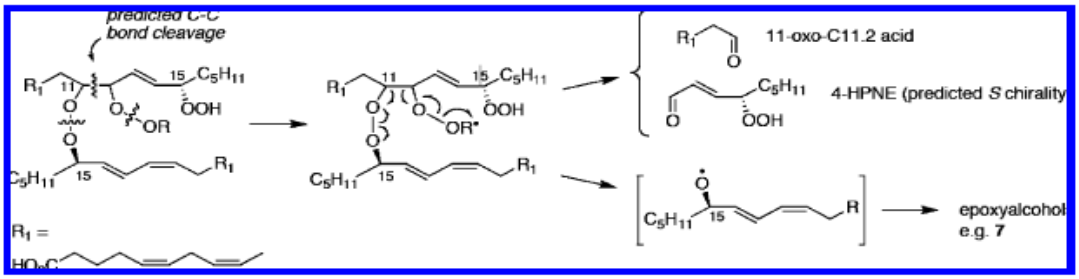

Figure 1.10: Proposed trimer and oligomer formation during 15(*S*)-HPETE decomposition (*38*).

1.6 Effects of AA-derived electrophiles on proteins and DNA

1.6.1 Carboxylic acid containing-electrophiles.

As discussed previously, carboxylic acid containing-electrophiles such as 15d-PGJ_2 (downstream metabolite of PGD_2) can be formed from enzymatic pathways. All of these electrophiles contain an α-β unsaturated ketone and so can potentially react with proteins, GSH or DNA. The possible detoxification pathways are to reduce the conjugated ketone or the double bond to undergo GST-mediated conjugation with GSH. The metabolites are then secreted from the cells. These carboxylate-containing α,β-unsaturated ketone metabolites can have significant biological effects before they degrade. For example, 15d-PGJ_2 is a ligand for the peroxisome proliferator-activated receptor gamma (PPARγ) receptor and once 15d-PGJ_2 binds to PPARγ it translocates from the cytosol into the nucleus. The PPARγ then binds to DNA and regulates the transcription of target genes. The up- or down-regulation of these genes can activate adipocyte differentiation, reduce inflammation and also have anti-proliferation effects. (*4*)

1.6.2 Non-carboxylic acid containing-electrophiles.

As discussed previously, aldehydes that are generated by lipid oxidation such as MDA, HNE and ONE are bifunctional electrophiles that can react with numerous cellular targets. The effects of these aldehydes on modifying proteins, DNA and GSH have been intensively studied as described below.

1.6.2.1 Modification of proteins:

Lipid peroxidation generated electrophiles tend to modify proteins through covalent conjugation with cysteine, histidine, and lysine residues. Immunostaining measured protein adducts from glycoxidation, lipid oxidation, and acrolein has been analyzed in healthy subjects or patients with diabetic nephropathy (DN) or with IgA nephropathy (IgA-N) (Table 1.2) (*39*). This study clearly showed that the lipid oxidation products, MDA and HNE form proteins adducts in DN or IgA subjects, while there are only trace adducts in healthy subjects, which highlights the relationship between lipid oxidation and DN or IgA nephropathy development.

Group	Grade	CML	Pentosidine	MDA-Lysine	HNE-Protein Adduct	Acrolein-Protein Adduct
Healthy subjects		±	±	±	±	±
DN	I	±	+	+	±~+	±~+
	II	+	+~++	+~++	+	+
	III	+~++	++	++	+~++	++
IgA	I	±	±	±	±	±
	II	±	±	±~+	±~+	±
	III	±	±	+~++	+~++	±

Table 1.2 Results of immunostaining for glycoxidation products, lipid oxidation products, and acrolein-protein adduct in healthy subjects and patients with diabetic nephropathy (DN) or IgA nephropathy (IgA-N). CML, carboxymethyllysine; MDA-lysine, malondialdehyde-lysine; HNE-Protein, 4-hydroxy-nonenal-lysine.

HNE generated from COX-mediated AA oxidation can even up-regulate the expression of COX-2, and function as a positive feedback loop, which further increases COX-2 products, resulting in "carbonyl stress" and oxidative stress. (*40*)

1.6.2.2 Modifications of DNA:

2'-Deoxynucleosides (except thymidine) have primary amine groups, which are good nucleophiles and could be the targets of electrophiles. The reactions of different lipid oxidation-derived electrophiles with 2'-deoxyguanosine (dGuo) and 2'-deoxyadenine (dAdo) are shown in Figure 1.11 (*41*). It has been reported that dGuo adducts are detected *in vivo* at higher levels than dAdo and 2'-deoxycytidine (dCyd) adducts. ONE and HNE DNA adducts can only come from lipid oxidation, while MDA can arise from other sources such as during thromboxane A2 biosynthesis. Therefore, ONE- and HNE-derived DNA-adducts are good biomarkers for lipid oxidation. Normally, cells have an efficient DNA repair system, and once damaged DNA is recognized, they either remove the damaged oligonucleotides (nucleotide excision repair, NER) or only the damaged bases (base excision repair, BER). The excised damaged oligonucleotides or bases would be excreted, and it might be possible to detect them in urine. Thus, the HNE and ONE modified oligonucleotides or bases could potentially be lipid oxidation and DNA damage biomarkers. These DNA adducts are mutagenic if not repaired, they would accumulate and could be ultimately responsible for tumorigenesis.

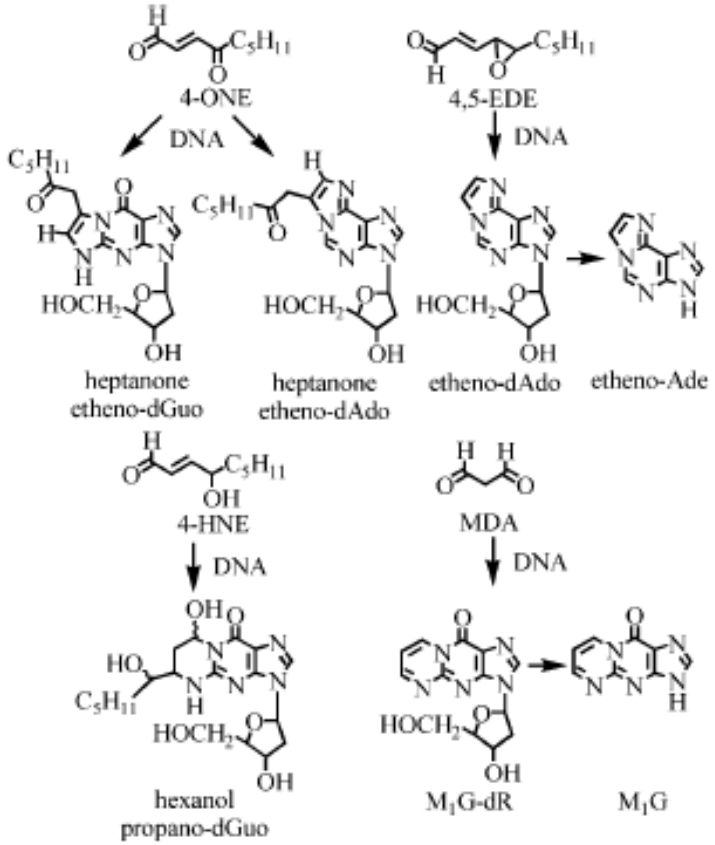

Figure 1.11, Scheme of dGuo or dAdo adducts from ONE, HNE, MDA and trans-4,5-epoxy-2(E)-decenal (EDE) (*41*).

1.6.2.3 Inactivation of HNE

Similar to the inactivation of carboxylate-containing electrophiles, the aldehyde moiety of HNE is also subject to reduction to an alcohol by aldo-keto reductases (AKRs), particularly the AKR1B subfamily isoenzyme: AKR1B1. Moreover, HNE is also the substrate of GSTs (*42*), which catalyze the addition of GSH (Figure 1.12). Conjugation can also occur directly

through a chemical reaction in the absence of GSTs. Thus, measurement of HNE-GSH adduct could be strategy to monitor the lipid peroxidation level.

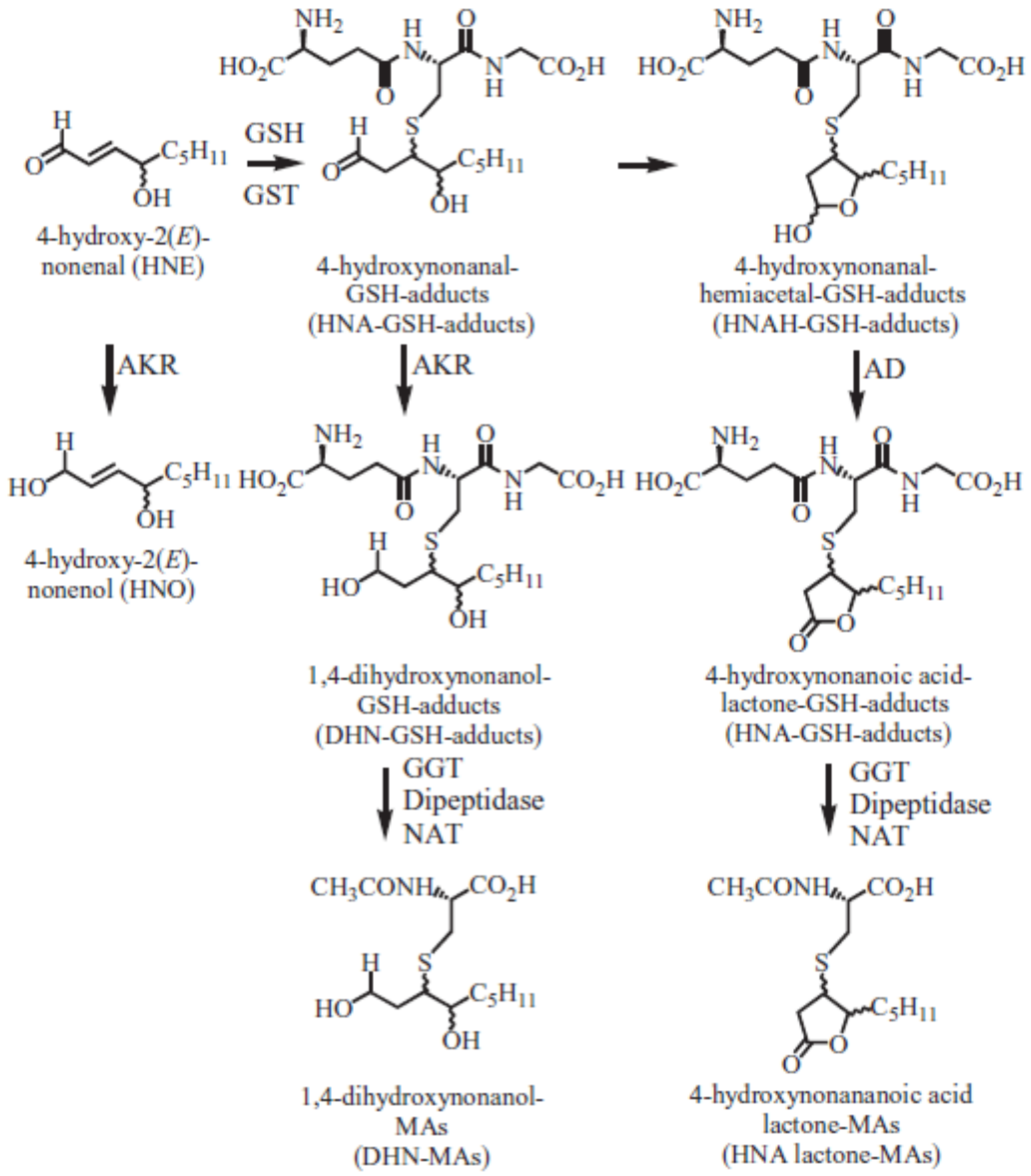

Figure 1.12 The detoxification of HNE by GST and AKR. Modified from (*42*)

1.7 Brief description of mass spectrometry (MS) methods

1.7.1 Three components:

All mass spectrometers have three components, an ion source, an analyzer and a detector.

The most widely used ion source uses atmospheric pressure ionization (API), which is usually coupled with liquid chromatography (LC). Analytes are charged in solution by adjusting the pH of the mobile phase. They are allowed to evaporate from the liquid mobile phase into the gas phase (electrospray ionization, ESI) or by applying a charged needle under atmospheric pressure (atmospheric pressure chemical ionization, APCI). High temperature (200 to 400 °C) and nitrogen gas help the desolvation process.

The mass analyzer is used to distinguish ions with different mass to charge ratios (*m/z*). The ability of the mass spectrometer to distinguish ions of different *m/z* depends upon the resolving power of the mass spectrometer that is used. The definition of resolution is the minimum *m/z* peak separation divided by *m/z*. For high resolution, such as the LTQ-Orbitrap (Thermo Electron, San Jose, CA), it could be up to 150,000, which means that it would be possible to distinguish two ions that differ in mass by only 0.001 Da. In contrast, low resolution instruments, which typically operate at unit mass resolution, can only distinguish two ions that differ in mass by 0.1 Da. Low resolution mass spectrometers include triple stage quadrupole (TSQ) and linear ion trap (LTQ) instruments. TSQs are normally used for quantitative studies, while ion traps are more widely used for structure elucidation due to its multiple fragmentation function.

1.7.2 TSQ quantitation:

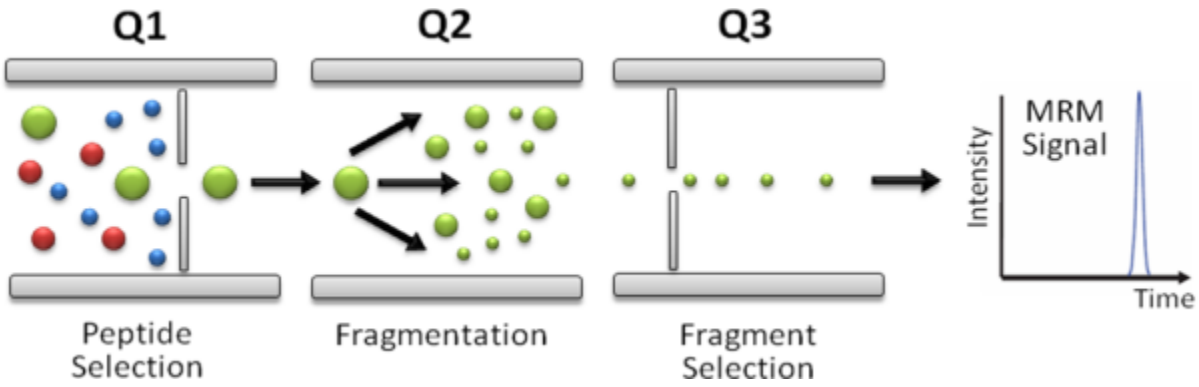

Figure 1.13 A simplified example of how the TSQ separates peptide ions with different m/z values.

The TSQ instrument has three quadrupoles (Q) in serial. Q1 and Q3 can work in scanning mode, where all of the ions are allowed to pass through and recorded by detector, while Q2 is designed to function as a collision cell, which means the voltage and collision gas will apply to this cell and fragment the ions coming from Q1. The most frequently applied mode with the TSQ is selected reaction monitoring (SRM). Under this mode, Q1 is responsible for allowing only a selected parent ion to pass through, while in Q2, this ion is fragmented and only selected product ion is allowed to fly to Q3 and recorded. (MRM usually refers to multiple product ions from a single parent ion). LC-SRM/MS is highly selective even with only unit resolution because specificity is conferred by the fragmentations process. The method is also highly sensitive and reproducible. Thus, this LC-SRM/MS is widely used in lipid metabolite and quantification.

Chapter 2 11-Oxo-Eicosatetraenoic Acid is a Cyclooxygenase-2/15-Hydroxyprostaglandin Dehydrogenase-Derived Anti-Proliferative Eicosanoid

2.1 ABSTRACT

Previously, the Blair laboratory established that 11(*R*)-HETE was a significant COX-2-derived AA metabolite in epithelial cells. Stable isotope dilution chiral LC-electron capture atmospheric pressure chemical ionization (ECAPCI)/MS was used to quantify COX-2-derived eicosanoids in the human colorectal adenocarcinoma (LoVo) epithelial cell line, which expresses both COX-2 and 15-PGDH. 11(*R*)-HETE secretion reached peak concentrations within minutes after AA addition before rapidly diminishing, suggesting further metabolism had occurred. Surprisingly, 15-PGDH, which is normally specific for oxidation of eicosanoid 15(*S*)-hydroxyl groups, was found to convert 11(*R*)-HETE to 11-oxo-ETE. Furthermore, LoVo cell lysates converted 11(*R*)-HETE to 11-oxo-ETE and inhibition of 15-PGDH with 5-[[4-ethoxycarbonyl) phenyl]azo]-2-hydroxy-benzeneacetic acid (CAY 10397) (50 μM) significantly suppressed endogenous 11-oxo-ETE production with a corresponding increase in 11*(R)*-HETE. These data confirmed COX-2 and 15-PGDH as enzymes responsible for 11-oxo-ETE biosynthesis. Finally, addition of AA to the LoVo cells resulted in rapid secretion of 11-oxo-ETE into the media, reaching peak levels within 20 min of starting the incubation. This was followed by a sharp decrease in

11-oxo-ETE levels. GST was found to metabolize 11-oxo-ETE to the 11-oxo-ETE-GSH (OEG)-adduct in LoVo cells, as confirmed by LC-MS/MS analysis. Bromodeoxyuridine (BrdU)-based cell proliferation assays in human umbilical vein endothelial cells (HUVECs) revealed that the half-maximal inhibitory concentration (IC_{50}) of 11-oxo-ETE for inhibition of HUVEC proliferation was 2.1 μM. These results show that 11-oxo-ETE is a novel COX-2/15-PGDH-derived eicosanoid, which inhibits endothelial cell proliferation with a potency that is similar to that observed for 15d-PGJ_2.

2.2 INTRODUCTION

In an earlier study, the Blair laboratory established that 11(*R*)-HETE was a significant COX-2-derived AA metabolite in epithelial cells (*43*). However, the consequences of this finding were not clear at that time. A number of toxic substances including arsenite (*44*), dioxin (*45*) benzo[*a*]pyrene-diol-epoxide (*46*), and cigarette smoke (*47*) up-regulate COX-2 expression, which in turn regulates numerous intracellular biochemical pathways. This occurs primarily through the biosynthesis of COX-2-derived AA metabolites, which can exert cell-specific effects on inflammation, cell growth, and proliferation. For example, COX-2-derived prostaglandin (PG) E_2 increases tumor proliferation through multiple mechanisms including activation of plasma membrane G-protein-coupled receptors and the nuclear peroxisome proliferator-activated receptor (PPAR)γ.(*48*)

Steady-state levels of PGE_2 are maintained by PGE-synthase-mediated biosynthesis from COX-2-derived PGH_2 and catabolism by 15-PGDH-mediated

inactivation to 15-oxo-PGE_2 (Figure 2.1).(*49,50*) The 15-oxo-PGE_2 is then converted to 13,14-dihydro-15-oxo-PGE_2 by 15-oxo-prostaglandin-Δ^{13} reductase.(*51*) Loss of 15-PGDH expression is associated with tumor formation in bladder, breast, colon, intestine, kidney, lung, pancreas, stomach, and skin cancer.(*49,50,52-54*) Thus, up-regulation of COX-2 (*48*) and down-regulation of 15-PGDH (*52*) provides a switch towards endogenous mediators that are significant contributors to cancer progression.(*57*)

PGD_2, another COX-2-derived metabolite, is also metabolized by 15-PGDH to form 15-oxo-PGD_2, which is then converted to the corresponding inactive 13,14-dihydro-derivative (Figure 2.1).(*58*) Alternatively, PGD_2 undergoes albumin-mediated dehydration to give PGJ_2, followed by a further dehydration to give 15-deoxy-$\Delta^{12,14}$-prostaglandin J_2; (15d-PGJ_2) (Figure 2.2).(*59*) Previous studies have shown that 15d-PGJ_2 is a PPARγ agonist,(60) which inhibits HUVEC proliferation in culture.(*61*) In addition, 15d-PGJ_2 can induce caspase-mediated endothelial cell apoptosis(*62*) and inhibit the nuclear factor κB (NFκB) pathway.(*63-64*) It can also increase levels of p53 in HUVECs, activate p53 phosphorylation, and induce p21.(*65*)

Studies of purified COX enzymes have shown that 11(*R*)-HETE, 15(*S*)-HETE, and 15(*R*)-HETE are the major HETEs that are formed.(*66*) The HETEs arise from reduction of the corresponding HPETEs primarily through the peroxidase (POX) activity of COXs (Figure 2.1).(*67*) 11(*R*)-HETE was a significant eicosanoid secreted by AA-treated rat intestinal epithelial cells that stably express COX-2 (RIES cells) but it was rapidly metabolized.(*43*) 15(*S*)-HETE

was formed in lower abundance and metabolized to 15-oxo-ETE (*66,68*) as expected from its 15(*S*)-configuration and the substrate specificity of 15-PGDH. 15-Oxo-ETE was also found to inhibit endothelial cell proliferation, although at concentrations higher than 15d-PGJ_2.(*68*) However, there is little evidence that 15d-PGJ_2 can be formed *in vivo* at concentrations commensurate with an endogenous anti-proliferative role.(*69*) In our earlier study, (*43*) the metabolic fate of 11(*R*)-HETE secreted by the RIES cells was not established. 11-Oxo-ETE has now been synthesized and a LC-selected reaction monitoring (SRM)/MS method for its analysis has been developed. This has made it possible to determine whether 11-oxo-ETE is secreted by human epithelial cell lines with up-regulated COX-2 expression and to identify the dehydrogenase responsible. The ability of 11-oxo-ETE to modulate HUVEC proliferation has also been examined.

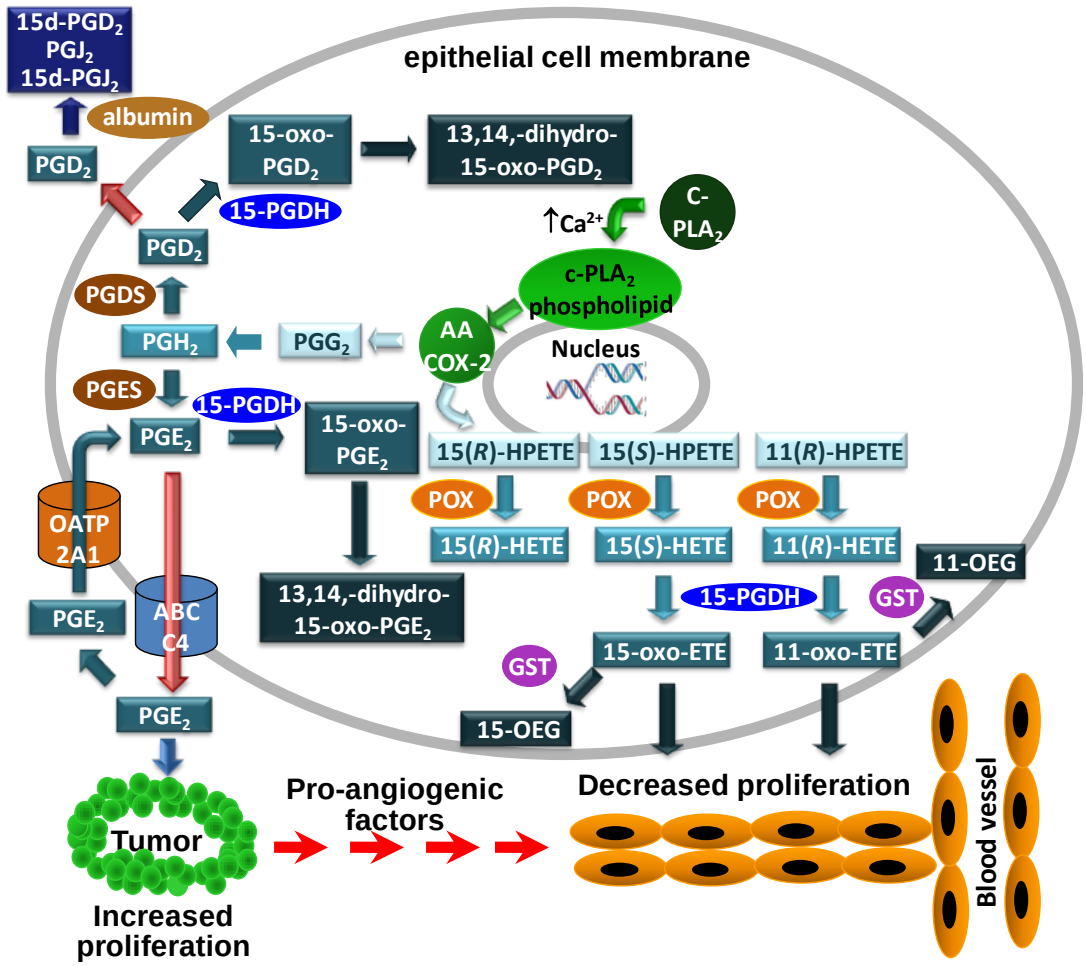

Figure 2.1. Formation and action of COX-2-derived eicosanoids in epithelial cell models. AA is released from membrane phospholipids by calcium-dependent cytosolic phospholipase A2 (cPLA2). The released AA undergoes COX-2-medaited metabolism to PGs or forms the lipid hydroperoxides, 15(*S*)-hydroperoxyeicosatetraenoic acid; (HPETE), 15(*R*)-HPETE and 11(*R*)-HPETE, which are reduced to the corresponding HETEs. PGD_2 and PGE_2 are inactivated by 15-PGDH-mediated conversion to their 15-oxo-metabolites. Both 15-oxo-PGD_2 and 15-oxo-PGE_2 are converted to 13,14-dihydro-5-oxo-PG metabolites. Intact PGD_2 secreted by the epithelial cells can undergo albumin-mediated dehydration to 15d-PGJ_2. PGE_2 secreted from the epithelial cells by the ABCC4 transporter is pro-proliferative for tumor cells. Re-uptake of PGE_2 by OATP2A1 into the epithelial cells leads to further 15-PGDH-mediated inactivation. In contrast to PGE_2 and PGD_2, 15(*S*)-HETE and 11(*R*)-HETE are activated by 15-PGDH-mediated oxidation to 15-oxo-ETE and 11-oxo-ETE, respectively. The oxo-ETEs are further conjugated to form OEGs. Secreted 15- and 11-oxo-ETE that escape further

metabolism can then inhibit endothelial cell proliferation. Therefore, down-regulation of 15-PGDH and OATP2A1 would result in increased PGE_2-mediated tumor and endothelial cell proliferation.

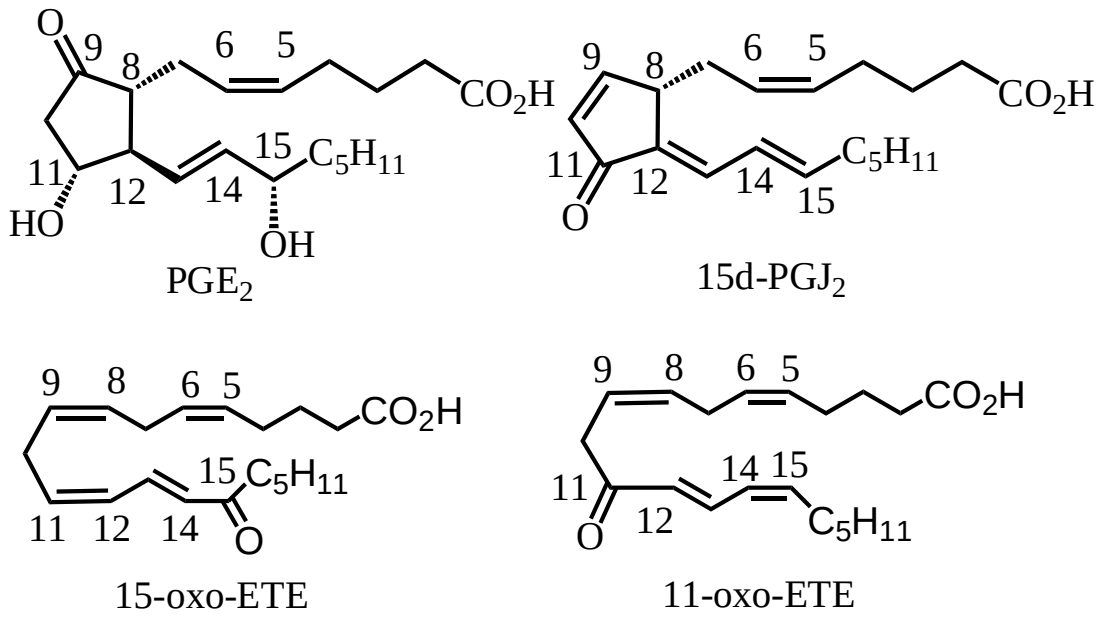

Figure 2.2. Chemical structures of COX-2 derived eicosanoids.

2.3 EXPERIMENTAL PROCEDURES

2.3.1 Chemicals and Reagents.

AA (peroxide-free), 11(*R,S*)-HETE, 15(*R,S*)-HETE, [$^2H_8$]-15(*S*)-HETE, [$^{13}C_{20}$]-15-oxo-ETE, 15-oxo-ETE, PGE_2, [$^2H_4$]-PGE_2, 13,14-dihydro-15-keto-PGE_2, [$^2H_4$]-13,14-dihydro-15-keto-PGE_2, 15d-PGJ_2, CAY10397, protease inhibitor cocktail and recombinant human 15-PGDH were purchased from Cayman

(Ann Harbor, MI). The Dess-Martin reagent [1,1,1-Tris(acetyloxy)-1,1-dihydro-1,2-benziodoxol-3-(1*H*)-one], 2,3,4,5,6-pentafluorobenzyl (PFB) bromide, Trizma-HCl, lipoxidase from Glycine max (soybean), sodium borohydride, and NAD^+ were purchased from Sigma-Aldrich (St. Louis, MO). Fetal bovine serum (FBS) was from Gemini Bioproducts (West Sacramento, CA). F12K medium, DMEM medium, Medium 200 (M200), Minimum Essential Medium (MEM), D-glucose, L-glutamine, low-serum growth supplement (LSGS) kit, penicillin, and streptomycin were supplied by Invitrogen (Carlsbad, CA). LC-MS grade water, hexane, methanol, isopropanol, acetonitrile and dichloromethane were obtained from Fisher Scientific (Pittsburgh, PA). Gases were supplied by The Linde Group (Munich, Germany). $[^{13}C_{20}]$-AA was obtained from Spectra Stable Isotopes (Columbia, MD).

2.3.2 Cell Culture.

Human colorectal adenocarcinoma LoVo cells (ATCC, Manassas, VA) were cultured in F12K medium supplemented with 10% FBS, 2 mM/L glutamine, 100,000 units/l penicillin and 100 mg/l streptomycin. Human colonic adenocarcinoma HCA-7 Colony 29 cells (Sigma-Aldrich, St. Louis, MO) were grown in DMEM supplemented with 10% FBS, 2 mM L-glutamine, 110 mg/L sodium pyruvate, 100,000 units/l penicillin and 100 mg/l streptomycin. For lipidomics analysis, the culture media was replaced with serum-free F12K or DMEM media before the treatment. HUVECs were obtained from Invitrogen (Carlsbad, CA), and cultured on collagen I-coated tissue culture dishes in

Medium 200 supplemented with LSGS kit. Caco-2 cells were grown in MEM containing 20% FBS 2 mM/L glutamine, 100,000 units/l penicillin and 100 mg/l streptomycin. Cell proliferation assays were performed using HUVECs from passage 4.

2.3.3 Mass Spectrometry.

A triple stage quadrupole (TSQ Quantum) mass spectrometer (Thermo Electron, San Jose, CA) equipped with an APCI source was used for the quantitative lipidomics analyses. Targeted chiral LC-ECAPCI/SRM/MS analysis was conducted using PFB derivatives of 7 lipids and 4 heavy isotope analog internal standards. For the lipidomics profile, the instrument was operated in the negative ion mode, and unit resolution was maintained for both precursor and fragment ions. Operating conditions for the TSQ Quantum were: vaporizer temperature at 450°C; heated capillary temperature at 250 °C with the corona discharge needle set at 30 μA; nitrogen as sheath (25 psi) and auxiliary (5 arbitrary units) gas. Collision-induced dissociation (CID) was performed using argon as the collision gas at 2.7 mtorr in the RF-only quadrupole. The following SRM transitions were used: 11-oxo-ETE-PFB, *m/z* 317 → 165 (collision energy (CE), 25 eV), 15-oxo-ETE-PFB, *m/z* 317 → 113 (CE, 18 eV), [$^{13}C_{20}$]-15-oxo-ETE-PFB, *m/z* 337 → 120 (CE, 18 eV), 11(*R*)-HETE-PFB, *m/z* 319 → 167 (CE, 16 eV), [$^{2}H_{8}$]-15(*S*)-HETE-PFB, *m/z* 327 → 226 (CE, 13 eV), PGE_2-PFB, *m/z* 351 → 271 (CE, 18 eV), [$^{2}H_{4}$]-PGE_2-PFB, *m/z* 355 → 275 (CE, 18 eV). 13,14-dihydro-15-keto-PGE_2-PFB, *m/z* 351 →

235 (CE, 22 eV), [$^2H_4$]-13,14-dihydro-15-keto-PGE_2-PFB, *m/z* 355 → 239 (CE, 22 eV).

For GSH adduct analysis, the mass spectrometer was operated in the positive ion mode with an electrospray ionization (ESI) source. The operating conditions were: spray voltage at 4 kV; capillary temperature at 350°C; nitrogen as sheath (35 psi) and auxiliary (13 arbitrary units) gas. CID was performed using argon as the collision gas at 2.7 mtorr in the Rf-only quadrupole. The following SRM transition (m/z 626 → 497) was monitored for 11-oxo-ETE-GSH (CE, 18 eV).

2.3.4 Liquid Chromatography.

LC separations were conducted using a Waters® Alliance 2690 HPLC system. A Chiralpak AD-H column (250 × 4.6 mm inner diameter, 5 μm; Daicel) was employed for normal phase separation (flow-rate 1 ml/min) of PFB-derivatives of eicosanoids. Gradient 1 was used for separating PFB-derivatives of HETEs and PGE_2, whereas gradient 2 was used for PFB derivatives of oxo-ETEs. For gradient 1, solvent A was hexane, and solvent B was methanol/isopropanol (1:1; v/v). Gradient 1 was as follows: 2% B at 0 min, 2% B at 3 min, 3.6% B at 11 min, 8% B at 15 min, 8% B at 27 min, 50% B at 30 min, 50% at 35 min, and 2% B at 37 min. Separations were performed at 30°C using a linear gradient. For gradient 2, solvent A was hexane, and solvent B was isopropanol/hexane (6:4; v/v). Gradient 2 was as follows: 2% B at 0 min, 2% B at 14.5 min, 12% B at 15 min, 23% B at 19 min, 90% B at 19.5 min, 90% B at 23.5 min, and 2% B at 24 min.

A Chiralpak AD-RH column (150 × 4.6 mm inner diameter, 5 μm; Daicel) was used for reverse phase (isocratic method 1, flow-rate 0.5 ml/min) separation of the un-derivatized 11-oxo-ETE. The mobile phase for isocratic separations was methanol/water/formic acid (95:5:0.1; v/v).

Chemically synthesized 11-oxo-ETE was purified by normal-phase (isocratic method 2) preparative LC (Ultrasphere™ 250 × 10 mm, inner diameter, 5 μm; Beckman) using Hitachi LC system by monitoring the UV absorbance at 236 nm. The mobile phase for isocratic method 2 (flow-rate 2.5 ml/min) was hexane/isopropanol/acetic acid (98.5:1.5:0.1; v/v).

GSH adducts were separated by reverse phase using gradient 3 on Waters® Alliance 2690 HPLC system. The separation employed a Phenomenex Synergi Hydro-RP column (150 × 4.6 mm inner diameters, 5 μm). Solvent A was 0.1% aqueous formic acid, and solvent B was methanol/acetonitrile (50:50; v/v). Gradient 3 was as follows: 2% B at 0 min, 2% B at 14 min, 30% B at 20 min, 42% B at 21 min, 65% B at 27 min, 80% B at 29 min, 90% B at 33 min, 90% B at 34 min, 2% B at 35 min. The flow rate was 0.4 ml/min. The separation was performed at ambient temperature using a linear gradient.

2.3.5 PFB Derivatization.

Eicosanoids were dissolved in 100 μl of acetonitrile, and then reacted with 100 μl of PFB bromide in acetonitrile (1:19; v/v) and 100 μl of diisopropylethylamine in acetonitrile (1:9; v/v) at room temperature for 30 min. The derivatives were evaporated to dryness, dissolved in 100 μl of hexane/ethanol (95:5; v/v) and analyzed by chiral LC-ECAPCI/SRM/MS.

2.3.6 Enzymatic Conversion of 11(*R*)-HETE by 15-PGDH.

Various concentrations of 11(*R*)-HETE (0, 2.3 μM, 4.6 μM, 6.9 μM, 9.2 μM and 23 μM) were incubated with 4 nM of recombinant human 15-PGDH (50 ng, 1.8 pmol) and cofactor NAD^+ (400 μM) in 50 mM Tris-Cl (pH 7.9) for 3.5 min at 37 °C. Each total reaction volume was 200 μl. After a 3.5 min incubation, the enzymatic reaction was quenched with 400 μl of ice cold methanol and [$^{13}C_{20}$]-15-oxo-ETE (8 ng) added as the internal standard. Eicosanoids were extracted with 1.2 ml of dichloromethane/methanol (8:1; v/v). The lower organic layer was then evaporated to dryness under nitrogen and reconstituted in methanol (100 μl). An aliquot (25 μl) was separated using isocratic method 1 and analyzed by LC-ESI/MS as described above. The retention time for 11-oxo-ETE was 8.7 min. In separate experiments, the formation of 11-oxo-ETE was found to be linear for the first 5 min. Eicosanoids were quantified by interpolation from a standard curve prepared with 11-oxo-ETE using [$^{13}C_{20}$]-15-oxo-ETE as the internal standard.

2.3.7 Chemical Synthesis and Purification of 11-Oxo-ETE.

The Dess-Martin reagent (5 mg, 12.0 μmol) was added to a solution of 11(*R,S*)-HETE (10 mg, 31.0 μmol) in dichloromethane (0.5 ml) and stirred for 2 h at room temperature. The reaction was monitored by LC-MS using gradient 1 as described above, after PFB derivatization until there was no starting material left. There was only one major product, which corresponded to 11-oxo-ETE. The reaction mixture was centrifuged twice at 3,400 rpm (10 min) and the supernatant was evaporated. The residue was

dissolved in the mobile phase (800 μl) and purified by isocratic method 2 as described above. The retention time for 11-oxo-ETE was 13.1 min. High resolution accurate mass measurements were obtained using electrospray ionization on a Thermo LTQ-FT mass spectrometer at a resolution of 100,000 (data not shown). NMR spectra were obtained on a Bruker 500 MHz NMR instrument.

2.3.8 15-PGDH inhibition in LoVo or HCA-7 Cell Lysates by CAY10397.

LoVo or HCA-7 cells were grown to 90% confluence, washed with 10 ml of phosphate-buffered saline (PBS) buffer (2 times), and then gently scraped in 600 μl of lysis buffer containing 0.1 M Tris-HCl (pH 7.9) and the protease inhibitor. Cell suspension was transferred to 2 ml Eppendorf tubes, and sonicated for 60 seconds on ice (power 5). Cell lysate was then incubated with or without the selective 15-PGDH inhibitor (CAY10397, 50 μM) and its co-factor (NAD^+, 500 μM) for 10 min at 37°C. The pH was then adjusted to 4 with 10% aqueous acetic acid (10 μl) followed by addition of the internal standard mix, [$^{13}C_{20}$]-15-oxo-ETE, [$^2H_8$]-15(*S*)-HETE and [$^2H_4$]-PGE_2 (50 pg/μl, 20 μl). Diethyl ether (600 μl) was added, and samples were vortex-mixed and centrifuged (15000 rpm×2 min). The organic layer was evaporated under nitrogen, and then the eicosanoids were derivatized with PFB bromide as mentioned above. Finally, samples were re-dissolved in hexane/ethanol (95:5; v/v, 100 μl), and analyzed (20 μl) by normal phase LC-ECAPCI/MS. The amounts of eicosanoids were normalized by protein concentrations of each lysate, which were determined by BCA assay.

2.3.9 Metabolism of AA by LoVo or HCA-7 Cells.

LoVo or HCA-7 cells were grown to 90% confluence in 6-well plates as described above, and then fed fresh serum-free F-12K or DMEM medium. Cells were then incubated with AA (10 μM) for 0, 5, 10 and 30 min, 1 and 2.5 h at 37°C. At each time point, 0.6 ml medium was taken out, 20 μl 10% aqueous acetic acid was added to adjust pH to 3-4, together with 20 μl internal standards mixture (50 pg/ μl [$^{12}C_{20}$]-15-oxo-ETE, [$^{2}H_{8}$]-15(S)-HETE, [$^{2}H_{4}$]-PGE_2 and [$^{2}H_{4}$]-13,14-dihydro-15-keto-PGE_2-PFB). Then diethyl ether (1 ml) was added, and the mixture was vortex-mixed and centrifuged (15000 rpm × 2 min). The upper ether layer was evaporated under nitrogen, and PFB derivatives were synthesized as described above and analyzed by normal phase LC-ECAPCI/MS.

2.3.10 Standard curves for Eicosanoid Quantification.

To quantify eicosanoids excreted in the medium, Eppendorf tubes containing 0.6 ml F12K medium were spiked with lipid standards, together with internal standards for ([$^{12}C_{20}$]-15-oxo-ETE, [$^{2}H_{8}$]-15(S)-HETE ,[$^{2}H_{4}$]-PGE_2 and [$^{2}H_{4}$]-13,14-dihydro-15-keto- PGE_2-PFB 1 ng each). To quantify eicosanoids in the cell lysate, lipids standards and internal standards mixture were spiked into 0.2 ml Tris-HCl buffer. The extraction and PFB derivatization methods are the same as mentioned above.

2.3.11 Analysis of 11-OEG adducts in LoVo cell lysate.

LoVo cells were grown to 90% confluence and then washed with PBS (10 ml). Cells were gently scraped in 600 µl Tris-HCl buffer (0.1 M, pH=7.9), containing protease inhibitor. Cell lysates were transferred to 2 ml Eppendorf tubes, and sonicated for 60 seconds on ice (power 5). 11-oxo-ETE (20 ng in ethanol) was added to the lysate together with 1 mM GSH. After incubation for 25 min at 37°C, 10 µl of 10% acetic acid was added, and the sample was loaded onto SPE column (oasis HLB, 30 mg) pre-conditioned with methanol and then 0.1% formic acid. The column was washed with 1 ml water and eluted with 250 µl methanol, and then 20 µl was analyzed by reverse phase LC-ESI/MS using gradient 3, as described above.

2.3.12 Conversion of 11-oxo-ETE and 15-oxo-ETE to 11(*S*)-HETE and 15(*S*)-HETE in Caco-2 cell lysate.

Caco-2 cell lysate was prepared in the same way as LoVo cell lysate, and then NADH (100 µM), NADPH (100 µM), 11-oxo-ETE (100 nM) and [$^{13}C_{20}$]-15-oxo-ETE (100 nM) were added. For the control sample, no oxo-ETEs were added. The mixtures were kept at 37 °C for 10 min before lipid extraction. The extraction and PFB derivatization procedures were the same as described above.

2.3.13 Cell proliferation assay.

BrdU incorporation in HUVECs was used to assess the effects of 11-oxo-ETE on cell proliferation. The BrdU assay was performed in a 96-well format using a commercially available colorimetric enzyme-linked immunosorbent assay (ELISA) kit (Roche), and also by immunofluorescence microscopy. Equal

numbers of HUVECs in passage 4 were plated in either, collagen-I coated 96-well plates (2000 cells/well), or collagen-I coated 8-chamber tissue culture glass slides (10000 cells/chamber). Cells were allowed to attach overnight in 0.25% DMSO containing media. Eicosanoids were dissolved in DMSO, such that the final concentration of DMSO in cell media was always 0.25% or lower. Cells were then treated for 24 h with either vehicle (0.25% DMSO), 11-oxo-ETE (1 nM-100 μM), or 15d-PGJ_2 (1 nM-100 μM). After 18 h of treatment, BrdU (final concentration, 10 μM in 0.25% DMSO) was added to each treatment group for an additional 6 h.

For the colorimetric ELISA, the manufacturer's protocol was followed to perform the assay. The absorbance at λ = 370 nm obtained from the assay was transformed to the cell numbers using a standard curve constructed by plating known number of HUVECs in triplicate. The IC_{50} values for eicosanoid inhibition of HUVEC proliferation were defined as the half maximal inhibitory concentration for endothelial cell proliferation over 24 h when compared with vehicle-treated cells. They were determined from the regression lines of the log inhibitor vs. response curves using a least squares fit.

For the immunofluorescence staining, cells were fixed with neutral buffered formalin for 10 min, permeabilized with methanol for 20 min, and then DNA was denatured by pressure cooking the slides in 10 mM citric acid buffer, pH 6 for 1 h. Cells were then incubated overnight with rat anti-BrdU antibody (1:1000, Accurate Chemical & Scientific Corp.) at 4°C, followed by 30 min incubation at 37 °C with Cy3-conjugated donkey anti-rat secondary antibody

(1:600, Jackson Immuno Research). Cells were counterstained with 4',6-diamidino-2-phenylindole (DAPI, Invitrogen) and visualized using a Nikon E600 microscope equipped with differential interference contrast (Nomarski) optics and photographed (x200 magnification) with a Fast 1394 QICam (QImaging). Positive BrdU staining was quantified by image analysis using IVision Analysis Software (Biovision). The percentage of proliferating cells was determined by counting the BrdU-positive cells versus the total number of cells in randomly selected microscopic fields (10/replicate) for each treatment group.

Statistical Analyses. All experiments were conducted in triplicate, unless otherwise indicated. Statistical significance (p value < 0.05) was determined using a two-tailed unpaired t-test employing GraphPad® Prism software (v 5.01).

2.4 RESULTS

2.4.1 Biosynthesis of 11-oxo-ETE by 15-PGDH.

Various concentrations of 11(*R*)-HETE were incubated with recombinant human 15-PGDH and NAD+ at 37 °C. A Michaelis-Menten kinetic analysis of 11-oxo-ETE formation revealed that the V_{max} (296 nmol/min/mg), K_m (3.42 μM), and k_{cat} (8.6 min^{-1}) values for oxidation of 11(*R*)-HETE (Figure 2.3) were similar to those for 15(*S)*-HETE (K_m = 1.65 μM, k_{cat} =8.6 min^{-1};). Therefore, the catalytic efficiency (Kcat/Km) for 15-PGDH-mediated oxidation of 11(*R*)-

HETE (2513 $min^{-1}mM^{-1}$, Figure 2.3) was similar to that for 15(*S*)-HETE (7091 $min^{-1}mM^{-1}$;).

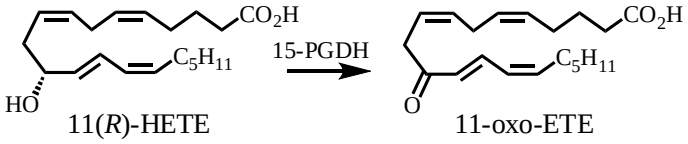

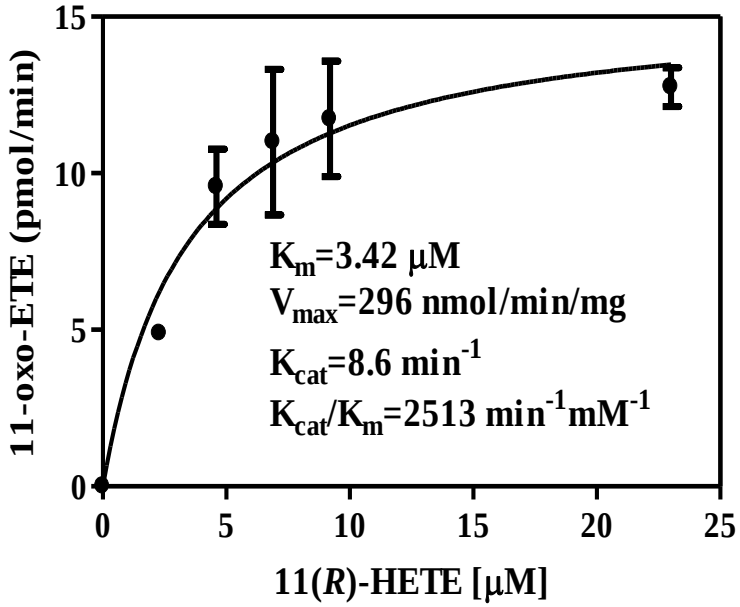

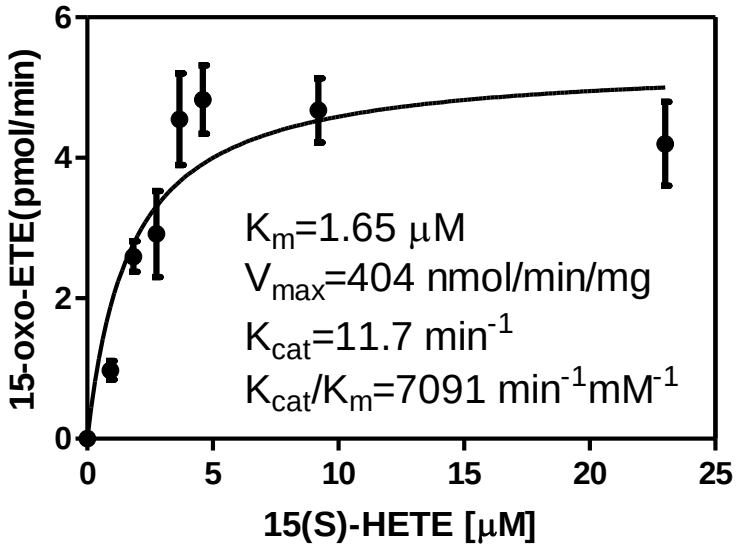

Figure 2.3. Kinetic plot of the formation of 11-oxo-ETE and 15-oxo-ETE by 15-PGDH. Various concentrations of 11(*R*)-HETE or 15(*S*)-HETE (0-23 μM) were incubated with 4 nM 15-PGDH and cofactor NAD+. Determinations for 11-oxo-ETE were conducted in triplicate (means ± S.E.M.) by stable isotope dilution LC-ESI/MS analyses.

2.4.2 Chemical Synthesis of Authentic 11-oxo-ETE.

11-Oxo-ETE was synthesized chemically by oxidizing racemic 11(*R,S*)-HETE using the Dess-Martin reagent, and then purified using chromatographic separation. A combined total of 10 mg of the racemic 11(*R,S*)-HETE resulted in the isolation of 4.9 mg of pure 11-oxo-ETE (overall yield of 49%). High resolution electrospray ionization-MS of 11-oxo-ETE revealed accurate masses of *m/z* 319.2263 and *m/z* 341.2079 for the protonated and sodiated molecules, respectively [calculated accurate mass for protonated ($C_{20}H_{31}O_3$) and sodiated ($C_{20}H_{30}O_3Na$) molecules, *m/z* 319.2273 and *m/z* 341.2093, respectively]. 500 MHz ^{1}H-NMR (δH, $CDCl_3$;) 7.55 (dd, J_1 = 11.5 Hz, J_2 =15.5, 1H), 6.21(d, J =15.5Hz, 1H), 6.15-6.11 (m, 1H), 5.97-5.92 (m, 1H), 5.60-5.58 (m, 2H), 5.41-5.38 (m, 2H), 3.35 (d, J =4.5Hz, 2H), 2.83-2.81 (m, 2H), 2.38-2.31 (m, 4H), 2.17-2.12 (m, 2H), 1.74-1.25 (m, 8H), 0.89 (t, J = 7.0 Hz, 3H). Analysis of purified 11-oxo-ETE as its PFB derivative by LC-ECAPCI/MS (Figure 2.5a) revealed an intense negative ion at *m/z* 317 corresponding to [M-PFB]$^-$. CID of [M-PFB]$^-$ (*m/z* 317) and MS/MS analysis revealed major product ions at *m/z* 273, 219, 165, 149, and 123. The UV spectrum was consistent with the presence of a conjugated dienone with a UV λ_{max} at 279 nm and molecular extinction coefficient (ε) of 18,985 $M^{-1}cm^{-1}$. The NMR spectrum data is shown in Figure 2.4.

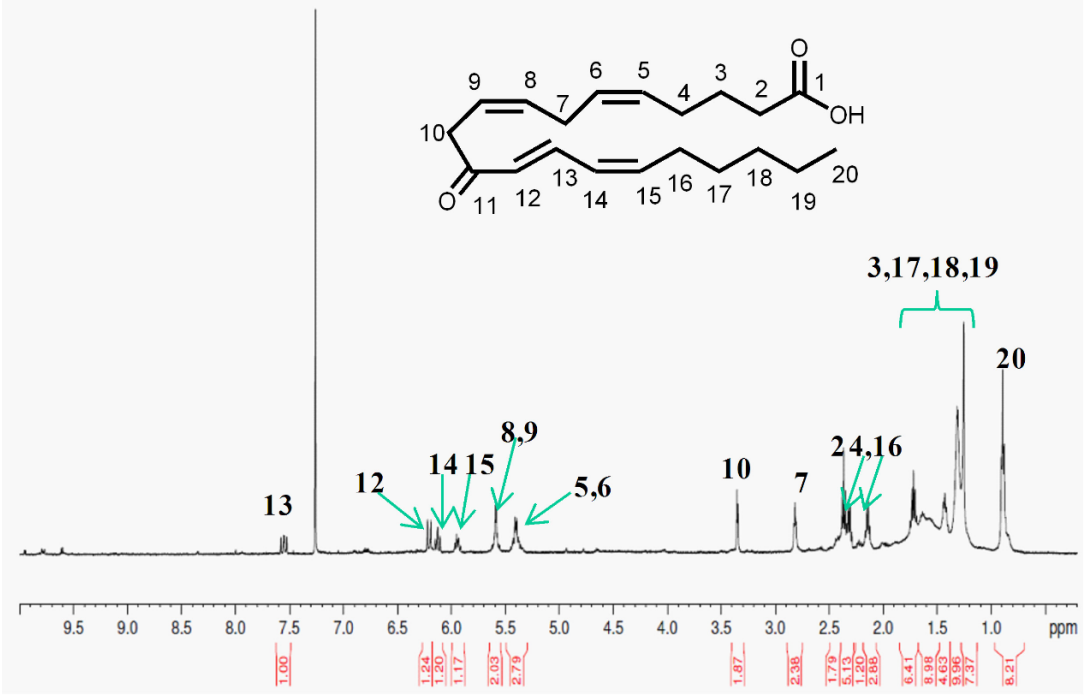

Figure 2.4 500 MHz ^{1}H NMR spectrum of 11-oxo-ETE in $CDCl_3$.

2.4.3 Confirmation of 11-oxo-ETE Identity by LC-MS and MS/MS Analyses.

The LoVo cell line is known to express both COX-2 and 15-PGDH and only trace amounts of COX-1,(52,60) this was confirmed by Western blot analysis (data not shown). Cell lysates were incubated with 100 nM 11(*R*)-HETE in the presence of 500 μM NAD^+ for 10 min. LC-MS analysis of PFB derivatives of eicosanoids extracted from the LoVo cell lysate showed that there was a single major metabolite, which eluted at 12.8 min (data not shown). The full scan mass spectrum of this metabolite had only one major ion at *m/z* 317 corresponding to $[M\text{-}PFB]^-$ (Figure 2.5b). CID and MS/MS analysis revealed the formation of intense product ions at *m/z* 123, 149, 165, 219, and 273 (Figure 2.5b). The product ion spectrum was identical with that obtained

from authentic synthetic 11-oxo-ETE-PFB (Figure 2.5a), which confirmed the identity of 11-oxo-ETE from LoVo cells. The product ion at *m/z* 165 in LoVo cell-derived and synthetic 11-oxo-ETE-PFB corresponded to cleavage between C-9 and C-10 and *m/z* 123 was formed from cleavage between C-11 and C-12 (Figure 2.5).

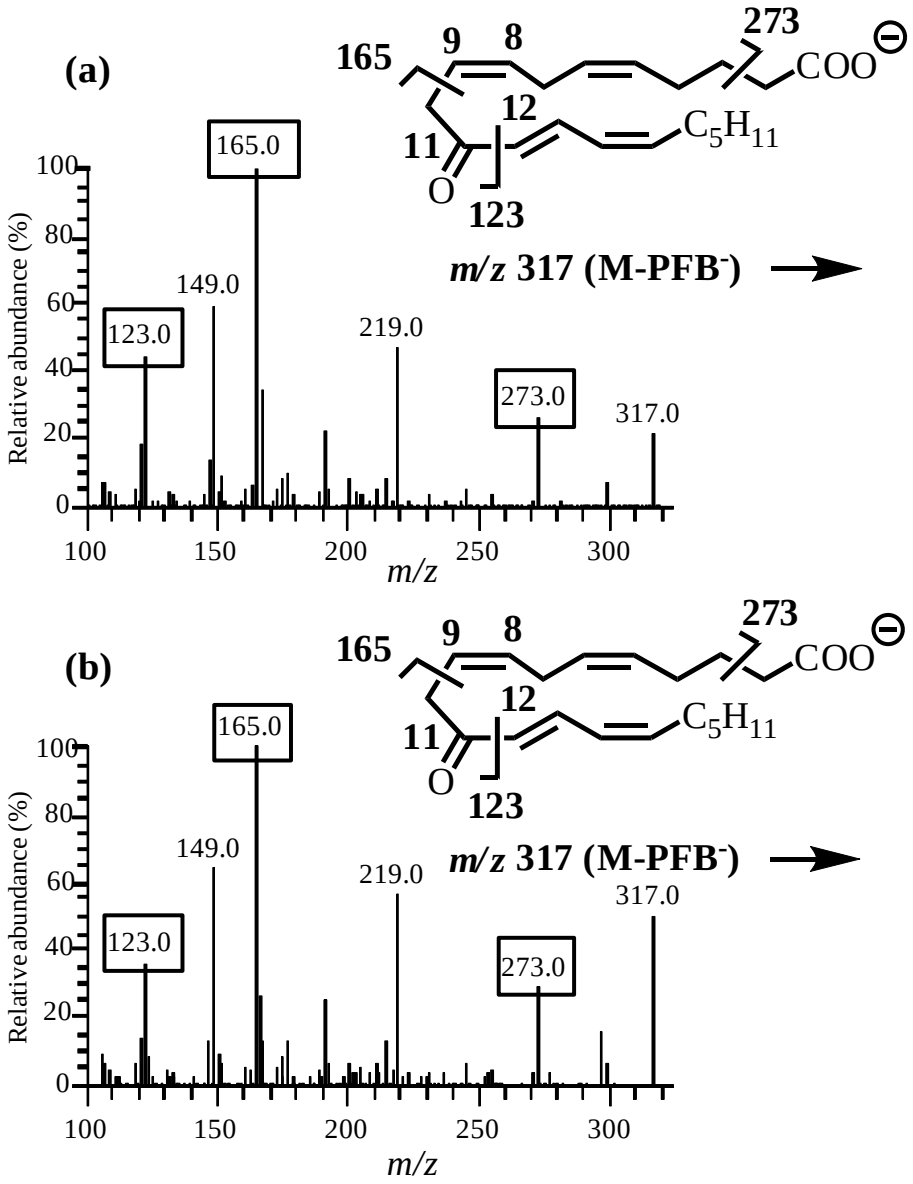

Figure 2.5. Confirmation of 11-oxo-ETE formation by LC-MS/MS analysis. Specific product ions observed by CID and MS/MS analysis of [M-

PFB]· (m/z 317), corresponding to 11-oxo-ETE are shown on the relevant chemical structures. (a) Synthetic 11-oxo-ETE-PFB standard; (b) 15-PGDH-derived 11-oxo-ETE-PFB from LoVo cell lysate to which 100 nM 11(*R*)-HETE had been added.

2.4.4 Separation of Eicosanoids by Chiral LC-ECAPCI/SRM/MS.

Lysates from LoVo cells were extracted for the eicosanoids, which were then analyzed (after PFB derivatization) by LC-ECAPCI/SRM/MS. A representative chromatogram (Figure 2.6) reveals the separation of 11-oxo-ETE (retention time 12.8 min) and 15-oxo-ETE (retention time 12.0 min) that were formed in the LoVo cell lysate. Additional eicosanoids that were observed (Figure 2.6) include, 13,14-dihydro-15-keto-PGE_2 (retention time, 33.6 min), 11(*R*)-HETE (retention time, 10.0 min), and PGE_2 (retention time, 29.4 min).

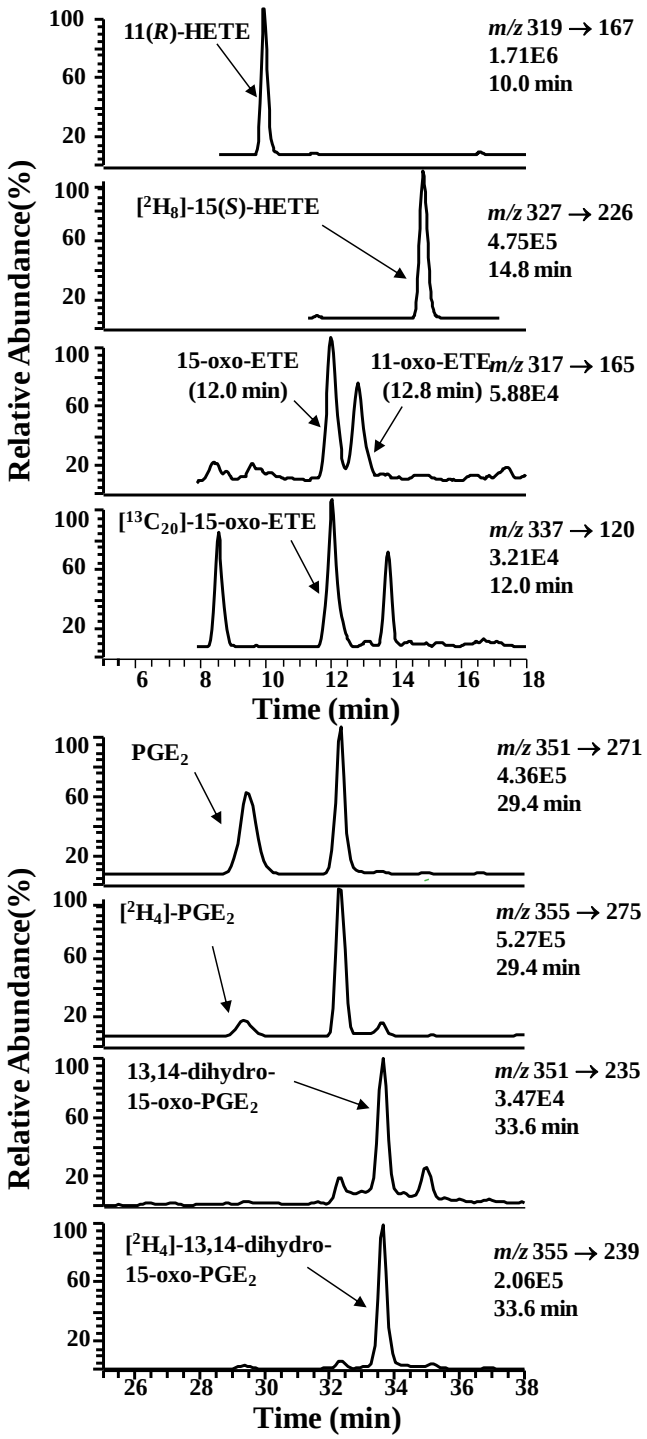

Figure 2.6. Targeted chiral lipidomics analysis of COX-2 derived eicosanoids from LoVo cells. LoVo cells were lysed; eicosanoids were extracted, derivatized with PFB bromide, and analyzed by LC-ECAPCI/SRM/MS. LoVo cell lysates were pre-treated with 50 μM CAY10397 to inhibit 15-PGDH to be able to detect the 11-, 15-HETEs and PGE_2.

Representative chromatograms are shown for (a) 11(*R*)-HETE-PFB (m/z319 →167), (b) [$^{2}H_{8}$]-15(*S*)-HETE-PFB internal standard (m/z 327→226), (c) 11-oxo-ETE-PFB (m/z 317→165), (c) 15-oxo-ETE-PFB (m/z 317→165), (d) [$^{13}C_{20}$]-15-oxo-ETE-PFB internal standard (m/z 337→120), (e) PGE_2-PFB (m/z 351→271), (f) [$^{2}H_{4}$]-PGE_2-PFB (m/z 355→275), (g) 13,14-dihydro-15-oxo-PGE_2-PFB (m/z 351→235), (h) [$^{2}H_{4}$]-13,14-dihydro-15-oxo-PGE_2-PFB (m/z 355→239).

2.4.5 Inhibition of 15-PGDH by CAY10397 in LoVo and HCA-7 cell lysates.

In contrast to LoVo cells, the HCA-7 cell line is known to express COX-2 and only trace amounts of COX-1 and 15-PGDH (*52, 71*). This was confirmed by Western blot analysis (data not shown). LoVo (Figure 2.7a) or HCA-7 (Figure 2.7b) cell lysates were incubated with 500 μM NAD+, with or without the 15-PGDH-inhibitor, CAY10397 (50 μM) for 10 min. Inhibition of 15-PGDH significantly abolished the formation of endogenous 11-oxo-ETE (Figure 2.7a) by 92%, along with the diminished formation of 15-oxo-ETE as well as 13,14-dihydro-15-oxo-PGE_2 (Figure 2.7a) in the LoVo cell lysate. However, since the oxo-ETEs and 13,14-dihydro-15-oxo-PGE_2 were undetectable in HCA-7 cell lysate, their precursors were quantified instead, and CAY10397 had no effect on their levels (Figure 2.7b).

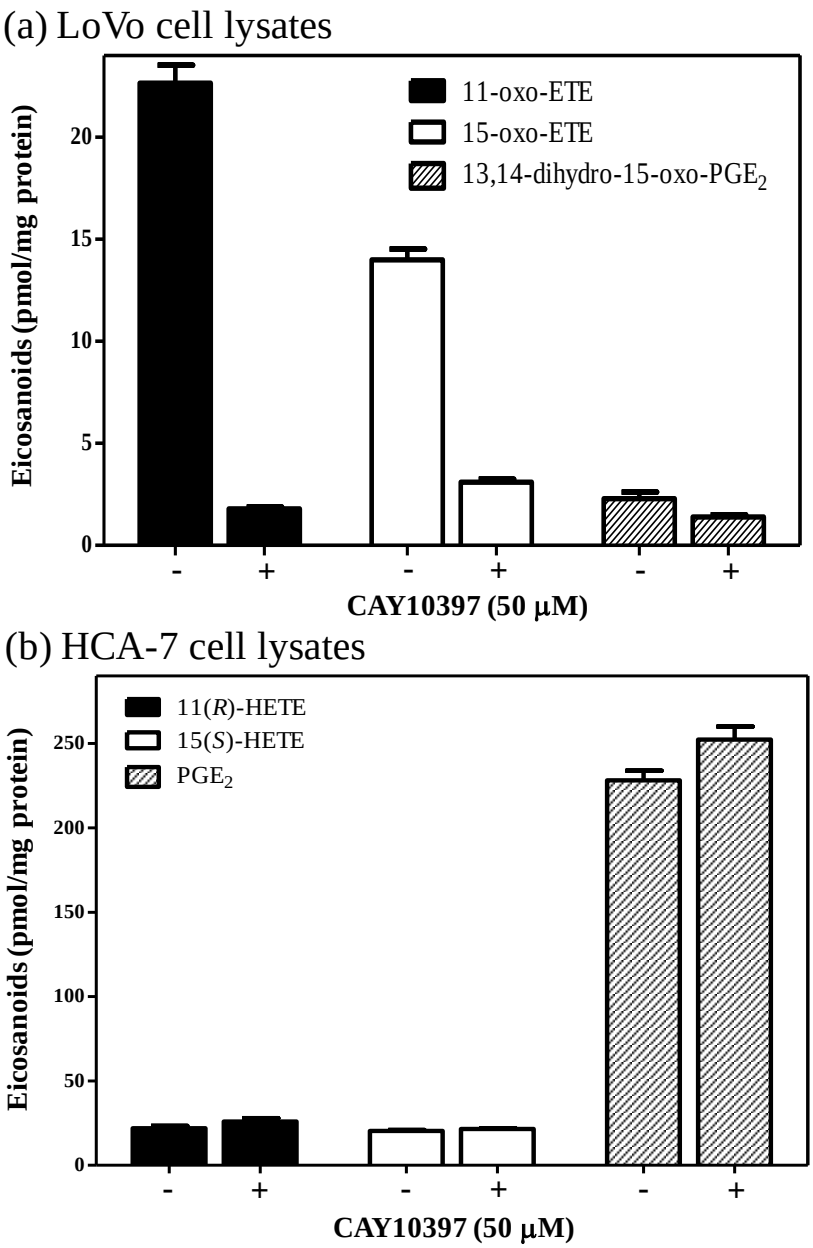

Figure2.7. Inhibition of 15-PGDH in LoVo and HCA-7 cell lysates by CAY10397. (a) LoVo or (b) HCA-7 cell lysate (1x106 cells/treatment group) was incubated with or without CAY10397 (50 μM, to inhibit 15-PGDH). Eicosanoids were extracted from the lysates and their levels were determined by chiral LC-ECAPCI/SRM/MS. Analyses were performed in triplicates, and error bars show S.E.M.

2.4.6 Secretion of eicosanoids from LoVo and HCA-7 cells following AA addition.

Time-course analyses for the amount of different eicosanoids secreted by LoVo and HCA-7 cells following AA incubation for 0-2.5 h are shown in Figure 2.8a and Figure 2.8b, respectively. 11-Oxo-ETE was secreted into the cell media by LoVo cells along with 15-oxo-ETE and 13,14-dihydro-15-oxo-PGE_2 (Figure 2.8a). Interestingly, both 11-oxo-ETE and 15-oxo-ETE reached maximum concentrations 10 min after the addition of AA to the cells. This was followed by a decline of both eicosanoids to steady-state levels after 2.5 h (Figure 2.8a) in LoVo cells. In contrast, 13,14-dihydro-15-oxo-PGE_2 levels did not peak until 1 h after the addition of AA (Figure 2.8a) and remained constant throughout the remainder of the incubation period. In contrast, none of the eicosanoids resulting from 15-PGDH-mediated metabolism were detected in the media of HCA-7 cells incubated with AA (Figure 2.8b).

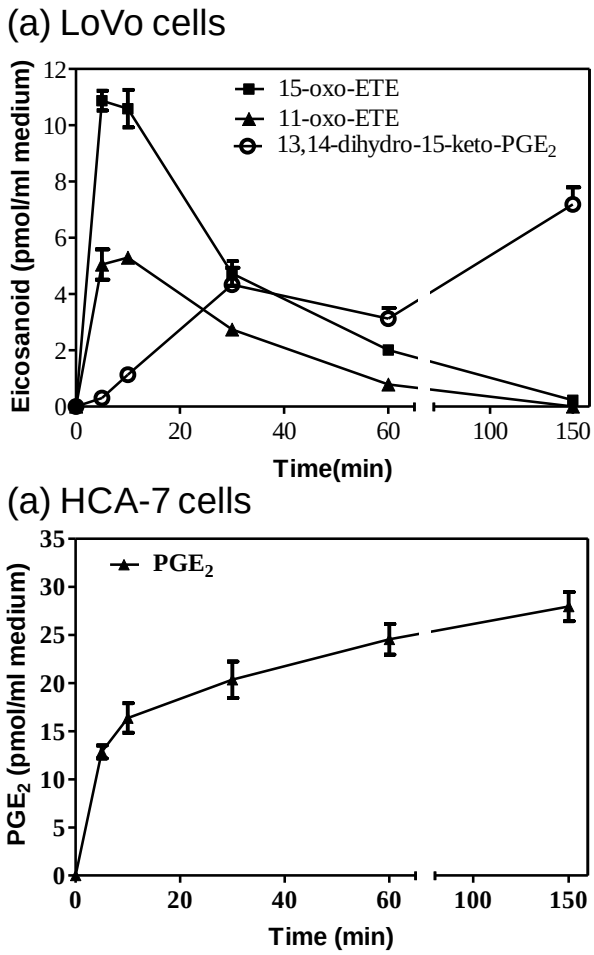

Figure 2.8. Time course for eicosanoids secreted from LoVo and HCA-7 cells following AA incubation. (a) LoVo or (b) HCA-7 cells were incubated with 10 μM AA for 0-6 h. The different eicosanoids secreted into the media at various time-points were extracted and their levels were determined by stable isotope dilution LC-ECAPCI/SRM/MS analysis of their PFB derivatives. Determinations were conducted in triplicate (means ± S.E.M.), and the quantitation was performed using the standard curves generated for these eicosanoids.

2.4.7 Formation of 11-OEG in LoVo Cell Lysates.

Biosynthesis of 11-OEG was monitored in the cell lysate after the addition of 100 nM 11-oxo-ETE and 1 mM GSH to the LoVo cell lysate. 11-OEG formation

was detected and confirmed by LC-MS/MS monitoring of the major metabolite formed after a 30 min incubation. OEG (retention time, 32.2 min, data not shown) was observed as an intense peak in the LC-ESI/MS chromatogram when analyzed by gradient 3 (as described above). CID and MS/MS analysis revealed the formation of intense product ions at *m/z* 497, 319, 308, and 179 (Figure 2.9).

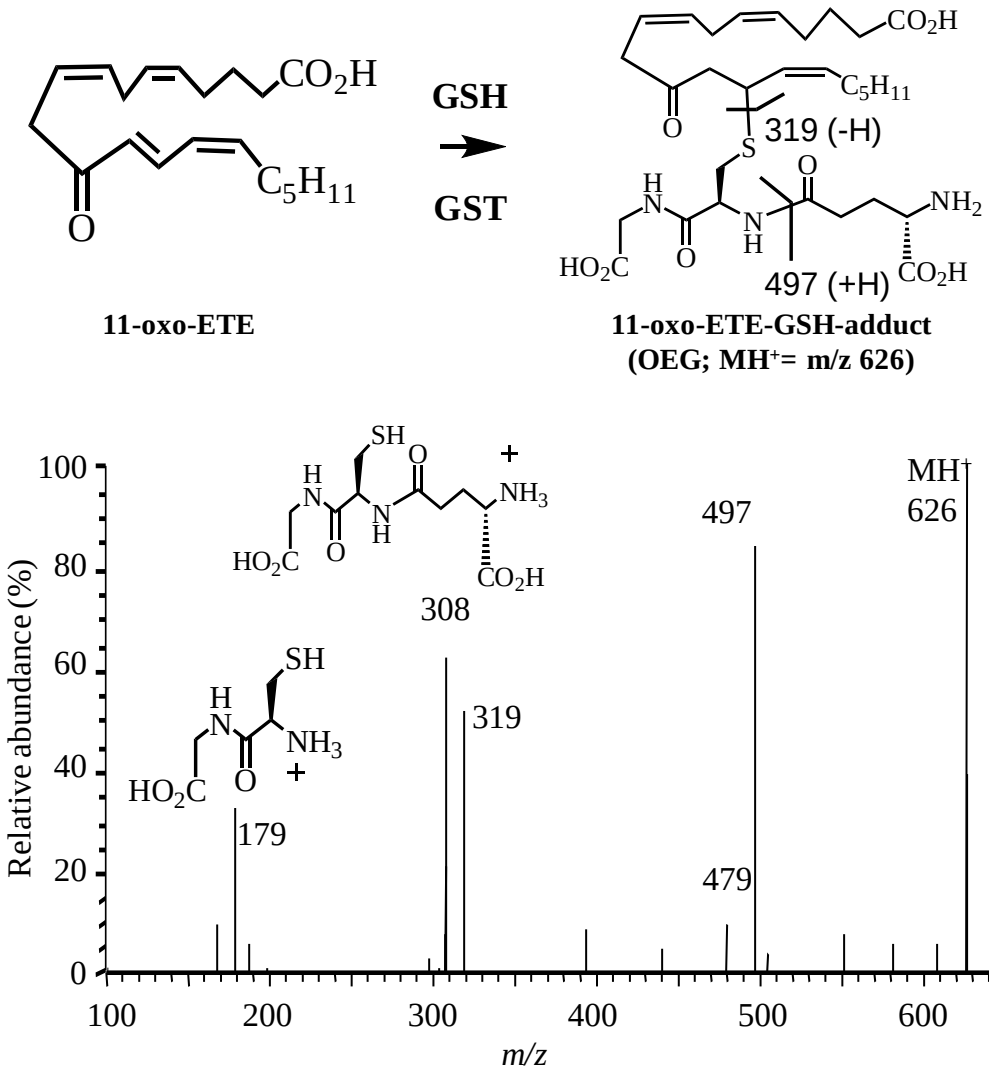

Figure 2.9. LC-MS/MS analysis of 11-OEG adduct. 11-OEG was synthesized by reacting 200 nM 11-oxo-ETE and 1 mM GSH in LoVo cell lysate for 25 min at 37°C. The product was extracted by solid-phase

extraction and analyzed by LC-ESI/MS/MS. Specific product ions observed by CID of [MH]+ (m/z 626) are shown with their relevant chemical structures in the MS/MS analysis of 11-OEG.

2.4.8 Conversion of 11-oxo-ETE and 15-oxo-ETE to 11(*S*)-HETE and 15(*S*)-HETE in Caco-2 cell lysate.

Besides detoxification by GST/GSH pathway, oxo-ETEs can also be reduced to their alcohol form. This biotransformation was tested in Caco-2 cells by adding exogenous 11-oxo-ETE and [$^{13}C_{20}$]-15-oxo-ETE to the cells lysate, together with potential cofactor NADH/NADPH. After analyzing the eicosanoids in the lysate, the formation of 11(*S*)-HETE and [$^{13}C_{20}$]-15(*S*)-HETE was observed. The data are shown in Figure2.10.

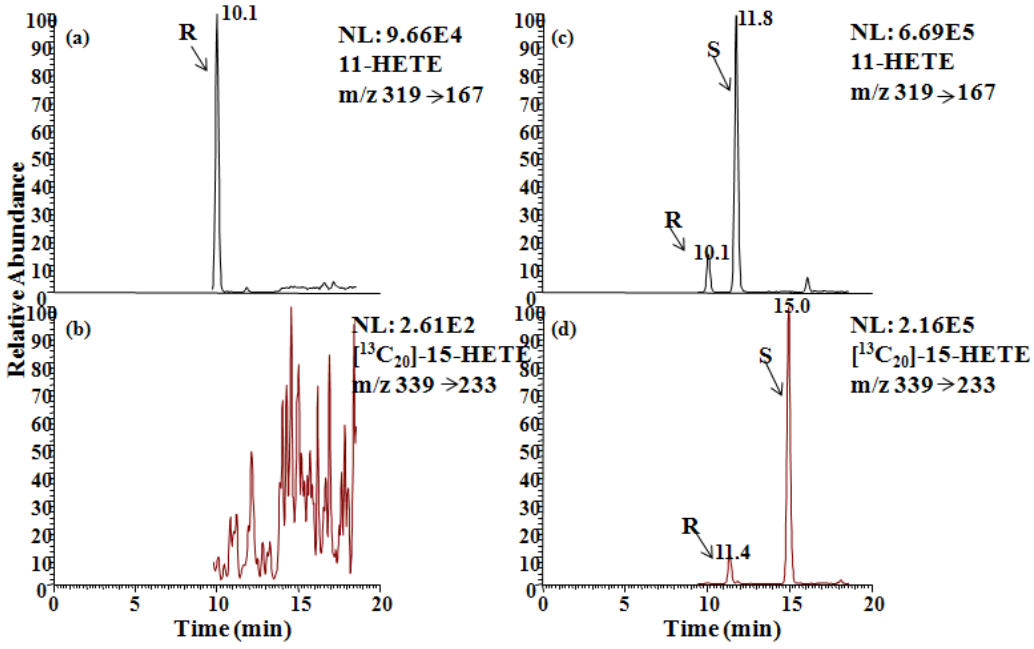

Figure 2.10 Reduction of 11-oxo-ETE and [$^{13}C_{20}$]-15-oxo-ETE to 11(*S*)-HETE and [$^{13}C_{20}$]-15(*S*)-HETE in Caco-2 cell line. Figure2.10(a) and 2.10(b) show the basal level of 11-HETE and [$^{13}C_{20}$]-15(*S*)-HETE in Caco-2 cell lysate, while 2.10(c) and 2.10(d) represent the formation of 11(*S*)-HETE and [$^{13}C_{20}$]-15(*S*)-HETE after treating Caco-2 cell lysate with 100 nM 11-oxo-ETE and [$^{13}C_{20}$]-15(*S*)-HETE for 10 min at 37 °C. 11-HETE was monitored as PFB derivative in negative mode by SRM m/z 319→167, while [$^{13}C_{20}$]-15(*S*)-HETE was monitored by 339→233. The peak in 9(a) and (c) at 10.1 min is corresponding to 11(*R*)-HETE, while 11.8 min is 11(*S*)-HETE. The retention time of [$^{13}C_{20}$]-15(*R*)-HETE is 11.4 min, while its (S) form is 15.0 min.

2.4.9 Effects of Eicosanoids on HUVEC Proliferation.

Proliferation by HUVECs was assessed by quantifying the BrdU incorporation into the cells actively synthesizing new DNA. The BrdU assay was performed using a quantitative colorimetric 96-well format ELISA as well as by immunofluorescence microscopy for observing the morphological effects of eicosanoids in HUVECs. For the BrdU ELISA, HUVECs (2000 cells/well) were treated with different doses (0-100 μM) of 11-oxo-ETE and 15d-PGJ_2 for a period of 24h. The cell numbers corresponding to each treatment dose were computed and used to calculate cell proliferation (%) as compared to the vehicle-treated controls. 11-Oxo-ETE (IC_{50} = 2.1 μM) was equipotent with 15d-PGJ_2 (IC_{50} = 2.3 μM), a known potent inhibitor of endothelial cell proliferation (Figure 2.11a). For the immunofluorescence analysis, HUVECs (8000 cells/chamber) were treated with 2 μM of either 11-oxo-ETE or 15d-PGJ_2 for 24 h. BrdU incorporation was assessed by counting the BrdU-positive cells as compared to the total number of cells counted in randomly selected microscopic fields (10 fields/treatment). The photomicrographs

clearly show that treatment with 11-oxo-ETE as well as 15d-PGJ_2 remarkably reduced the total number of BrdU-positive cells (stained red) as compared to vehicle-treated controls (Figure 2.11b). Moreover, there was a distinct change in the morphological appearance of the DAPI-stained (stained blue) cells in the eicosanoid-treated slides that failed to incorporate BrdU (Figure 2.11b).

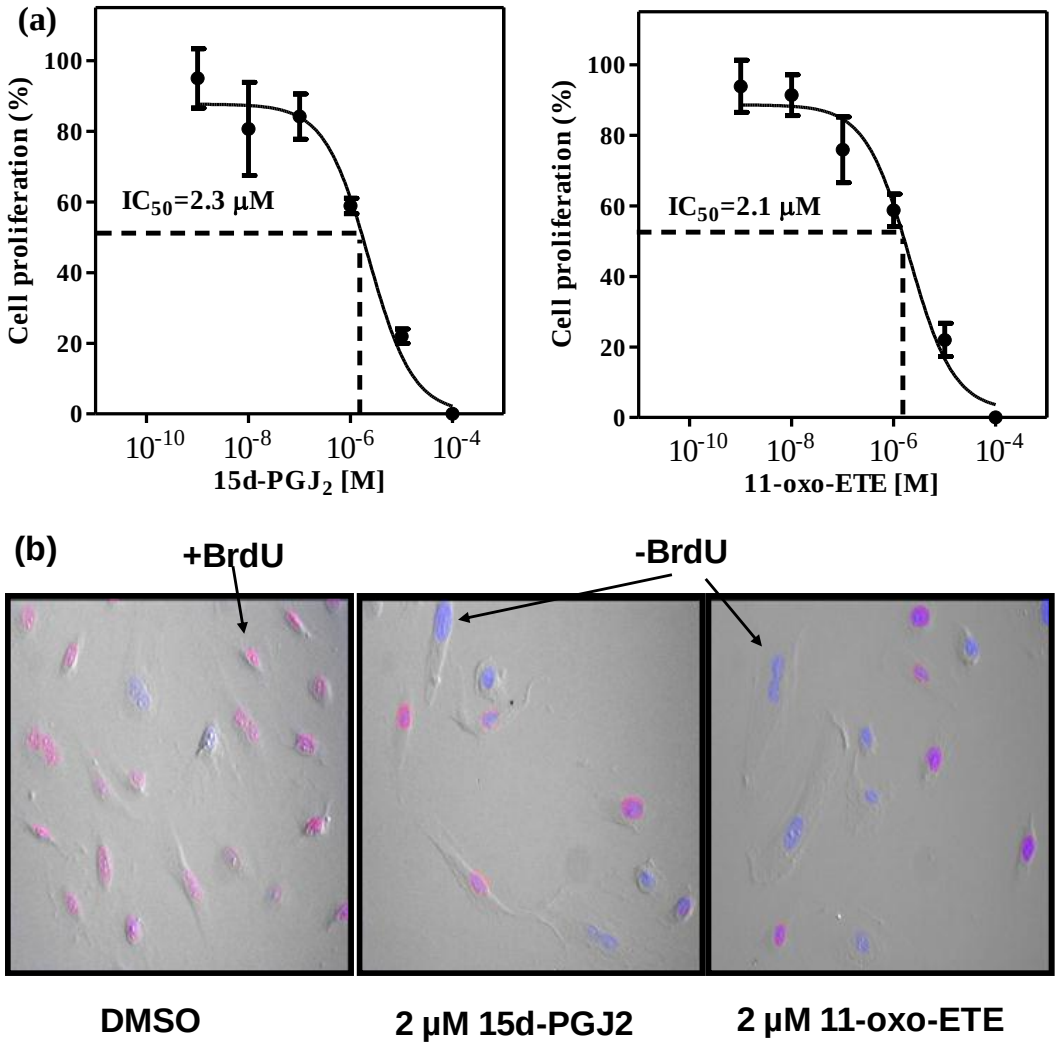

Figure 2.11. Effect of eicosanoids on cell proliferation of HUVECs. (a) For BrdU ELISA, HUVECs (2000 cells/well) were treated with various doses of 11-oxo-ETE and 15d-PGJ_2 for a period of 24 h. Cell proliferation (means +

S.E.M.) was assessed by measuring absorbance at 370 nm and converting it to cell numbers using a standard curve and thereby used to construct the IC_{50} plots. All experiments were conducted three times in triplicate. Representative data from one experiment conducted in triplicate are shown as means ± S.E.M. (b) For immunofluorescence, HUVECs (8000/chamber) were treated with 2 μM of 15d-PGJ_2 or 11-oxo-ETE for 24 h and then stained for BrdU and counterstained with DAPI (cells stained blue). Photomicrographs were taken at x200 magnification, and BrdU-positive (stained purple) cells were counted in randomly selected microscopic fields (10/replicate) as compared to the total number of cells in these fields. All experiments were conducted in triplicate. Representative photomicrographs from one set of replicates are shown.

2.5 DISCUSSION

15-PGDH catalyzes NAD^+-mediated oxidation of the 15(*S*)-hydroxyl moiety of PGs and other eicosanoids (Figure 2.1) (*52, 58, 68*). Previous studies had established that 15-PGDH is also responsible for metabolizing the 15-LOX-derived 15(*S*)-HETE in macrophages and monocytes to 15-oxo-ETE (*68*). Surprisingly, it was found that 11(*R*)-HETE is also metabolized by 15-PGDH to a novel eicosanoid, that was identified as 11-oxo-ETE (Figure 2.3). Moreover, the catalytic activity of human 15-PGDH for oxidation of 11(*R*)-HETE (Figure 2.3) was very similar to that observed for 15(*S*)-HETE. These results were very surprising in view of the lack of a 15(*S*)-hydroxyl group on 11(*R*)-HETE as well as the incorrect 11(*R*)-stereochemistry. The structure of 11-oxo-ETE metabolite was established by chemically synthesizing authentic 11-oxo-ETE from racemic 11-HETE. 11-Oxo-ETE was formed in both LoVo cell lysates (Figure 2.7a) and secreted from intact cells (Figure 2.8a); whereas 11-oxo-ETE was not formed by HCA-7 cell lysates (Figure 2.7b) or

secreted from intact cells (Figure 2.8b). Since LoVo cells express COX-2 as well as 15-PGDH, whereas HCA-7 cells express COX-2 but not 15-PGDH (*52, 70*, *71*), these data convincingly prove that 11-oxo-ETE is an endogenous product formed enzymatically by a combination of COX-2 and 15-PGDH.

11-oxo-ETE is isomeric with 15-oxo-ETE (Figure 2.2) and also has very similar LC properties. Therefore, a reversed phase LC-SRM/MS method was developed to separate the un-derivatized oxo-ETEs, and normal phase was implemented to separate their PFB derivatives. This made it possible to readily analyze the two oxo-ETEs. Endogenous eicosanoids formed by LoVo and HCA-7 epithelial cells and cell lysates as well as those formed after the addition of AA were analyzed as PFB derivatives by chiral LC-ECAPCI/MS (*72, 73*). Representative chromatograms of the eicosanoids produced endogenously in the LoVo cell lysates are shown in Figure 2.6. Inhibition of 15-PGDH enzyme by CAY10397 significantly diminished the formation of endogenous 11-oxo-ETE in LoVo cell lysates (Figure 2.7a). In addition, the formation of 15-oxo-ETE as well as 13,14-dihydro-15-oxo-PGE_2, the other two 15-PGDH-dependent metabolites, were also significantly reduced in LoVo cell lysates treated with CAY10397 (Figure 2.7a). In contrast, the three 15-PGDH products, namely, 11-, 15-oxo-ETE and 13,14-dihydro-15-oxo-PGE_2, were undetectable in HCA-7 cells as these cells do not express any 15-PGDH (*52, 70*). Instead, the corresponding precursors for these three metabolites were observed in the lysates. Furthermore, treatment with CAY10397 had no effect on levels of 11(*R*)-HETE, 15(*S*)-HETE or PGE_2 (Figure 2.7b). Intact LoVo cells also secreted 11-oxo-ETE, 15-oxo-ETE as well as 13,14-dihydro-

15-oxo-PGE_2. However, the 11-oxo-ETE was cleared very rapidly (Figure 2.8a), suggesting that further metabolism was occurring. Subsequently, it was observed that 11-oxo-ETE underwent GST-mediated metabolism to 11-OEG, similar to the formation of 15-OEG in RIES cells (Figure 2.9) (*43*). Moreover, it was observed that 11-oxo-ETE and [$^{13}C_{20}$]-15-oxo-ETE could be converted to 11(*S*)-HETE and [$^{13}C_{20}$]-15(*S*)-HETE in the Caco-2 cell line, which does not express 15-PGDH. Therefore, a reductive pathway could be responsible for the formation of endogenous 11(*S*)-HETE.

11-Oxo-ETE differs from 15d-PGJ_2 in the lack of a C-8 to C-12 bond, in having a *cis*-8,9- rather than *cis*-9,10-double bond, and a *cis*- rather than *trans*-14,15-double bond (Figure 2.2). This suggested that 11-oxo-ETE might be a more effective inhibitor of HUVEC proliferation than 15-oxo-ETE (*68*) with a potency similar to that observed for 15d-PGJ_2 (*61*). In fact, 11-oxo-ETE was six times more potent than 15-oxo-ETE (data not shown) and equipotent with 15d-PGJ_2 at inhibition of HUVEC proliferation (Figure 2.10). Dose-response studies revealed that its IC_{50} was 2.1 μM compared to an IC_{50} value of 2.3 μM for 15d-PGJ_2 (Figure 2.10a). Moreover, immunofluorescence microscopy revealed that 11-oxo-ETE not only inhibited BrdU incorporation into the HUVECs but it also caused a dramatic change in the shape and morphology of these cells (Figure 2.10b). Although the total number of cells counted in the eicosanoid-treated groups were quite similar to the vehicle-treated group, the BrdU-negative cells were significantly distorted (Figure 2.10b). Typically, if the cells are undergoing death by apoptosis, they would appear more compact and round. However, 11-oxo-treated cells were

elongated and stretched (Figure 2.10b), which could be indicative of extensive cytoskeletal remodeling, cell cycle arrest and/or differentiation. Interestingly, 11-oxo-ETE formation could not be detected in HUVEC lysate that was incubated with 11(*R*)-HETE (data not shown). Finally, immunoblot analysis of HUVEC cell lysate failed to detect COX-2 protein (data not shown). Taken together, these data suggest a paracrine role for 11-oxo-ETE on endothelial cell proliferation.

As noted above, inhibition of 15-PGDH resulted in significant decreases in 11-oxo-ETE formation in LoVo cells (Figure 2.7). 15-PGDH is down-regulated in numerous cancers types (*49, 52-56*), which would cause a decrease in 11-oxo-ETE biosynthesis by preventing the *in vivo* conversion of 11(*R*)-HETE to 11-oxo-ETE (Figure 2.1). This could be particularly devastating as COX-2 becomes up-regulated during tumorigenesis, which would result in elevated PGE_2 biosynthesis along with decreased 15-PGDH-mediated inactivation to 15-oxo-PGE_2 (Figure 2.1). Ultimately, this would result in an increase in PGE_2-mediated pro-proliferative activity (*48,57*) without the counter effect of anti-proliferative oxo-ETEs. Increased PGE_2 activity can also arise through down-regulation of the influx PG transporter - the organic anion transporter polypeptide (OATP) 2A1 (Figure 2.1) (*74,75*).

There is some evidence that 11-oxo-ETE can activate nuclear PPARγ.(*76*) PPARγ is a ligand-dependent transcription factor responsible for the regulation of a number of cellular events ranging from lipid metabolism to apoptosis.(*77*) 15d-PGJ_2 is a PPARγ agonist, which might account for its

ability to inhibit endothelial cell proliferation (*60,61*). However, this effect is only observed with pharmacological amounts of 15d-PGJ_2 rather than endogenous concentrations (*69*). Besides PPARγ agonistic activity, 15d-PGJ_2 is also known to be an inhibitor of NFκB signaling, a pathway critical to cell proliferation as well as tumorigenesis (*78,79*). In view of the ability of COX-2/15-PGDH to rapidly metabolize AA to nM amounts of oxo-ETEs, together with the structural similarity of oxo-ETEs and 15d-PGJ_2 (Figure 2.2), it will be important to determine which of these activities are shared by both classes of eicosanoids. It is noteworthy that docosahexaenoic acid and docosapentaenoic acid can be metabolized by the sequential action of COX-2 and dehydrogenises into oxo-eicosanoids that modulate the antioxidant response (*21*). Similarly 5-LOX-drived 5(*S*)-HETE is metabolized by 5-hydroxyeicosanoid dehydrogenase into the chemoattractant 5-oxo-ETE (*80*). Therefore, the oxo-eicosanoids represent a family of oxidized lipids with diverse biological activities.

In summary, these studies have revealed that down-regulation of 15-PGDH inhibits the formation of the endogenous anti-proliferative eicosanoid, 11-oxo-ETE. Therefore, 15-PGDH has two quite distinct properties; it can either inactivate PGs or activate HETEs to oxo-ETEs that exert a paracrine effect on endothelial cells (Figure 2.1). 11-Oxo-ETE, a member of the oxo-ETE family (*80-82*), was observed previously as an endogenously-derived lipid in human atherosclerotic plaques (*83*). However, the biosynthesis of 11-oxo-ETE and its biological activity were not evaluated in that study. Furthermore, there does not appear to be any subsequent report of its formation either, *in vitro*

or *in vivo*. In fact 11-oxo-ETE is derived from COX-2/15-PGDH-mediated AA metabolism and it inhibits endothelial cell proliferation with an IC_{50} that is very similar to that of 15d-PGJ_2.

Chapter 3 Cyclooxygenase-2-mediated reactive aldehyde formation

3.1 ABSTRACT

HNE and ONE are major products of lipid. These bifunctional electrophiles have many biological effects, which is probably due in part to their high reactivity with endogenous nucleophiles, such as glutathione, proteins and DNA. HNE has a chiral center at C4. Some recent research has revealed that the chirality of HNE is significant since its two enantiomers differ in their ability to damage proteins and undergo detoxification. Thus, it is important to study the formation of HNE with respect to chirality. In order to accomplish this goal, HNE was analyzed as its GSH-adduct form, which allowed increased detection sensitivity. It was found that in the presence of GSH, PGG_2 and 15(S)-HPETE mainly produced 4(*S*)-HNE-GSH. In contrast 11(*R*)-HPETE produced racemic HNE-GSH while 15(*R*)-HPETE produced 4(*R*)-HNE-GSH. This new finding that HNE formed from different lipid hydroperoxides possessing different chiral characteristics suggested a new decomposition mechanism for lipid hydroperoxides. Interestingly, it was observed that 4(*S*)-HNE-GSH was the predominant isomer arising from incubations of recombinant COX-2 with AA in the presence of GSH. However, with aspirin-modified COX-2, 4(*R*)-HNE-GSH was the major product. This observation is in keeping with the known activity of aspirin, which converts COX-2 into a

15(*R*)-LOX and produces mainly 15(*R*)-HPETE. Human colorectal adenocarcinoma (LoVo) epithelial cells, which over-expressed COX-2, also mainly generated 4(*S*)-HNE-GSH (86%) in the cell lysate when they were treated with AA. This result together with the eicosanoid quantification assay showed that in LoVo cells, HNE and ONE were formed mainly from PGG_2 and not from the HPETEs as has been previously thought. ONE formed on nuclear membranes can covalently modify DNA due to its close proximity, resulting in mutagenic DNA adducts, such as heptano-etheno-2'-deoxyguanosine (H-εdGuo).

3.2 INTRODUCTION

PGG_2 (Figure 1.1) has been implicated in many inflammatory diseases, since PGG_2 is the precursor of pro-inflammatory prostaglandins. However, before PGG_2 is converted to PGH_2, PGE_2 and other PGs, it could also undergo decomposition to malondialdehyde (MDA), together with HNE, and ONE have been characterized as cytotoxic and genotoxic lipid peroxidation products (32). MDA forms Schiff-base adducts with proteins or DNA bases, while HNE and ONE form adducts through Michael addition (32). When MDA is at physiological pH, it exists mainly in the enolate form, which has lower reactivity compared to HNE and ONE. HNE formation has been implicated as a reactive intermediate in many diseases, such as atherosclerosis, Alzheimer's disease, diabetes and Parkinson's disease *(84-86)*. HNE has one chiral center and different strategies have been applied to study HNE

enantiomers, including chiral LC-UV, LC-MS, NMR, fluorescence, as well as anti-HNE antibody methods *(87-91)*. The Uchida group has studied the nature of HNE enantiomers selectively and differentially binding to proteins *(91, 92)*, while the Picklo group showed that HNE detoxification by GST or AKR is also stereoselective *(93, 94)*. Furthermore, the Brash group has demonstrated that 4(*S)*-HNE is formed with high enantioselectivity from the decomposition of 15(*S*)-HPETE *(89)*. It was established that in LoVo cells, PGs were the major COX-2 mediated arachidonic acid metabolites *(95)*. Therefore, this provided an excellent model system to examine the mechanism of formation of COX-2-derived HNE (Figure 1.1) and ONE. This would then make it possible to definitively identify the source of ONE-derived DNA-adducts such as H-εdGuo.

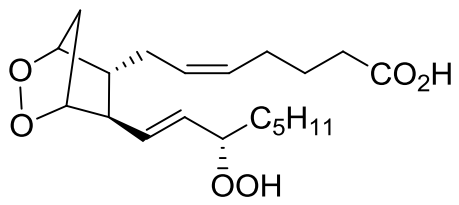

PGG$_2$

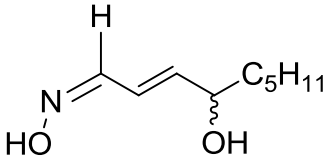

4(*R,S*)-HNE-oxime

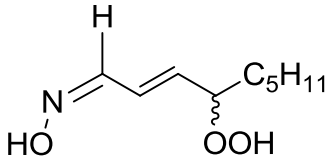

4(*R,S*)-HPNE-oxime

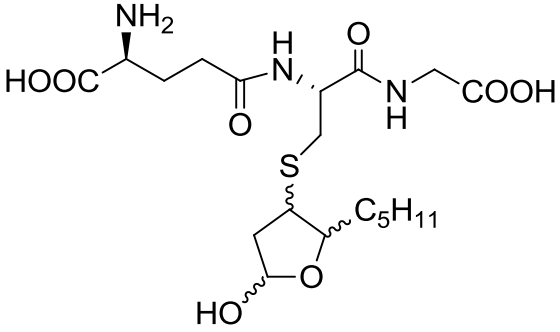

HNE-GSH adduct

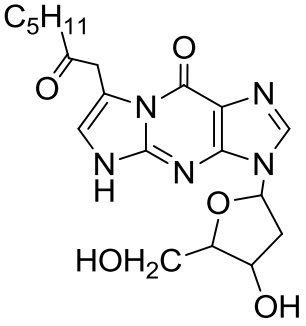

H-εdG

Figure 3.1 Structures of PGE_2, HNE-oxime, HNE-GSH-adducts and H-εdGuo.

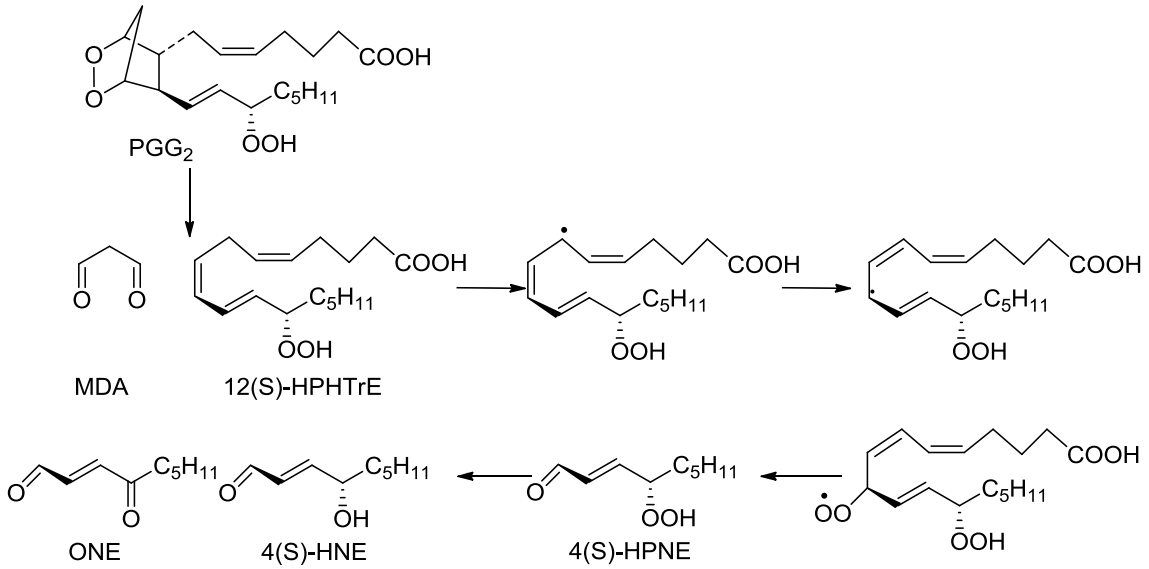

Figure 3.2. The proposed mechanism of the transformation of PGG_2 into HNE and ONE. There might be an intermediate hydroperoxide, 12(*S*)-HPTrE, which is formed together with MDA from PGG_2 decomposition. The hydrogen attached to C7 is abstracted, followed by the formation of a carbon-centered radical at C7, and then the double bond between C8 and C9 relocates to C7 and C8, together with the relocation of C7 radical to C9 radical. A hydroperoxide radical is formed after an oxygen molecule radical to C9 radical. A hydroperoxide radical is formed after an oxygen molecule inserts to C9 position, followed by hock rearrangement and the formation of 4(*S*)-HPNE. The 4(*S*)-HPNE is then converted to 4(*S*)-HNE and ONE.

3.3 EXPERIMENTAL PROCEDURES

3.3.1 Chemicals and Reagents.

AA (peroxide-free), 11(*R,S*)-HETE, 15(*R,S*)-HETE, [$^2H_8$]-15(*S*)-HETE, [$^2H_8$]-12(*S*)-HETE, 12(*S*)-HHT, PGE_2, [$^2H_4$]-PGE_2, $PGF_{2\alpha}$, [$^2H_4$]-$PGF_{2\alpha}$, [$^2H_3$]-4-HNE,

PGG_2, protease inhibitor cocktail (100X), recombinant ovine COX-1 and human COX-2 were purchased from Cayman (Ann Harbor, MI). 2,3,4,5,6-pentafluorobenzyl (PFB) bromide, Trizma-HCl, ethacrynic acid, hematin porcine, hydroxylamine hydrochloride, L-glutathione, phenol, L-ascorbic acid, zopolrestat, 2'-deoxyguanosine monohydrate and lipoxidase from *Glycine max* (soybean) were purchased from Sigma-Aldrich (St. Louis, MO). Rofecoxib was purchased from Sequoia Research Products (UK). Fetal bovine serum (FBS) was from Gemini Bioproducts (West Sacramento, CA). F12K medium, D-glucose, L-glutamine, penicillin, and streptomycin were supplied by Invitrogen (Carlsbad, CA). LC-MS grade water, hexane, methanol, isopropanol, acetonitrile and dichloromethane were obtained from Fisher Scientific (Pittsburgh, PA). Gases were supplied by The Linde Group (Munich, Germany).

3.3.2 Cell Culture.

LoVo cells (ATCC, Manassas, VA) were cultured in F12K medium supplemented with 10% FBS, 2 mM L-glutamine, 100,000 units/l penicillin and 100 mg/l streptomycin.

3.3.3 MS conditions.

A triple stage quadrupole (TSQ Quantum) mass spectrometer (Thermo Electron, San Jose, CA) equipped with an APCI source was used for the quantitative lipidomics analyses. Targeted chiral LC-ECAPCI/SRM/MS analysis was conducted using PFB derivatives of 7 lipids and 4 heavy isotope analog internal standards. For the lipidomics profile, the instrument was operated in

the negative ion mode, and unit resolution was maintained for both precursor and fragment ions. Operating conditions for the TSQ Quantum were: vaporizer temperature at 450°C; heated capillary temperature at 250 °C with the corona discharge needle set at 30 μA; nitrogen as sheath (25 psi) and auxiliary (5 arbitrary units) gas. Collision-induced dissociation (CID) was performed using argon as the collision gas at 1.5 mtorr in the RF-only quadrupole. The following SRM transitions were used: 11(*R*)-HETE-PFB, *m/z* 319 → 167 (CE, 16 eV), 15-HETE-PFB, *m/z* 327 → 226 (CE, 13 eV), 12(*S*)-HHT-PFB, *m/z* 279 → 217 (CE, 18 eV), [$^2H_8$]-15(*S*)-HETE-PFB, *m/z* 327 → 226 (CE, 13 eV), [$^2H_8$]-12(S)-HETE-PFB, *m/z* 327 → 184(CE, 14 eV), PGE_2-PFB, *m/z* 351 → 271 (CE, 18 eV), [$^2H_4$]-PGE_2-PFB, *m/z* 355 → 275 (CE, 18 eV), PGD_2-PFB, *m/z* 351 → 271 (CE, 18 eV), [$^2H_4$]-PGD_2-PFB, *m/z* 355 → 275 (CE, 18 eV), $PGF_{2\alpha}$-PFB, m/z 353→ 193 (CE, 25 eV), [$^2H_4$]- $PGF_{2\alpha}$-PFB, m/z 357→ 197(CE, 25 eV).

For oxime derivatives analysis, the Finnigan LTQ mass spectrometer (Thermo Electron, San Jose, CA) was used in the positive ion mode with an electrospray ionization (ESI) source. The operating conditions were: spray voltage at 4 kV; capillary temperature at 250 °C; capillary voltage at 35 V; nitrogen as sheath (40 psi) and auxiliary (20 arbitrary units) gas. CID was performed using helium as the collision gas in the ion trap. The following SRM transition (m/z 188 → 154) was monitored for HPNE-oxime (normalized CE, 25 %), and SRM transition (m/z 172 → 99) was monitored for HNE-oxime (normalized CE, 25%).

For GSH adduct analysis, the TSQ Quantum was operated in the positive ion mode with an ESI source. The operating conditions were: spray voltage at 4 kV; capillary temperature at 350°C; nitrogen as sheath (35 psi) and auxiliary (13 arbitrary units) gas. CID was performed using argon as the collision gas at 1.5 mtorr in the Rf-only quadrupole. The following SRM transition (m/z 464 → 308) was monitored for HNE-GSH (CE, 14 eV).

For H-εdGuo analysis, the TSQ Quantum was operated in the positive ion mode with an ESI source. The operating conditions were: spray voltage at 4 kV; capillary temperature at 320°C; nitrogen as sheath (25 psi) and auxiliary (10 arbitrary units) gas. CID was performed using argon as the collision gas at 1.5 mtorr in the Rf-only quadrupole. The following SRM transition (m/z 404 → 288) was monitored for H-εdGuo (CE, 18 eV).

3.3.4 LC methods.

LC separations were conducted using a Waters Alliance 2690 HPLC system (Waters Corp., Milford, MA, USA). A Chiralpak AD-H column (250 × 4.6 mm inner diameter, 5 μm; Daicel Chemical Industries, Ltd., Tokyo, Japan) was employed for normal phase separation (flow-rate 1 ml/min) of PFB-derivatives of eicosanoids. Gradient 1 was used for separating PFB-derivatives of HETEs and PGE_2. For gradient 1, solvent A was hexane, and solvent B was methanol/isopropanol (1:1; v/v). Gradient 1 was as follows: 2% B at 0 min, 2% B at 3 min, 3.6% B at 11 min, 8% B at 15 min, 8% B at 27 min, 50% B at 30 min, 50% at 35 min, and 2% B at 37 min. Separations were performed at 30 °C using a linear gradient.

A Chiralpak AD-RH column (150 × 4.6 mm inner diameter, 5 μm; Daicel Chemical Industries, Ltd., Tokyo, Japan) on Waters Alliance 2690 HPLC was used for reverse phase (isocratic method 1, flow-rate 0.5 ml/min) separation of the HNE and HPNE oxime derivatives. The mobile phase for isocratic separations was methanol/water (85:15; v/v) with 0.1% formic acid. 4(*R,S*)-HNE was separated on the same column connected to Hitachi L-6200 LC with mobile phase of methanol/water (85:15, v/v), and the UV absorbance was set at 236 nm with L-4000 UV detector (isocratic method 2). For 4(*R,S*)-HPNE, the mobile phase was methanol/water (78:12, v/v, isocratic method 3). Separations were performed at room temperature.

Chemically synthesized Me-15(*S*)-HPETE was purified by normal-phase (isocratic method 4) preparative LC (Ultrasphere™ 250 × 10 mm, inner diameter, 5 μm; Beckman) using Hitachi LC system by monitoring the UV absorbance at 236 nm. The mobile phase for isocratic method 2 was hexane/isopropanol (197:3, v/v) containing 0.1% acetic acid.

Chemically synthesized Me-15(*R*)-HPETE was purified by normal-phase (isocratic method 5) LC (Chiralpak AD-H 250 × 4.6 mm, inner diameter, 5 μm) using Hitachi LC system by monitoring the UV absorbance at 236 nm. The mobile phase for isocratic method 4 (flow-rate 1 ml/min) was hexane/ethanol (100:2; v/v). The separation was performed at ambient temperature using a linear gradient.

GSH adducts were separated by reversed phase using gradient 2 on Waters Alliance 2690 HPLC system. The separation employed a Phenomenex Synergi

Hydro-RP column (150 × 4.6 mm inner diameters, 5 μm). Solvent A was 0.1% aqueous formic acid, and solvent B was methanol/acetonitrile/formic acid (50:50:0.1; v/v). Gradient 2 was as follows: 2% B at 0 min, 12% B at 14 min, 30% B at 20 min, 42% B at 21 min, 65% B at 27 min, 80% B at 29 min, 90% B at 33 min, 90% B at 34 min, 2% B at 35 min. The flow rate was 0.4 ml/min. The separation was performed at ambient temperature using a linear gradient.

H-εdGuo was separated by reversed phase using gradient 3 on Waters Alliance 2690 HPLC system. The column used was Phenomenex Kinetex C18 (100 × 2.1 mm inner diameters, 2.6 μm). Solvent A was 0.1 % aqueous formic acid, and solvent B was acetonitrile/formic acid (100:0.1; v/v). Gradient 3 was as follows: 10% B at 0 min, 10% B at 3 min, 30% B at 3.5 min, 90% B at 15 min, 90%B at 22 min, 10% B at 23 min. The flow rate was 0.2 ml/min. The separation was performed at ambient temperature using a linear gradient.

3.3.5 Chirality of HNE-GSH adduct formed from eicosanoids.

HPETEs or PGG_2 (1.7 μM) were incubated at 37 ^{o}C with hematin (100 nM) and GSH (4 mM) in 200 μl 100 mM Tris-Cl (pH 7.9) for 30 min, and reaction mixtures were loaded onto SPE column (oasis HLB, 30 mg) pre-conditioned with methanol and then 0.1% formic acid. The column was washed with 1 ml water and eluted with 250 μl methanol, and then 20 μl was analyzed by reverse phase LC-ESI/MS using gradient 2, as described above. Each sample was prepared in triplicate.

3.3.6 Formation of the ONE dGuo adduct (H-εdGuo) from PGG_2.

PGG_2 or 15(S)-HPETE (15 μM) in 200 μl Chelex-treated 100 mM MOPS buffer(pH 7.2), containing 150 mM NaCl was incubated with 100 μM $NH_4Fe(SO_4)_2$ and 100 μM dGuo at 37 °C for 24 hrs. Ethyl acetate (2 × 800 μl) was added to extract products. Organic layer was evaporated and dissolved to 100 μl MeOH/H_2O (1:9; v/v). 20 μl of each sample was injected to LC-ESI/MS (gradient 3).

3.3.7 Kinetic study of AA metabolism by COX.

6.7 nM recombinant ovine COX-1 or 14 nM recombinant human COX-2 was pre-incubated with cofactor hematin (100 nM), phenol (1 mM) and GSH (4 mM) in 100 mM Tris-Cl (pH 7.9) for 60 sec at 37°C before adding various concentrations of AA (0, 2.5 μM, 5 μM, 10 μM, 20 μM and 50 μM). Each total reaction volume was 200 μl. In separate experiments, the formation of eicosanoids was found to be linear for the first 45 sec. After 30 sec incubation, the enzymatic reaction was quenched by adding 400 μl of ice-cold methanol and strong vortex. 20 μl 10% aqueous acetic acid was added to adjust pH to 3-4, together with 20 μl internal standards mixture (50 pg/ μl [$^2H_8$]-15(*S*)-HETE, [$^2H_8$]-12(*S*)-HETE, [$^2H_4$]-PGE_2 and [$^2H_4$]-$PGF_{2\alpha}$). The control samples were prepared by incubating same concentrations of AA with denatured COX for 30 sec in the same buffer as above. Eicosanoids were extracted with 1.2 ml of dichloromethane/methanol (8:1; v/v). The lower organic layer was then evaporated to dryness under nitrogen and reconstituted in acetonitrile (100 μl). PFB derivatives were synthesized as

described above and analyzed by normal phase LC-ECAPCI/MS. Here, hematin stock solution (1mM in 0.1N NaOH) was prepared weekly, while phenol and GSH solutions were freshly prepared.

Eicosanoids were quantified by interpolation from a standard curve prepared with 15-HETE, 11-HETE, 12(*S*)-HHT, PGE_2 and $PGF_{2\alpha}$ using [$^2H_8$]-15(*S*)-HETE, [$^2H_8$]-12(*S*)-HETE, [$^2H_4$]-PGE_2, and [$^2H_4$]-$PGF_{2\alpha}$ as the internal standard. Samples were prepared in duplicate.

3.3.8 Eicosanoids profile of AA metabolism by COX.

Recombinant ovine COX-1 or human COX-2 (25 nM) was incubated with 5 μM AA in 200 μl 100 mM Tris-Cl buffer (pH 7.9), containing 1 μM hematin, 1 mM phenol and 4 mM GSH. The incubation was kept at 37 °C for 30 min, and then the reaction mixtures were added with internal standards (50 pg/ μl [$^2H_8$]-15(*S*)-HETE, [$^2H_4$]-PGE_2 and [$^2H_4$]-$PGF_{2\alpha}$. The products were extracted with diethyl ether (2×600 μl) at pH 3-4. The organic layer was evaporated in N_2 flow and PFB derivatives were made before analysis by LC-ECAPCI /MS.

3.3.9 Standard curves for eicosanoid quantification.

To quantify eicosanoids from COX mediated AA metabolism, Eppendorf tubes containing 0.2 ml 100 mM Tris-Cl (pH 7.9) were spiked with lipid standards, together with internal standards for ([$^2H_8$]-15(*S*)-HETE , [$^2H_8$]-12(*S*)-HETE, [$^2H_4$]-PGE_2 and [$^2H_4$]-$PGF_{2\alpha}$, 1 ng each). The extraction and PFB derivatization methods are the same as mentioned above. Each sample was prepared in duplicate.

3.3.10 Chirality of HNE-GSH formed from COX mediated AA metabolism.

25 nM COX-1 or COX-2 were incubated with 5 μM AA in 100 mM Tris-Cl (pH 7.9) in the presence of hematin (1 μM), phenol (1mM), and GSH (4mM). The total volume reaction mixture volume was 200 μl. Here, arachidonic acid (10 μM) was pre-incubated with Girard T reagent (30 mM) in Tris-Cl buffer with 5% acetic acid for 20 min at R.T. Then 2 volume of hexane was added to extract arachidonic acid. Hexane layer was transfer to a separate tube, and evaporated in N_2 flow, and then re-dissolved to Tris-Cl buffer before adding to reaction mixture. After 30 min, the reaction mixtures were then acidified with 10% aqueous acetic acid (10 μl) to pH 3-4, followed by addition of the internal standard mix, [$^2H_3$]-HNE-GSH (5 pg/μl, 20 μl). Samples were centrifuged at 13500 rpm for 2 min. The supernatant was purified by SPE cartridge and analyzed by LC-ESI/MS, as described above. Samples were prepared in triplicate. Here, [$^2H_3$]-HNE-GSH was prepared by incubating 4-(*S*)-HNE and 4-(*R*)-HNE with GSH, respectively. 4(*S*)-HNE and 4-(*R*)-HNE were as described previously *(89)*, using isocratic method 2.

3.3.11 Standard curves for HNE-GSH quantification.

To quantify HNE-GSH adduct from COX-mediated AA metabolism, standard HNE (0.01, 0.1,0.5,2 and 10 ng) was incubated with GSH (4 mM) at 37 ºC for 30 min, and then [$^2H_3$]-HNE-GSH (5 pg/μl, 20 μl) was added to reaction mixtures. The reaction mixtures were purified by SPE cartridge and analyzed by LC-ESI/MS as previously described.

3.3.12 Chirality of HNE-GSH formed from LoVo cell lysate.

LoVo cells were grown to 90% confluence, washed with phosphate-buffered saline (PBS) buffer (2×10ml), and then gently scraped in 400 µl of lysis buffer containing 100 mM Tris-HCl (pH 7.9), protease inhibitor (diluted from 100X), GSH (4 mM), GST inhibitor ethacrynic acid (20 µM) and AKR inhibitor zopolrestat (50 nM). Cell suspension was transferred to 2 ml Eppendorf tubes, and sonicated for 60 seconds on ice (power 5). Cell lysate was then incubated for 15 min at 37°C. The pH was then adjusted to 3 to 4 with 10% aqueous acetic acid (10 µl) followed by addition of the internal standard mix, [$^2H_3$]-HNE-GSH (5 pg/µl, 20 µl). Samples were centrifuged at 13500 rpm for 2 min, and the supernatant was purified by SPE cartridge. The cartridge was eluted with 250 µl methanol, and 40 µl was analyzed by LC-ESI/MS. For the control samples, LoVo cells were pretreated with rofecoxib (50 µM) in F-12K medium at 37°C for 2 hrs to inhibit COX-2 activity, and then cell lysate was prepared as described above. To quantify eicosanoids formation under this condition, a separate set of samples were prepared, and the lipid extraction and PFB derivatization methods described previously were used.

3.3.13 Methylation of 15(*S*)-HPETE.

Ethereal diazomethane (CH_2N_2) was freshly prepared by reacting N-methyl-N-nitroso-p-toluensulfonamide with sodium hydroxide, employing a diazomethane generator from Wheaton (Millville, NJ). The manufacturer's procedures were followed, and the product was confirmed by both LC-MS and NMR.

3.3.14 Chemical synthesis and purification of 15(*R*)-HPETE methyl ester.

15(*R*)-HPETE methyl ester was synthesized according to Corey's method *(104, 105)*. Racemic 15-HPETE methyl ester was prepared by converting 15(*S*)-HETE methyl ester to the mesylate derivative, which was then treated with hydrogen peroxide in ether at -110 °C. 15(*R*)-HPETE methyl ester was isolated by normal phase-HPLC using isocratic method 5.

3.3.15 Separation and hydroxylamine derivatization of 4(*S*)-HPNE.

4(*R,S*)-HPNE from Cayman was separated by Chiralpak AD-RH column, as described previously (isocratic method 3). The first peak of the two enantiomers was collected and evaporated in N_2 flow, and then it was dissolved into 200 µl Chelex-treated MOPS buffer (100 mM, pH 7.2), containing 150 mM NaCl, followed by the addition of 1 mg hydroxylamine hydrochloride. The mixture was incubated at 37 °C for 1 h before extraction with ethyl acetate (2 × 800 µl). The organic layer was evaporated in N_2 flow, and then dissolved to 100 µl MeOH. 10 µl was analyzed by LC-LTQ/MS, as described above. The rest of the solution was added with 0.4 mg $SnCl_2$ and stayed at room temperature for 30 min. Water (900 µl) was added and then 3 ml ethyl acetate, and the mixture was centrifuged at 3000 rpm for 5 min. Then the ethyl acetate was evaporated and dissolved to 100 µl MeOH/water (85:15; v/v), and 10 µl was injected to LC-ESI/SRM/MS (isocratic method 1). 4(*S*)-HNE isolated from 4(*R,S*)-HNE (89) was also converted to the oxime derivative under the same condition as used for HPNE. By comparison of

4(*S*)-HNE oxime peak from standard 4(*S*)-HNE with that obtained from the reduction of HPNE-oxime, it was possible to conclude that the first peak, which eluted from the AD-RH column was 4(*S*)-HPNE.

3.3.16 Conversion of 4(*S*)-HPNE-oxime to 4(*S*)-HNE-oxime in the presence of Vit C.

4(*S*)-HPNE-oxime prepared as described above was separated with an AD-RH column using isocratic method 1. The two isomer peaks were collected separately, and then incubated 200 µl Chelex-treated MOPS buffer (100 mM, pH 7.2), containing 150 mM NaCl and 1 mM Vit C, 37 °C for 30 min. A similar ethyl acetate extraction workup was applied to purify the products. The samples were analyzed with the same LC-MS method as 4(*S*)-HNE-oxime.

3.4 RESULTS

3.4.1 Chirality of HNE-GSH formed from eicosanoids.

HNE was converted to its GSH-adduct in order to increase the sensitivity of detection. GSH also introduced new chiral centers, so the GSH-adduct diastereomer formed from 4(*S*)-HNE and the one formed from 4(*R*)-HNE could be readily separated with a non-chiral column. PGG_2, 11(*R*)-HPETE, 15(*S*)-HPETE, and 15(*R*)-HPETE-Me (1.7 µM) were incubated with hematin and GSH, resulting in the formation of different HNE-GSH diastereomers that could be readily analyzed. A representative chromatogram (Figure 3.3) reveals the separation of *R*-HNE-GSH (retention time 24.4 and 25.8 min) and

S-HNE-GSH (retention time 24.9 min). 11(*R*)-HPETE gave racemic HNE-GSH. 15(*S*)-HPETE gave (*S*)-HNE-GSH, while 15(*R*)-HPETE-Me gave (*R*)-HNE-GSH. PGG_2 only gave (*S*)-HNE-GSH.

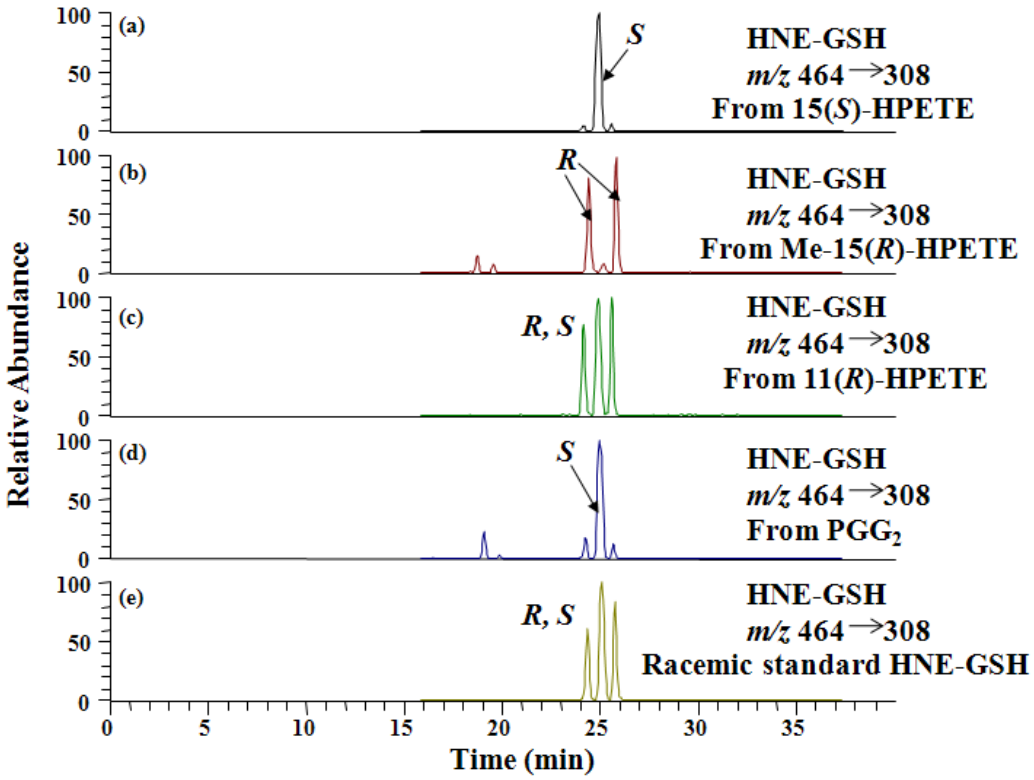

Figure 3.3. The chirality of HNE formed from eicosanoids. Figure (a), (b), (c) (d) show the chromatography of HNE-GSH formed from 15(*S*)-HPETE, 15(*R*)-HPETE methyl ester, 11(*R*)-HPETE and PGG_2, respectively. (e) is the chromatography of 4(*R,S*) HNE and GSH adduct standard. HNE-GSH is separated by reverse phase LC, and monitored by SRM transition m/z 464 to 308. The middle peak is 4(*S*)-HNE and GSH adduct. There are two peaks (the first and the third) corresponding to GSH adduct with 4(*R*)-HNE. This is because there are multiple chiral centers in HNE-GSH adducts.

3.4.2 Formation of H-εdGuo from PGG_2.

PGG_2 was incubated with dGuo in the absence or presence of Fe(II). PGG_2 decomposed to ONE in the presence of Fe(II) and ONE was trapped by dGuo

to form H-εdGuo. After 24 h incubation, the product was extracted with ethyl acetate. The organic layer was evaporated and dissolved into starting mobile phase. Samples were analyzed in LC-ESI/MS. The retention time of H-εdGuo is 14.7 min, as shown in Figure 3.4.

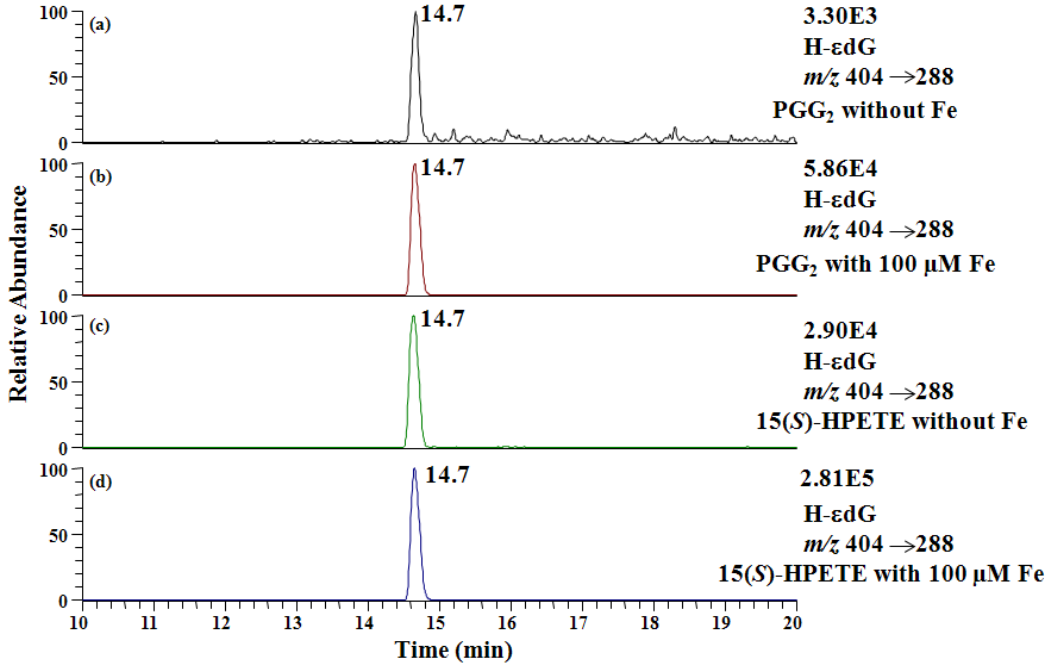

Figure 3.4. The formation of H-εdGuo from PGG_2 and 15(*S*)-HPETE. Samples were prepared from 15 μM PGG_2 or 15(*S*)-HPETE in Chelex-treated 100mM MOPS buffer, containing 150 mM NaCl buffer (pH 7.2) in the presence of 100 μM dGuo and in the presence or absence of 100 μM Fe(II) at 37 °C for 24 hr. Figure (a) and (b) show the H-εdGuo formation from PGG_2 in the absence and presence of Fe^{II}, respectively. Figure (c) and (d) show the H-εdGuo formation from 15(*S*)-HPETE in the absence and presence of Fe, respectively. Reverse phase LC coupled with SRM transition m/z 404 to 288 (collision energy 18 eV) was used to detect H-εdGuo.

3.4.3 Kinetic study of AA metabolism by COXs.

Various concentrations of AA were incubated with recombinant ovine COX-1 and human COX-2 at 37 °C. A Michaelis-Menten kinetic analysis of

eicosanoids formation revealed that the V_{max} values for conversion of AA to PGE_2, 11(*R*)-HETE, 15(*S*)-HETE, and 15(*R*)-HETE by COX-1 are 25.16, 13.86, 13.83, and 3.856 pmol/min, respectively, while Km values are 3.768, 9.434, 19.76, and 8.334 μM, respectively, and the corresponding k_{cat} values are 18.78, 10.34, 10.32, and 2.878 min^{-1}, respectively (Figure 3.5, Table 3.1).

COX-1 (ovine)	K_m (μM)	V_{max} (pmol/min)	k_{cat} (min^{-1})	k_{cat}/K_m (min^{-1} mM^{-1})
11(*R*)-HETE	9.434	13.86	10.34	1096
15(*S*)-HETE	19.76	13.83	10.32	522.3
15(*R*)-HETE	8.334	3.856	2.878	345.3
PGE_2	3.768	25.16	18.78	4985

COX-2 (human)	K_m (μM)	V_{max} (pmol/min)	k_{cat} (min^{-1})	k_{cat}/K_m (min^{-1} mM^{-1})
11(*R*)-HETE	3.916	6.754	2.412	615.9
15(*S*)-HETE	6.529	4.571	1.633	700.1
15(*R*)-HETE	13.74	4.325	1.545	112.4
PGE_2	0.8428	9.647	3.445	4088

Table 3.1. The K_m, V_{max}, k_{cat} and k_{cat}/K_m values of COX substrate AA with the respect of different products.

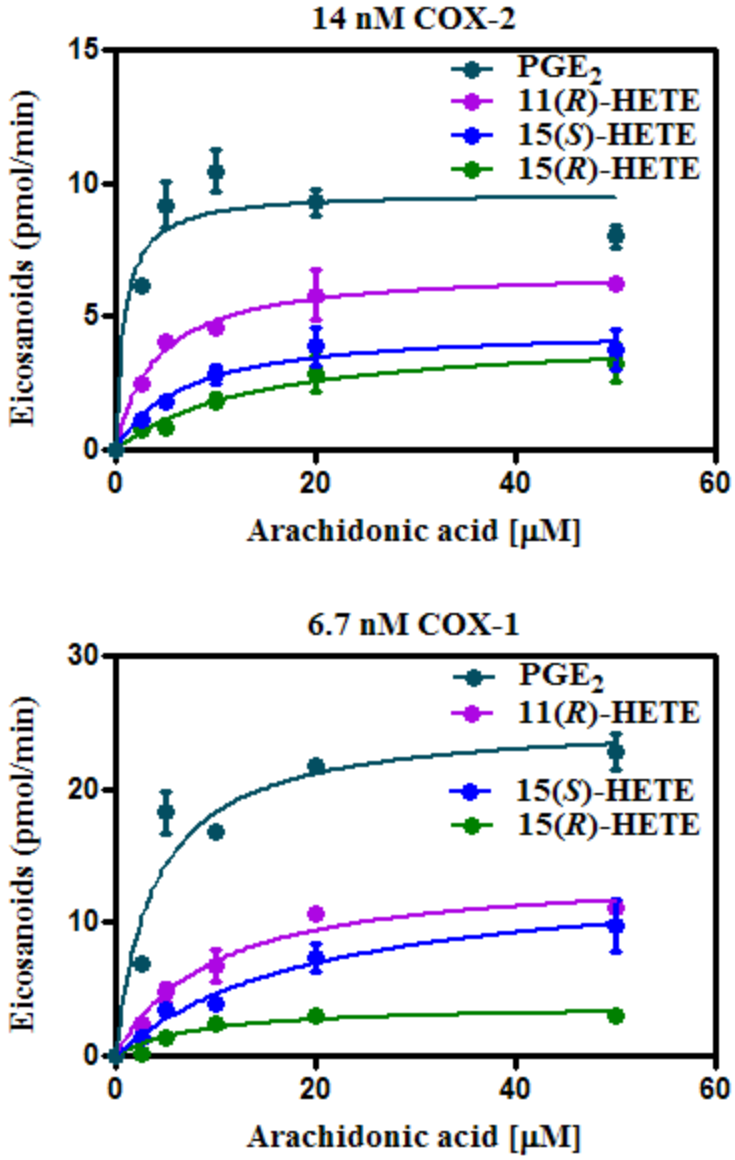

Figure 3.5. The saturation curves for recombinant ovine COX-1 and human COX-2 with AA as the substrate. All of the samples were prepared in duplicate (means ± S.E.M.)

3.4.4 Eicosanoid profile of AA metabolism by COX.

Recombinant ovine COX-1 or human COX-2 (25 nM) was incubated with 5 µM AA in 200 µl 100 mM Tris-Cl buffer (pH 7.9), containing 1 µM hematin, 1 mM

phenol and 4 mM GSH. The incubation was kept at 37 °C for 30 min, and then the reaction mixtures were added with internal standards (50 pg/ µl [$^2H_8$]-15(*S*)-HETE, [$^2H_4$]-PGE_2 and [$^2H_4$]-$PGF_{2\alpha}$). The products were extracted with diethyl ether (2 × 600 µl) at pH 3-4. The organic layer was evaporated in N_2 flow and PFB derivatives were made for LC-ECAPCI /MS analysis. The results are shown in Figure 3.6. If PGE_2, $PGF_{2\alpha}$ and 12-HHT are used to reflect the original PGG_2 level, and15-HPETE and 11-HPETE to reflect the LOX activity, then the PG pathway comprises > 88 % of the total COX-1 metabolites, and > 86 % for the COX-2 enzyme metabolites. The eicosanoids formation from LoVo cell lysate were extracted and quantified following a similar procedure. Figure 3.9 shows the products profiles from LoVo cell lysate. The product distribution was similar to that obtained from recombinant COX-2. PG metabolites comprised > 82 % of the overall eicosanoids, which indicates the initially formed PGG_2 was the major COX-2-derived metabolite.

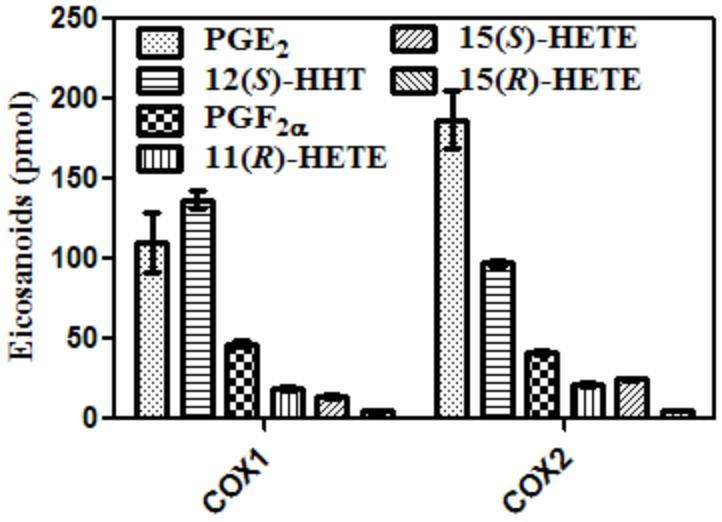

Figure 3.6. Eicosanoids formed from recombinant ovine COX-1 and human COX-2. Data is performed in triplicate (means ± S.E.M.)

3.4.5 Chirality of HNE-GSH formed from COX-mediated AA metabolism.

The HNE-GSH-adducts from 25 nM COX-1 or COX-2 incubation with 5 μM AA were purified by SPE and then analyzed by LC-ESI/SRM/MS. A representative chromatogram (Figure 3.7) reveals the separation of R-HNE-GSH (retention time 24.4 and 25.8 min) and S-HNE-GSH (retention time 24.9 min). A summary of the R, S percentage of HNE from different precursors is shown in Table 3.2.

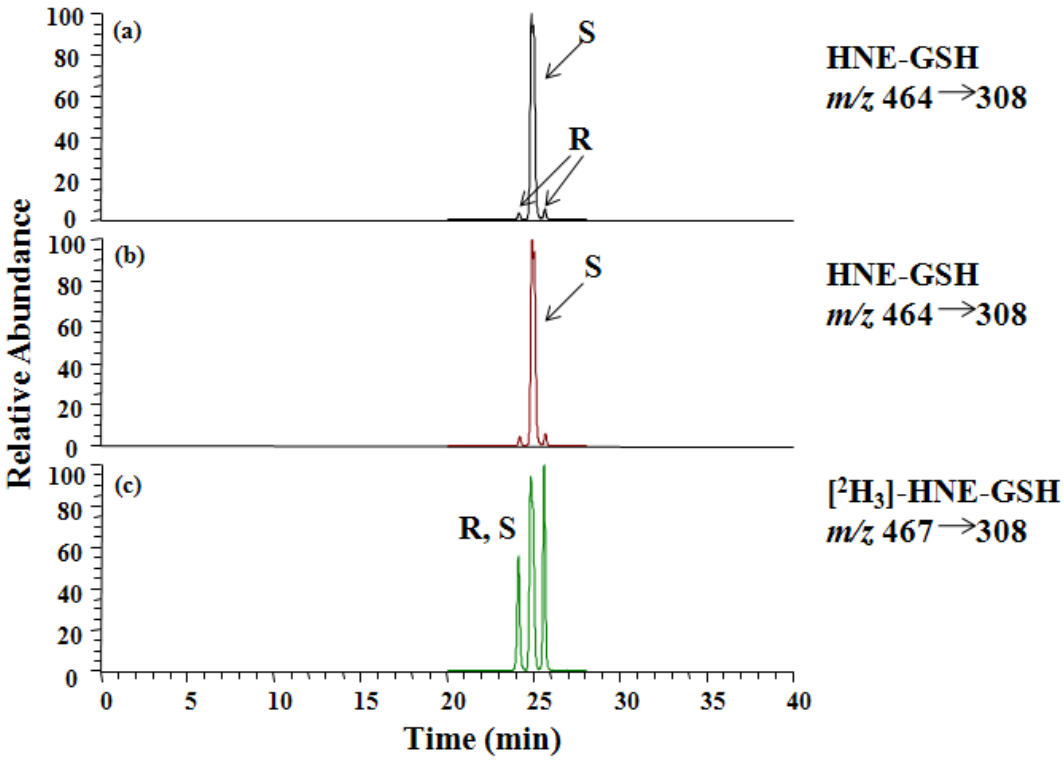

Figure 3.7. Chirality character of HNE-GSH formed from COX mediated AA metabolism Figure (a) shows HNE-GSH formed from COX-1 mediated AA metabolism, while HNE-GSH in Figure (b) comes from COX-2. [$^2H_3$]-HNE-GSH in Figure (c) is racemic internal standard, which is monitored by SRM transition m/z 467 to 308.

Substrates	4(*R*)-HNE(%)	4(*S*)-HNE(%)
11(*R*)-HPETE	52.0	48.0
15(*S*)-HPETE	7.0	93.0
15(*R*)-HPETE	94.0	6.0
COX-1 + AA	6.3	93.7
COX-2 + AA	8.5	91.5
PGG_2	11.0	89.0

Table 3.2 The chirality of HNE-GSH-adducts formed from different hydroperoxides and COX-mediated AA metabolism

3.4.6 Chirality of HNE-GSH-adducts formed from LoVo cell lysate.

LoVo cells are known to express COX-2. This was confirmed by Western blot analysis (data not shown). LoVo cell lysates were incubated with 100 mM Tris-Cl (pH 7.9), protease inhibitor, GSH (4 mM), GST inhibitor ethacrynic acid (20 μM) AKR inhibitor zopolrestat (50 nM). [$^2H_3$]-HNE (5 nM) or AA (20 μM) was added and incubation was kept for 15 min. Inhibition of GST abolished the effect of GST on enantioselective HNE-GSH-adduct formation. The AKR1B inhibitor stabilized HNE-GSH.*(23)* Racemic [$^2H_3$]-HNE was added to the lysate mixture, and racemic [$^2H_3$]-HNE-GSH was obtained (Figure 3.8c), which indicated that under this condition, the chirality of HNE-GSH from LoVo cell lysate supplemented with AA would represent the chirality of HNE formed from LoVo cell lysate (Figure 3.8b). Mainly, the *S*-HNE-GSH-adduct was detected, which was consistent with the chiral analysis of eicosanoids from LoVo cell lysates (Figure 3.9). Pre-treatment of rofecoxib inhibited > 90% of PGE_2 formation, so rofecoxib-treated LoVo cell lysate was used to provide a control sample.

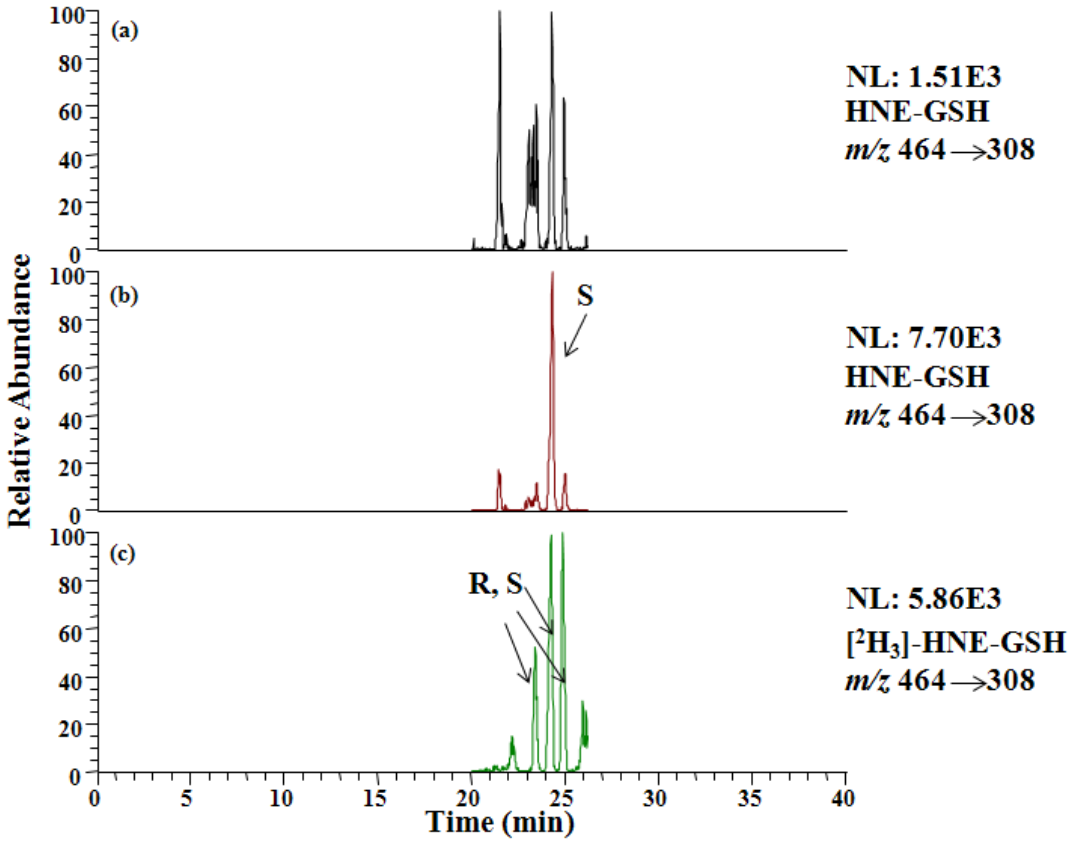

Figure 3.8. The formation of 4(*S*)-HNE and GSH adduct from LoVo cell lysate. Figure (a) displays HNE-GSH adduct from rofecoxib-treated LoVo cell lysate, which is used to represent the basal level of HNE-GSH adduct. Figure (b) shows HNE-GSH formed from LoVo cell lysate in the presence of ethacrynic acid, zopolrestat, and GSH Figure (c) is the formation of [$^2H_3$]-HNE-GSH after adding 250 pg [$^2H_3$]-HNE to LoVo cell lysate. All of these experiments were done in triplicate, and this Figure reflects one of the triplicates.

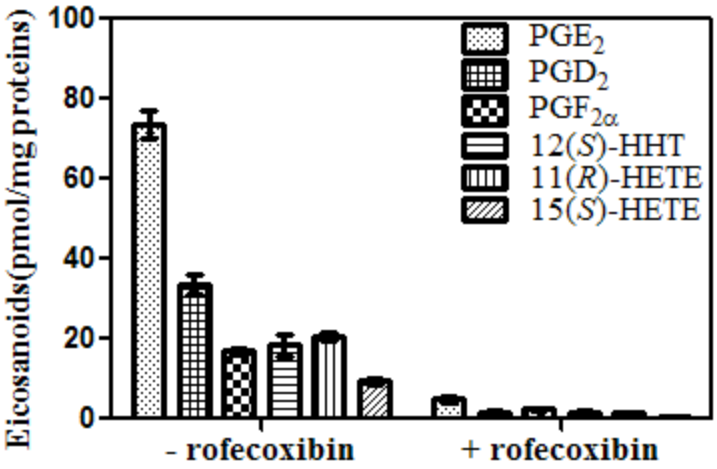

Figure 3.9. Eicosanoids formed from LoVo cell lysate in the presence of ethacrynic acid, ispolrestat, and GSH. All of the samples were prepared in triplicate. As shown above, PGE_2 was the major metabolite. 50 μM rofecoxib almost abolished the formation of eicosanoids from COX-2. All of these experiments were performed in triplicate (means ± S.E.M.).

3.4.7 Separation and oxime derivatization of 4(*R,S*)-HNE and 4(*R,S*)-HPNE

Both HNE and HPNE enantiomers could be separated on the same column, although the separation of 4(*R,S*)-HNE was more efficient(see Figure 3.10). A previous study had established that under these LC conditions, 4(*S*)-HNE is eluted first (7.6 min) followed by 4(*R*)-HNE. In order to confirm the chirality of the two HPNE enantiomers, the first eluting peak was collected and reacted with hydroxylamine in 200 μl 100 mM MOPS buffer with 150 mM NaCl, pH7.2. The resulting oxime was extracted with ethyl acetate (800 μl, twice), and the organic layer was evaporated under N_2. The HPNE-oxime was then re-dissolved into 100 μl methanol and 10 μl was then analyzed by LC-

MS on the LTQ instrument. It was also was reduced to HNE-oxime by adding $SnCl_2$, and the mixture was incubated at room temperature for 30 min. The product was again extracted with ethyl acetate. HNE-oxime formed from HPNE-oxime reduction was analyzed by the same LC-MS method. Figure 3.10 shows that the first peak (15.2 min) collected from 4(*R,S*)-HPNE was reduced to 4(*S*)-HNE only. The $SnCl_2$ reduction did not change the chirality of hydroperoxy group, so the 15.2 min peak corresponded to 4(*S*)-HPNE, while the 16.2 min peak was 4(*S*)-HPNE.

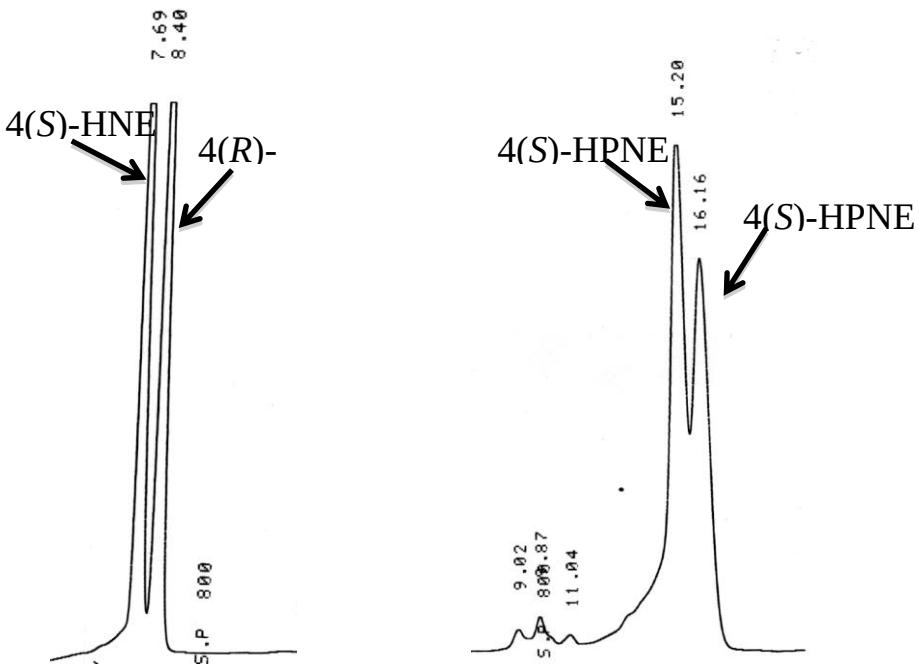

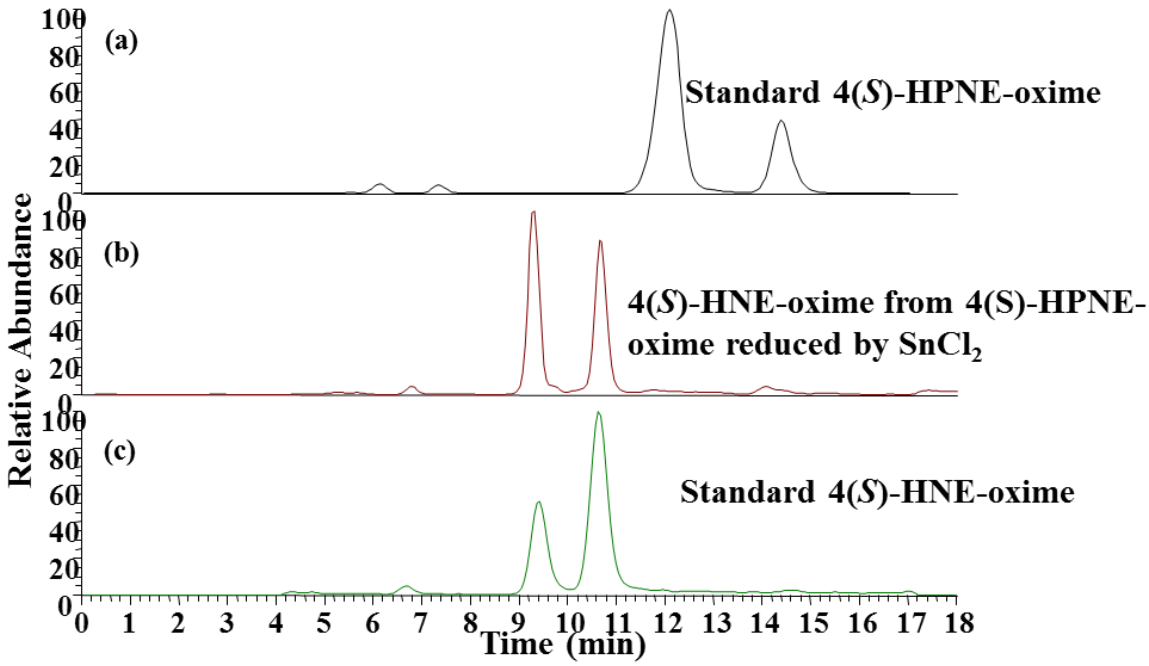

Figure 3.10. Chiral LC separation of 4(*R,S*)-HPNE and 4(*R,S*)-HNE and Chiral LC-MS analysis of their corresponding oxime derivatives.

Based on the data shown in Figure 3.10, the first peak eluted from AD-RH column using 78% MeOH/water as the mobile phase corresponded to 4(*S*)-HPNE. In the presence of Vit C, the 4(*S*)-HPNE could be converted to 4(*S*)-HNE without changing the chiral center at C4. Thus, monitoring the chirality of HNE would reflect the chiral character of HPNE.

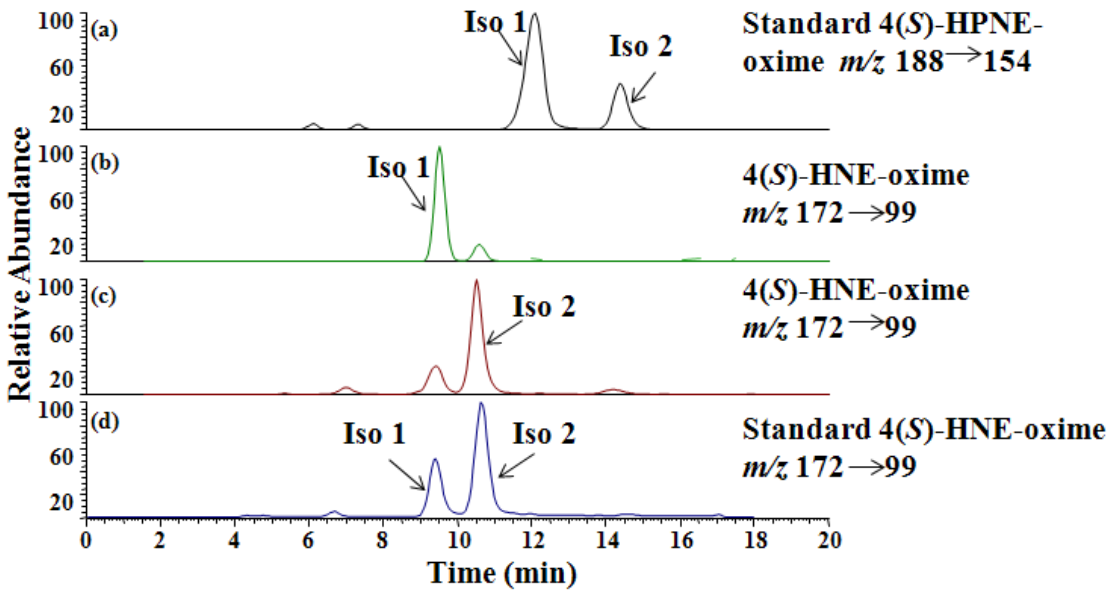

Figure 3.11 The conversion of 4(*S*)-HPNE-oxime to 4(*S*)-HNE-oxime in the presence of Vit C. Figure (a) shows 4(*S*)-HPNE-oxime (*syn*- and *anti*-isomers). Figure (b) is 4(*S*)-HNE-oxime isomer1 formed from 4(*S*)-HPNE-oxime isomer1, while (c) is 4(*S*)-HNE-oxime isomer 2 formed from 4(*S*)-HPNE-oxime isomer2. Figure (d) shows the two isomers from standard 4(*S*)-HNE-oxime. The 4(*R,S*)-HPNE and 4(*R,S*)-HNE enantiomers are separated by chiral AD-RH column. HPNE-oxime is monitored by SRM transition *m/z* 188 to 154 at collision energy 25%, while HNE-oxime was monitored by the SRM transition *m/z* 172 to 99 at the same collision energy.

3.4.8 Chemical synthesis and purification of 15(*R*)-HPETE methyl ester.

The synthesis of 15(*R*)-HPETE methyl ester was achieved by converting 15(*S*)-HETE methyl ester to racemic 15-HETE methyl ester. 15(*S*)-HPETE was prepared by oxidation of arachidonic acid from LO, and then methylated by CH_2N_2. The reduction of the hydroperoxy group at C15 to alcohol was via $NaBH_4$ reduction. Acidic and basic hydrolysis of the methyl ester were attempted to convert the methyl ester back to acid. However, the yield was

extremely low due to the relative instability of 15-HPETE. A chiral AD-RH column was applied to separate 15(*R,S*)-HPETE methyl ester as shown in Figure 3.12.In the left LC-UV chromatogram, the peak at 17.2 min corresponds to the *S* form of 15-HPETE-Me, while the peak at 18.2 min corresponds to the *R* form. Figure 3.12(a) shows LC-ESI/MS data of racemic 15-HPETE methyl ester, while 3.12(b) shows 15(*S*)-HPETE-Me only, so the peak at 10.6 min is 15(*R*)-HPETE-Me.

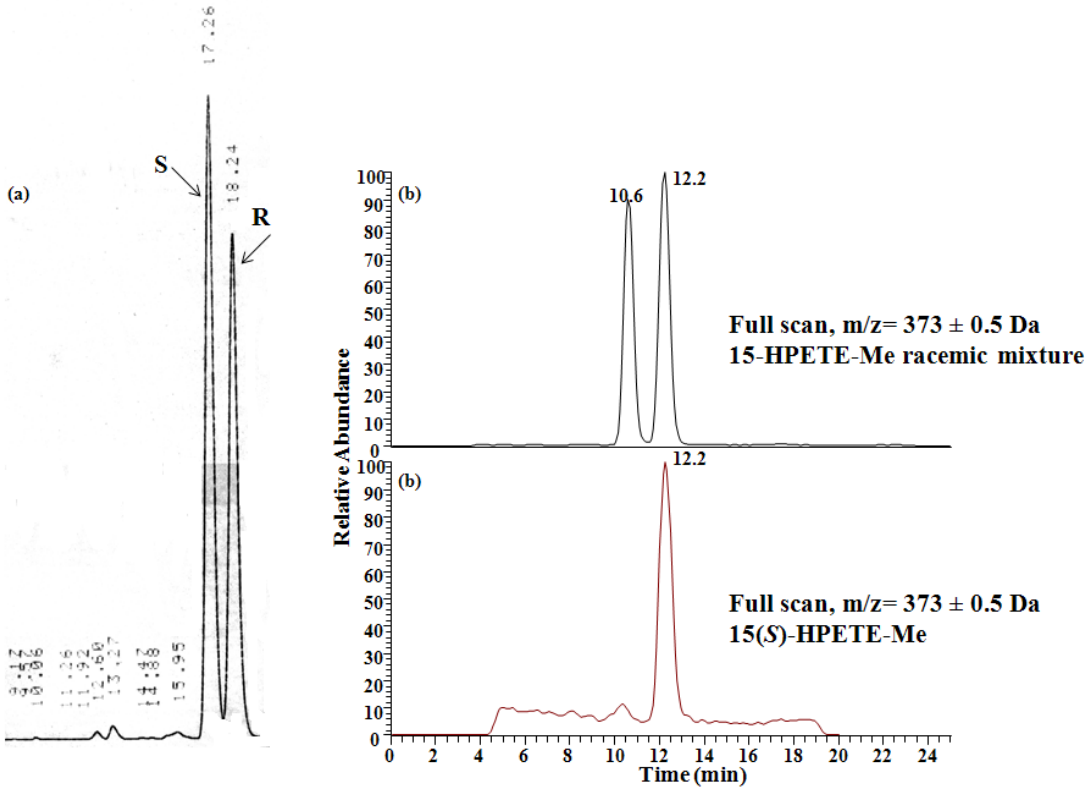

Figure 3.12, LC-UV purification and LC-MS confirmation of 15-HPETE methyl ester. The reaction mixture was purified by Chiralpak AD-H column with mobile phase of hexane/ethanol (100:2), and UV absorption at 236 nm was monitored. Figure (a) and (b) are 15-HPETE-Me samples analyzed by Chiralpak AD-RH column coupled with LTQ-ESI/MS. The LC-MS conditions are shown in the experimental procedures section.

3.5 DISCUSSION

HNE and ONE can be generated from linoleic acid and AA autoxidation *in vitro*. However, in cells the redox potential is strictly regulated, which means the free radical induced non-enzymatic autoxidation is very limited and the corresponding autoxidation products are at low levels. In contrast, when COXs and LOXs are present, linoleic acid or AA can be efficiently converted stereoselectively into lipid hydroperoxides in inflammatory cells and in many cancer tissues. The major product of COX-2 mediated AA oxidation is PGG_2. From analysis of HNE-GSH adduct generated from different eicosanoids, it was shown that PGG_2 could be converted into 4(*S*)-HNE; whereas, 11(*R*)-HPETE, which is the major acyclic lipid hydroperoxide, generated racemic 4(*R,S*)-HNE. Furthermore, 15(*S*)-HPETE, a major product of the 15-LOX/AA pathway, was converted into 4(*S*)-HNE, while 15(*R*)-HPETE, the major product of aspirin-treated COX-2, was converted into 4(*R*)-HNE. Characterization of the different eicosanoid-derived HNE enantiomers made it possible to evaluate the individual contributions of these eicosanoid precursor and their related pathways to formation of the reactive aldehydes HNE and ONE. Interestingly, 4(*S*)-HNE was the major form of HNE formed from either recombinant COX-mediated AA oxidation in the presence of hematin as well as from COX-2 expressed LoVo cell lysate. This result indicates that PGG_2 contributes is the major contributor to the formation of HNE. This means that COX-derived ONE, which shares the same precursor as HNE, also arises from PGG_2. This new finding implies that ONE-mediated DNA damage also arises from PGG_2 rather than from HPETEs as had been assumed previously (*67*).

The fact that PGG_2 is mainly converted into 4(*S*)-HNE suggests a novel decomposition mechanism. It is proposed that the 12-HPTrE formed when PGG_2 is converted to MDA forms a dihydroperoxide similar to that proposed for 5(*S*)-HPETE (*36*), which subsequently decomposes to 4(*S*)-HPNE via a Hock rearrangement. Furthermore, it further highlights the need for adequate intracellular reducing equivalents to convert PGG_2 into PGH_2 and so prevent the formation of MDA, HPNE, HNE, and ONE.

Chapter 4

Newly identified OUDE as the 15-HPETE and 11(*R*)-HPETE decomposition aldehyde

4.1 ABSTRACT

. HPNE and HPNE-derived HNE and ONE have been characterized previously. However, OUDE, which retains a carboxylic acid group from HPETEs has not been identified previously. The formation of OUDE from lipid hydroperoxide decomposition was shown to occur by comparing LC-MS and NMR information to an authentic standard prepared by organic synthesis. Chiral LC-MS analysis of oxime derivatives coupled with the use of [^{13}C]-analogs was employed in order to provide insight into the mechanism of formation of OUDE. An OUDE isomer, which was formed by C8-C9 double bond translocation to C9-C10 was also identified. This isomer possesses a reactive α,βunsaturated aldehyde analogous to HNE. It was found that there are two distinct pathways for 11(*R*)-HPETE and 15-HPETE to form OUDE and HPNE, based on the different chirality of HPNE generated from these lipid hydroperoxides. The findings of carboxylic acid containing aldehydes could be highly significant, considering that they could be generated on esterified lipids and disrupt the lipid membrane. This is different from HPNE, which cannot form an ester bond to membrane lipids. Thus, HPNE or HNE could

play quite different roles in regulating biological processes when compared to the corresponding carboxylate-containing OUDE isomers.

4.2 INTRODUCTION

15-HPETE and 11-HPETE are generated either from autoxidation of AA as racemic mixtures, or stereoselectively from enzymatic pathways. COX-2 converts free AA into 15(*S*)-HPETE and 11(*R*)-HPETE, while 15-LOX converts free AA or esterified AA into free 15(*S*)-HPETE or esterified 15(*S*)-HPETE (*109*). Both non-enzymatic pathways and enzymatic pathways are enhanced in cells under oxidative stress such as during inflammation and cancer. It has been known for many years that AA oxidation can generate aldehydes (*110,111*). However, previous research has focused primarily on AA-derived aldehydic products, which lack the α-carboxylate terminus.. Thus, HNE and ONE have been widely studied with regards to their mechanism of formation (32,*96*) and their biological effects (*97, 101-103, 107-108*). However, carboxylate containing aldehydes have attracted much less attention with respect to either their identification or their biological roles.

A number of research groups have studied the oxidized phospholipid products (OxPLs) that are present on the surface of LDL or apoptotic cells and function as potential CD36 ligand (*112,113,114*). The Hazen group has shown that some of these lipid oxidation products have aldehydes at the ω position (*115,116*). Through this research, a relationship between lipid oxidation and immune recognition has evolved, suggesting that oxidized lipids play important role in inflammation and that they are involved in the

development of atherosclerosis. Some of the OxPLs are pro-atherogenic and some are anti-atherogenic (*117,118*). Thus, the complexity of OxPL activity requires additional investigation into the characterization of these lipid aldehydes.

Previously, Jian et al. identified a novel carboxylate-containing aldehyde, 5,8-dioxo-6(*E*)-octenoic acid (DOOE), that was formed from 5(*S*)-HPETE, a 5-LOX-mediated AA oxidation product (36,*119*). One difference between 15-LOX and 5-LOX is that 15-LOX can use esterified AA or lipoprotein as substrate, while 5-LOX can only oxidize free arachidonic acid (*120)*. Thus, it was considered more worth studying the decomposition of 15-LOX-derived 15(*S*)-HPETE into reactive aldehydes. The resulting aldehyde could also potentially exist in an esterified form and so would be present on the surface of membrane where it could act as a signaling molecule.

The mechanism of HPETE decomposition to aldehydes is still not completely clear, although several groups have proposed some potential schemes (as shown in chapter 1). It is extremely challenging to capture the reactive intermediates that are precursors of the resulting aldehydes due to rapidity of potential radical reactions and the instability of any radical intermediates. Thus, we studied the chirality of the final aldehyde product, 4-hydroxy-nonenal (HPNE) at its C4 position, similar as the method used by the Brash Group (see Chapter 3). The chirality of HPNE formed from different precursors indicated that there were two distinct decomposition pathways

from 15-HPETE and 11(*R*)-HPETE. Furthermore, the made it possible to determine the relative contributions of different HPETEs to HPNE levels.

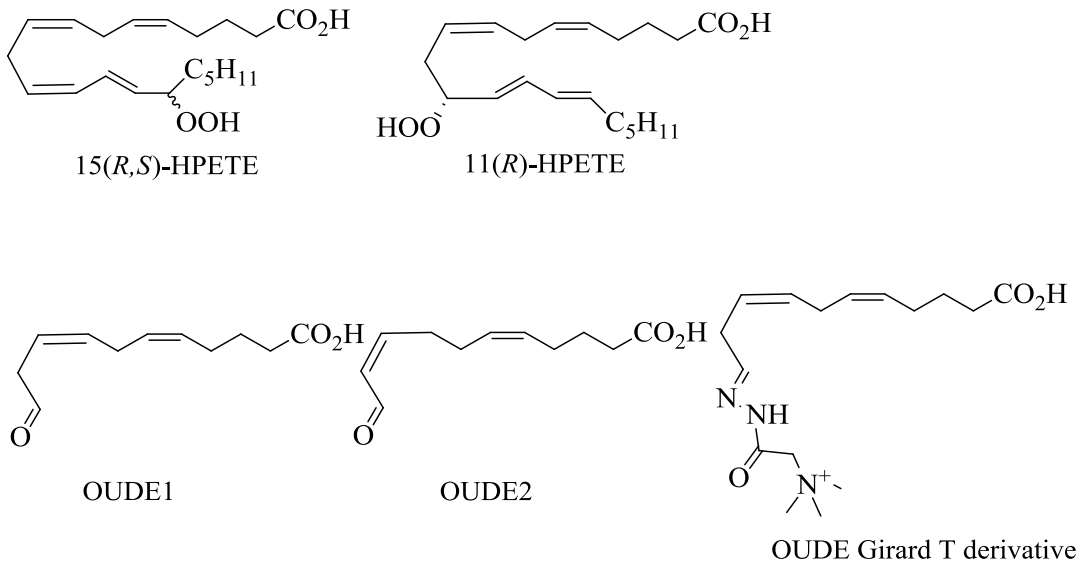

Figure 4.1 Chemical structures of 15-HPETE, 11-HPETE, OUDE1 and 2, and OUDE Girard T derivative

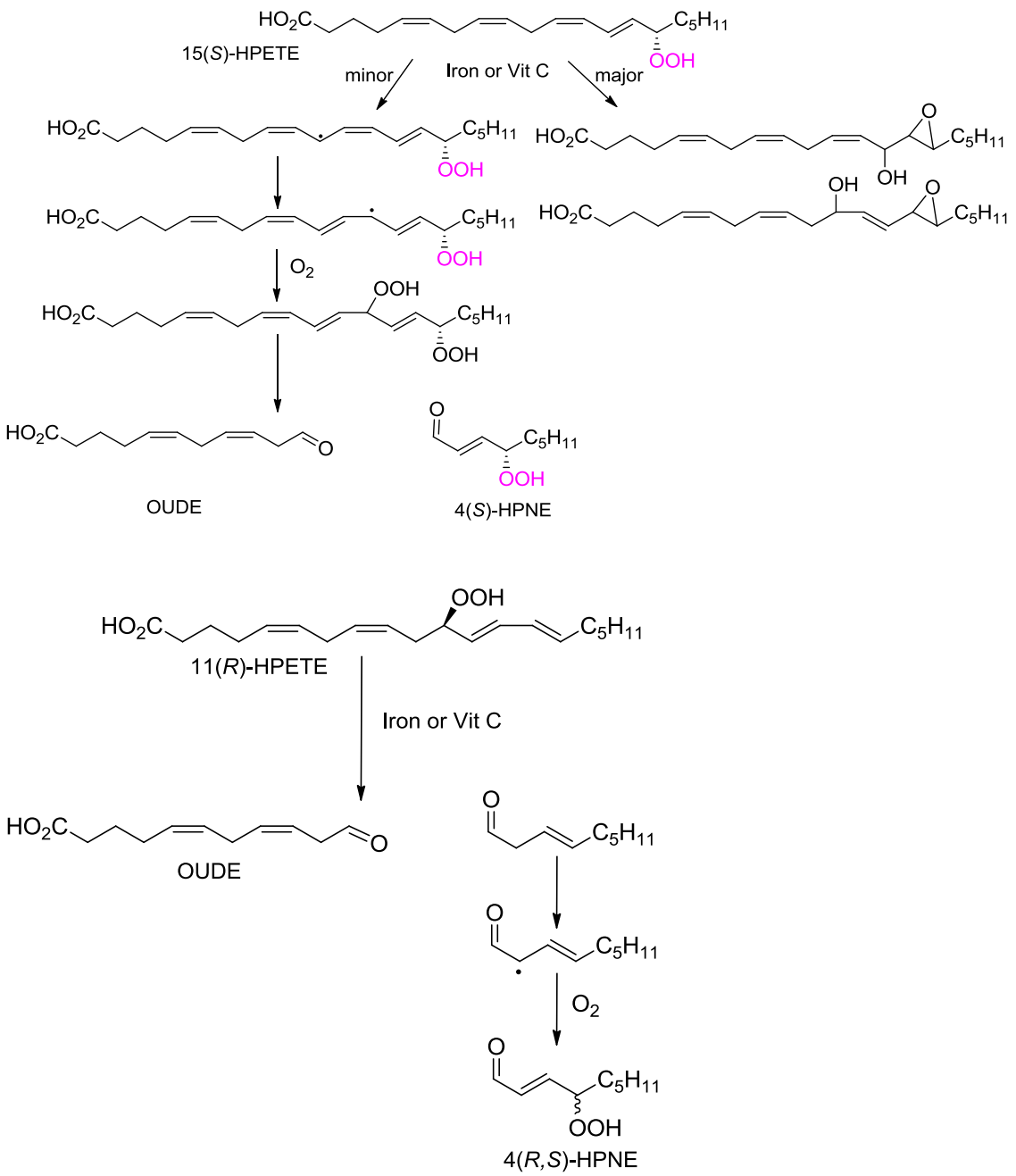

Figure 4.2. Proposed mechanism for formation of OUDE from 15(*S*)-HPETE and 11(*R*)-HPETE

4.3 EXPERIMENTAL PROCEDURES

4.3.1 Chemicals and Reagents.

AA, HPNE and [$^2H_3$]-4-HNE were purchased from Cayman (Ann Harbor, MI). Girard T reagent, hydroxylamine hydrochloride, L-glutathione, L-ascorbic acid, and lipoxidase from Glycine max (soybean) were purchased from Sigma-Aldrich (St. Louis, MO). LC-MS grade water, *tert*-Butyl methyl ether, methanol, isopropanol, acetonitrile and dichloromethane were obtained from Fisher Scientific (Pittsburgh, PA). Gases were supplied by The Linde Group (Munich, Germany).

4.3.2 MS conditions.

For oxime derivatives analysis, the Finnigan LTQ mass spectrometer (Thermo Electron, San Jose, CA) was used in the positive ion mode with an ESI source. The operating conditions were: spray voltage at 4 kV; capillary temperature at 250°C; capillary voltage at 35 V; nitrogen as sheath (40 psi) and auxiliary (20 arbitrary units) gas. CID was performed using helium as the collision gas in the ion trap. The following SRM transition (m/z 188 → 154) was monitored for HPNE-oxime (normalized CE, 25 %), and SRM transition (m/z 172 → 99) was monitored for HNE-oxime (normalized CE, 25%).

For GSH adduct analysis, the triple stage quadrupole (TSQ Quantum) mass spectrometer (Thermo Electron, San Jose, CA) equipped with an ESI source was used. TSQ Quantum was operated in the positive ion mode with an ESI source. The operating conditions were: spray voltage at 4 kV; capillary temperature at 350°C; nitrogen as sheath (35 psi) and auxiliary (13 arbitrary units) gas. CID was performed using argon as the collision gas at 1.5 mtorr

in the Rf-only quadrupole. The following SRM transition (m/z 464 → 308) was monitored for HNE-GSH (CE, 14 eV).

For high resolution mass analysis, the Thermo LTQ Orbitrap XL hybrid FTMS (Fourier Transform mass spectrometer) equipped with a Michrom nano ESI source was used. It was operated in negative mode for free fatty acid analysis, while in positive mode for Girard T derivatives analysis. The operating conditions were: spray voltage at 1.75kV; capillary temperature at 250 °C; capillary voltage at 49 V; helium as collision gas. For full scan, the resolution was set at 30 000. For MS/MS, the isolation width used was 2.5, the resolution for the products analysis was 30 000, and the collision energy was 35 %.

4.3.3 LC methods.

LC separations were conducted using a Waters Alliance 2690 HPLC system (Waters Corp., Milford, MA, USA). A Chiralpak AD-RH column (150 × 4.6 mm inner diameter, 5 μm; Daicel Chemical Industries, Ltd., Tokyo, Japan) was used for reverse phase (isocratic method 1, flow-rate 0.5 ml/min) separation of the HNE and HPNE oxime derivatives. The mobile phase for isocratic separations was methanol/water (85:15; v/v) containing 0.1 % formic acid.

OUDE was purified by preparative LC (Ultrasphere™ 250 × 10 mm, inner diameter, 5 μm; Beckman) using Hitachi LC system by monitoring the UV absorbance at 236 nm. The mobile phase for isocratic method 2 was hexane/isopropanol (97:3; v/v) with 0.1 % acetic acid as the modifier.

GSH-adducts were separated by reversed phase using gradient 1 on Waters Alliance 2690 HPLC system. The separation employed a Phenomenex Synergi Hydro-RP column (150 × 4.6 mm inner diameters, 5 μm). Solvent A was 0.1% aqueous formic acid, and solvent B was methanol/acetonitrile/formic acid (50:50:0.1; v/v). Gradient 1 was as follows: 2% B at 0 min, 12% B at 14 min, 30% B at 20 min, 42% B at 21 min, 65% B at 27 min, 80% B at 29 min, 90% B at 33 min, 90% B at 34 min, 2% B at 35 min. The flow rate was 0.4 ml/min. The separation was performed at ambient temperature using a linear gradient.

A Waters nanoAcquity UPLC system was coupled to the LTQ orbitrap XL. The column used to separate free fatty acids or Girard T derivatives was a Waters Acquity C18 (150 mm × 150 μm inner diameter, 1.7 μm). Solvent A was 0.1% aqueous formic acid, and solvent B was acetonitrile with 0.1% formic acid. The flow rate was 2 μl/min, and the column temperature was 35 °C.

For fatty acid analysis, gradient 2 was as follows: 35% B at 0 to 6 min, 90% B at 8 min, 98%B at 23 min to 26 min, and 35% B at 27 min till 37 min. For Girard T derivatives, Gradient 3 was as follows: 10% B from 0 min to 6 min, 50% B at 8 min, 80% B at 23 min, 98% B from 24 min till 27 min and 10% B from 28 min to 38 min.

4.3.4 NMR method.

NMR Spectra were determined at ambient temperature on a Bruker Avance 500 instrument. 1H experiments were carried out at 500 MHz. The samples (0.5-0.8 mg) were dissolved into 300 ml $CDCl_3$. The data processing was

performed on the spectrometer. Chemical shifts are expressed in parts per million (ppm) downfield from the residual solvent peak of 7.26 ppm for $CDCl_3$ for ^1H NMR. Splitting patterns are indicated as follows: br, broad; s, singlet; d, doublet; t, triplet; q, quartet; dd, doublet of doublets; dt, doublet of triplets.

4.3.5 GSH derivatization.

The lipid hydroperoxides decomposition reactions were performed in the presence of 4 mM GSH, and then the aldehydes GSH conjugates were formed during the incubation at 37 C for 30 min. Then the reaction mixtures were loaded to SPE cartridges (HLB, Oasis, 30 mg) which were pre-conditioned by adding 1 ml methanol and 1 ml water. After loading samples, the cartridges were washed with 1ml water to remove excess GSH, and then 0.5 ml methanol was added to elute the analytes. The elutent was directly analyzed by LC-ESI/SRM/MS or concentrated under N_2 flow.

4.3.6 Girard T derivatization.

Aldehydes in 200 μl buffer (100 mM MOPS, 150 mM NaCl, pH7.2) were added with 10 μl acetic acid and 1 mg Girard T reagent. The reaction mixture was kept at room temperature for 30 min and then transferred to SPE cartridge (HLB, Oasis, 30mg) pre-conditioned with 1 ml methanol and 1 ml water. The cartridge was then washed with 1 ml water, and then 0.5 ml methanol added to elute analyte. The elutent was evaporated to dryness in N_2 flow, and dissolved in 100 μl of water/acetonitrile (95:5; v/v). The solution was then transferred to Costar Spin-X nylon centrifuge filter (0.22 μm), and

centrifuged at 10 000 x g for 5 min. Then the clear solution was analyzed by nano UPLC-ESI/MS.

4.3.7 Preparation of OUDE.

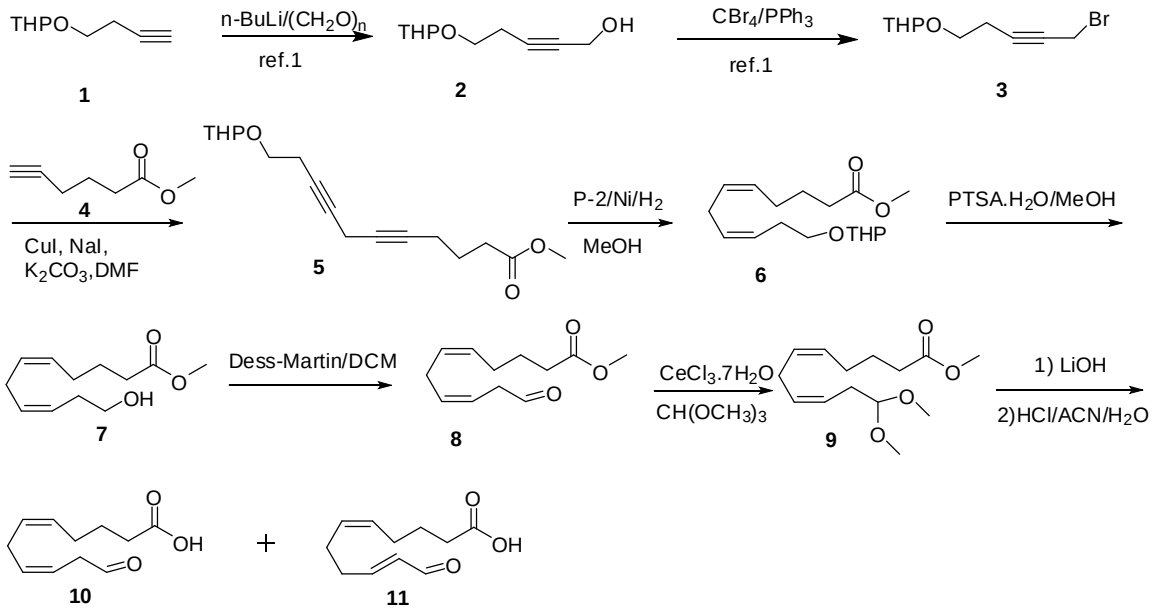

Figure 4.3 Synthesis of OUDE1 and OUDE2.

Methyl 11-(tetrahydro-2H-pyran-2-yloxy)undeca-5,8-diynoate (5). Methyl hex-5-ynoate 4 (2.76 g, 21.85 mmol) was added to a mixture of K_2CO_3 (5.03 g, 36.40 mmol), CuI (4.51 g, 23.67 mmol) and NaI (5.46, 36.40 mmol). The mixture was stirred for 30 min and 3 (*139*) was added. The reaction was stirred for 16 hrs. Ether (200ml) was added and washed with saturated NH_4Cl solution, water and brine. The solvent was evaporated for chromatography (10% EtOAc in Hexanes) to supply 5 (3.24 g, 61%). δH (500 MHz, $CDCl_3$) 3.92-3.67(m, 5H), 3.35 (s, 3H), 2.53-2.38 (m, 8H), 2.24-2.22 (m, 4H), 1.83-1.81 (m, 4H).

(5Z,8Z)-Methyl 11-(tetrahydro-2H-pyran-2-yloxy)undeca-5,8-dienoate (6). $NiOAc.4H_2O$ (0.68 g, 2.73 mmol) was dissolved in MeOH (20 mL) and the flask was flashed with H_2 three times. $NaBH_4$ (75 mg, 1.98 mmol) in NaOH (8 mL, 0.2 M) was added in one portion. After gas evolution had subsided, 0.8 mL of ethylenediamine was added and the mixture was stirred for 5 min. A (1.60 g 5.48 mmol) in methanol (2 mL) was added and the hydrogenation was continued for 4 hrs. The mixture was filtrated and the solvent was evaporated. The residue was taken up with EtOAc and washed with water. The organic layer was evaporated for flash chromatography (10% EtOAc in Hexanes) to provide 6 (1.0 g, 62%). δH (500 MHz, $CDCl_3$) 5.42-5.35(m, 4H), 4.59-4.58 (m, 1H), 3.87-3.83 (m, 1H), 3.75-3.70 (m, 1H), 3.65 (s, 3H), 3.50-3.47 (m, 1H), 3.42-3.37 (m, 1H), 2.79-2.77 (m, 2H), 2.36-2.29 (m, 4H), 2.10-2.07 (m, 2H), 1.82-1.69 (m, 8H).

(5Z,8Z)-Methyl 11-hydroxyundeca-5,8-dienoate (7). $PTSA.H_2O$ (1.83 g, 9.62 mmol) was added to a solution of 6 (0.95 g, 3.21 mmol) in methanol (20 mL) and stirred overnight. 20 mL sat. $NaHCO_3$ was added to the mixture and methanol was evaporated. The mixture was then extracted with EtOAc and washed with brine. The organic layer was evaporated for flash chromatography (20% EtOAc in Hexanes) to provide 7 (558 mg, 82%). δH (500 MHz, $CDCl_3$) 5.50-5.46 (m, 1H), 5.40-5.33 (m, 3H), 3.64-3.61 (m, 5H), 2.79-2.77 (m, 2H), 2.33-2.29 (m, 4H), 2.09-2.04 (m, 3H), 1.69-1.66 (m, 2H).

(5Z,8Z)-Methyl 11-oxoundeca-5,8-dienoate (8). Dess-Martin reagent (2.00 g, 4.71 mmol) was added to a solution of 7 in DCM (20 mL) and stirred for 2 hrs. Sat. $NaHCO_3$ (20 mL) was added to the mixture and the mixture was extracted with DCM. The organic layer was evaporated for flash chromatography (20% EtOAc in Hexanes) to supply 8 (490 mg, 99%). δH (500 MHz, $CDCl_3$) 9.66 (s, 1H), 5.65-5.49 (m, 4H), 3.66 (s, 3H), 2.33-2.319 (m, 5H), 2.16-2.09 (m, 1H), 1.69-1.66 (m, 4H).

(5Z,8Z)-Methyl 11,11-dimethoxyundeca-5,8-dienoate (9). Trimethylorthoformate (227 mg, 2.41 mmol) was added to a solution of 8 (50 mg, 0.238 mmol) and $CeCl_3.7H_2O$ (92 mg, 0.25 mmol) in MeOH (10 mL) and stirred for 2 hrs. 10 mL sat. $NaHCO_3$ was added to the mixture and the mixture was extracted with EtOAc. The organic layer was evaporated for flash chromatography (10% EtOAc in Hexanes) to provide 9 (40 mg, 66%). δH (500 MHz, $CDCl_3$) 5.49-5.36 (m, 4H), 4.39-4.38 (m, 1H), 3.67 (s, 3H), 3.33 (s, 6H), 2.79 (bs, 1H), 2.41-2.30 (m, 4H), 2.17-2.05 (m, 1H), 1.70-1.67 (m, 4H).

(5Z,8Z)-11-Oxoundeca-5,8-dienoic acid (10) and (5Z,9E)-11-oxoundeca-5,9-dienoic acid (11). 3N LiOH (2mL, 6 mmol) was added to a solution of 9 (40 mg, 0.156 mmol) in THF (5mL) and stirred for 2 hrs at 60 °C. The mixture was extracted with EtOAc after acidification with 3N HCl. The organic layer was evaporated for flash chromatography (EtOAc) to provide the crude acid (30 mg, 79%).

3N HCl (1 mL, 6 mmol) was added to the above crude acid in ACN (5 mL) and stirred for 2 hrs at r.t. The mixture was extracted with EtOAc. The organic layer was evaporated for HPLC (Beckman, Ultrasphere, 250x10 mm, UV: 236 nm, Hexane/isopropanol/acetic acid = 97:3:0.1, 2.5 mL/min, isocratic method 2).

4.3.8 Lipid hydroperoxides decomposition in the presence of Vit C or iron.

15(*S*)-HPETE (5 µg) in 200 µl Chelex-treated 100 mM MOPS buffer (pH 7.2), containing 150 mM NaCl was incubated with 1 mM Vit C at 37 °C for 24 hr. Ethyl acetate (2×800 µl) was added to extract products. The organic layer was evaporated and dissolved to 100 µl MeOH/H_2O (4:6, v/v). The solution was filtered by Costar nylon 0.22 µm filter and 2 µl of each sample was injected to UPLC-ESI-LTQ Orbitrap/MS (gradient 3). For GT derivatives, the method was described previously in section 4.3.6.

4.3.9 Chirality character of HPNE-oxime derivative formed from hydroperoxides.

HPETEs (300 µM) were incubated at 37 °C with 2 mM Vit C in 200 µl Chelex-treated MOPS buffer (100 mM, pH 7.2), containing 150 mM NaCl. After 1 h, 1 mg hydroxylamine hydrochloride was added to the reaction mixture and the incubation was continued for 1 h before extraction with diethyl ether (2 X 600 µl). Ethyl layer was evaporated in N_2. Samples were dissolved into 100 µl MeOH/water (85:15; v/v), and 20 µl was injected to LTQ-ESI/SRM/MS (isocratic method1).

4.3.10 Characterization of epoxide alcohol formed from 15(*S*)-HPETE.

To confirm the formation of epoxide alcohol from 15-HPETE, the reaction mixture was first purified by MTBE and then the organic phase was evaporated and re-dissolved into 200 μl acetonitrile containing 0.1 N HCl. Here acetonitrile instead of buffer was used to prevent water competing with chloride ion to attach to the epoxide. The mixture was kept for 30 min at room temperature, and then diluted 10 times before analyzed by nanoUPLC-LTQ orbitrap-ESI/MS.

4.4 RESULTS

4.4.1 Preparation and confirmation of OUDE.

OUDE was chemically synthesized as described above. When the reaction mixtures were purified using Hitachi a semi-preparative LC-UV system, two peaks collected, which shared the same molecular weight, the same retention time on UPLC C18 column and even the same MS/MS fragmentation when they were detected by the LTQ-Orbitrap (Figure 4.4) Thus, they were named OUDE as OUDE1 and 2, depending on the elution order from semi-preparative column. OUDE1 had a retention time of 13.4 min, while OUDE2 was eluted at 16.4 min.

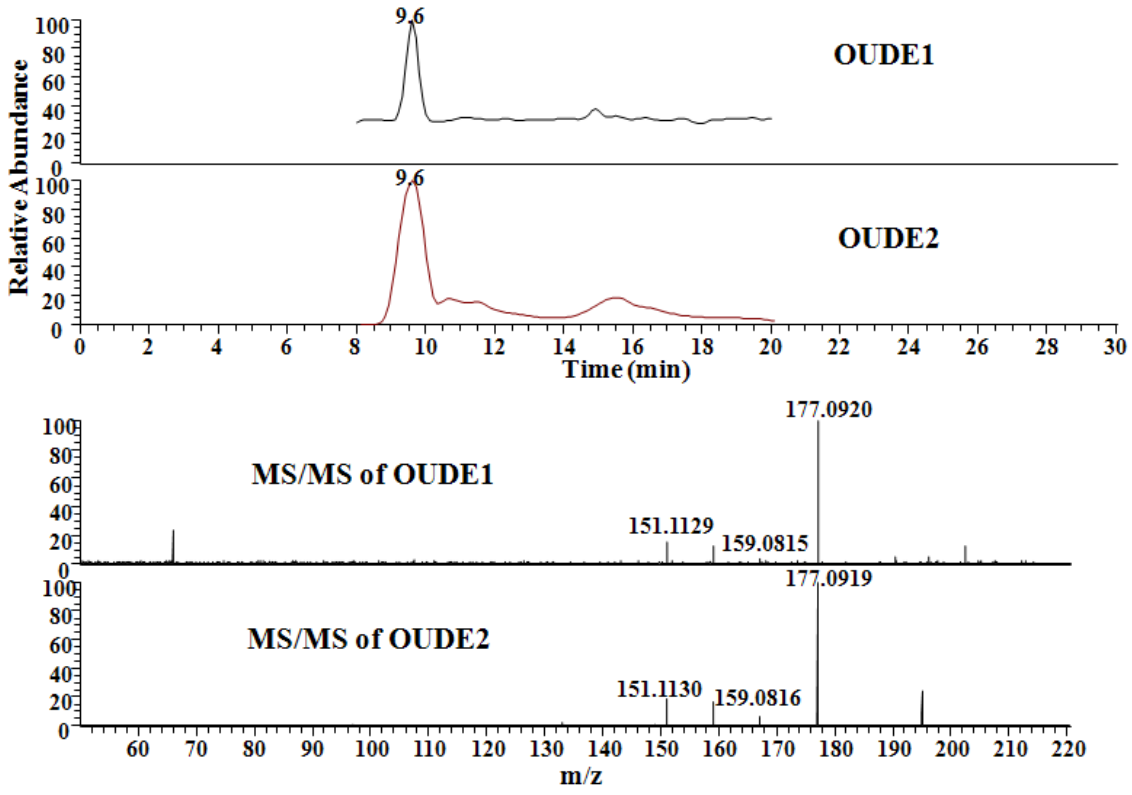

Figure 4.4. LC-orbitrap/MS/MS data of synthetic OUDE and its isomer. The top channels are corresponding the retention of OUDE1 and 2 on C18 column, while the lower spectrum show the MS/MS fragmentation of OUDE1 and 2 at collision energy 35%.

NMR was performed for these two isomers (Figure 4.5). For OUDE1: δH (500 MHz, $CDCl_3$) 9.68 (s, 1H), 5.69-5.40 (m, 4H), 2.80-2.78 (m, 2H), 2.44-2.32 (m, 2H), 2.15-2.02 (m, 2H), 1.73-1.61 (m, 4H). For OUDE2: δH (500 MHz, $CDCl_3$) 9.50 (d, J = 8.0 Hz, 1H, H-11), 6.85 (dt, J = 15.5, 8.0Hz, 1H, H-9), 6.15 (dd, J = 15.5, 8.0Hz, 1H, H-10), 5.43-5.37 (m, 2H), 2.79-2.73 (m, 2H), 2.42-2.24 (m, 4H), 1.73-1.64 (m, 4H). The insert in the OUDE2 NMR spectrum is the enlarged chemical shift range from 5.5 to 7 ppm. The doublet of triplets peak splitting pattern of H9 and the doublet of doublets pattern of H10 indicate the C9-C10 double bond, and also indicate C10 is the

one close to the terminal aldehyde. These patterns were not observed in OUDE1, so OUDE2 is the C8-C9 double bond translocation of OUDE1.

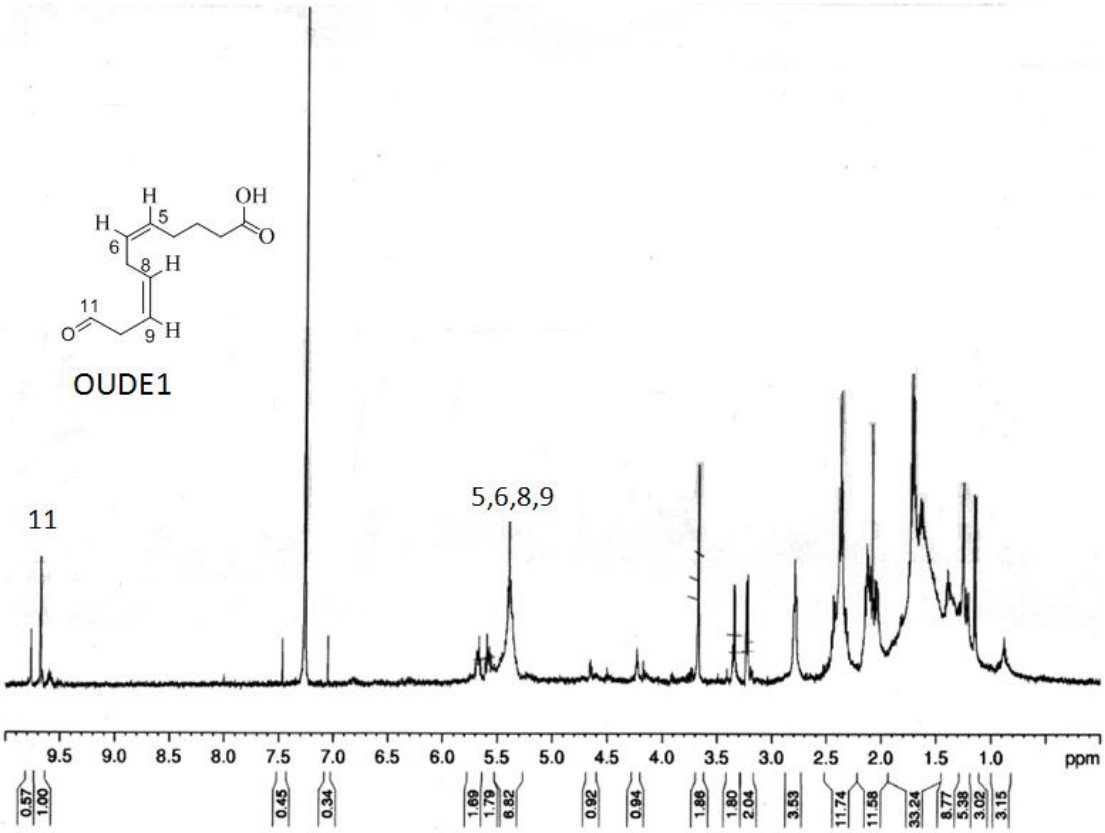

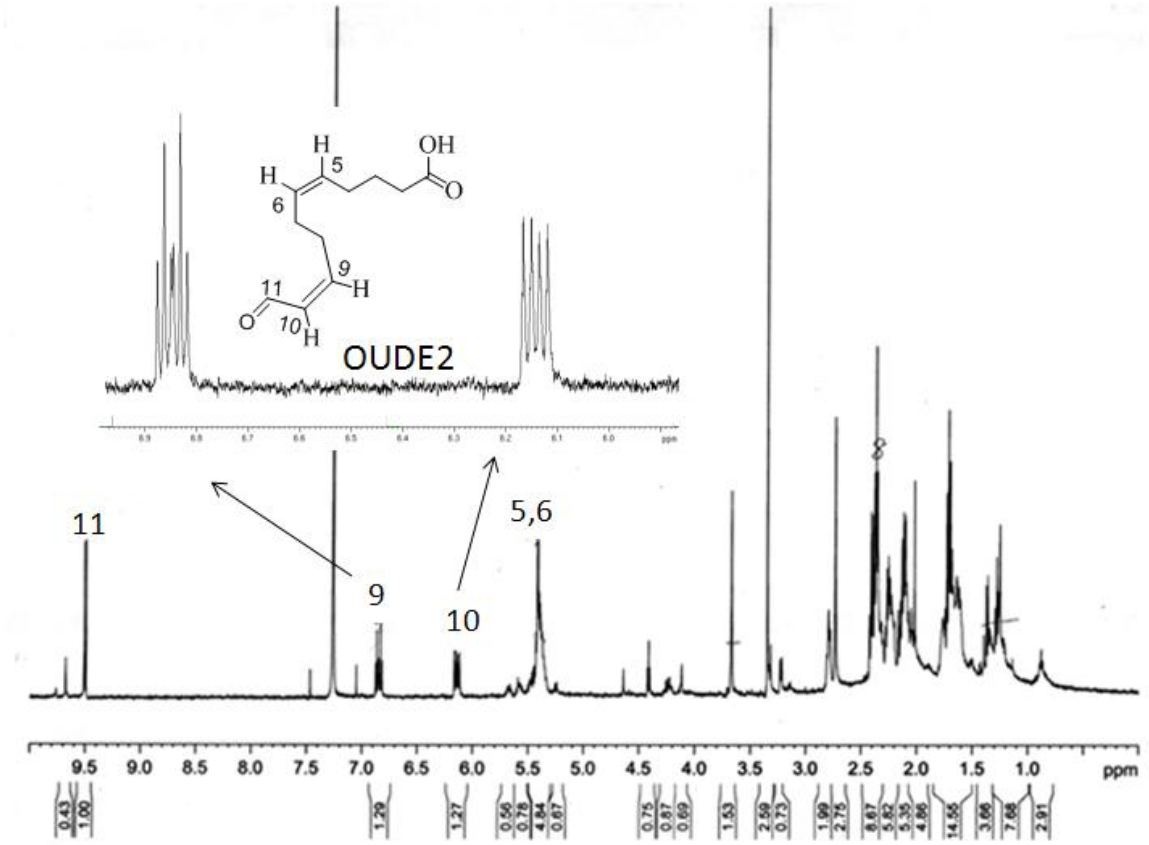

Figure 4.5. The NMR spectra of OUDE1 and OUDE2 at 500 MHZ.

4.4.2 Lipid hydroperoxides decomposition in the presence of Vit C or iron.

15-HPETE and 11(*R*)-HPETE underwent decomposition in the presence of Vit C or iron, and the decomposition products were analyzed by reverse phase LC coupled with high resolution orbitrap MS in the negative mode (Figure 4.6). To increase the detection sensitivity, the aldehydes products were converted to Girard T derivatives (Figure 4.7). [$^{13}C_{20}$]-11(*R*)-HPETE was synthesized from [$^{13}C_{20}$]-AA by 11-LOX enzyme (a kind gift from Dr. Alan

Brash, Vanderbilt University). The reaction conditions and purification conditions were same as for unlabeled 11(*R*)-HPETE or 15(*S*)-HPETE. Figure 4.7(g) shows a mass spectrum of the [$^{13}C_{11}$]-OUDE GT derivative derived from [$^{13}C_{20}$]-11(*R*)-HPETE decomposition, Figures 4.7(d) to 4.7(f) shows the product ions from the MS/MS analysis of OUDE GT at collision energy of 35%, while the lower mass spectrum shows the product ions from [$^{13}C_{11}$]-OUDE GT at same collision energy. It is clear that the product ions observed in Figure 4.7(g) mass spectrum have an 11 Da mass shift when compared to the product ions in Figures 4.7(d) to 4.7(f). This not only indicates that OUDE contains eleven carbons, but also indicates that these ions arise from cleavage of a Girard T moiety.

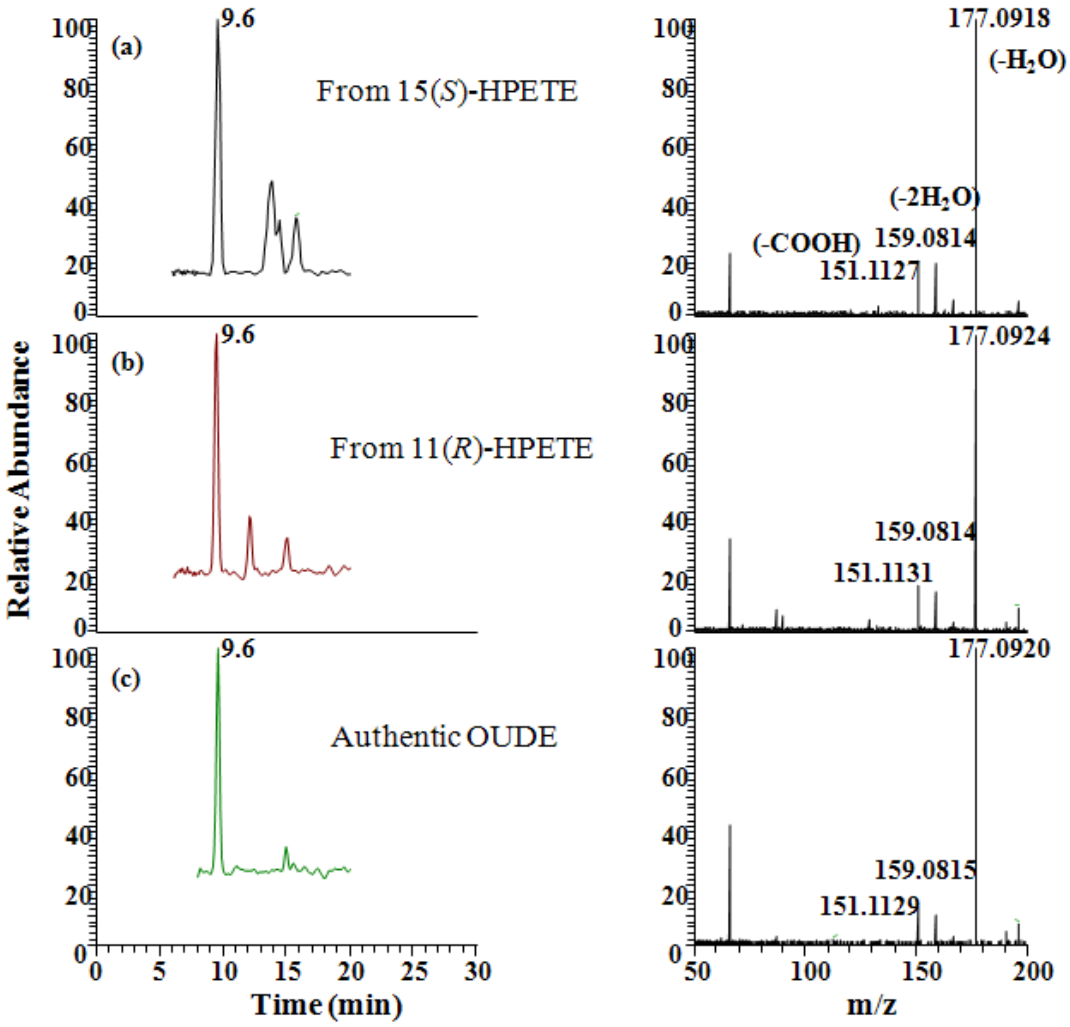

Figure 4.6. LC-MS detection of OUDE from 15(*S*)-HPETE and 11(*R*)-HPETE.

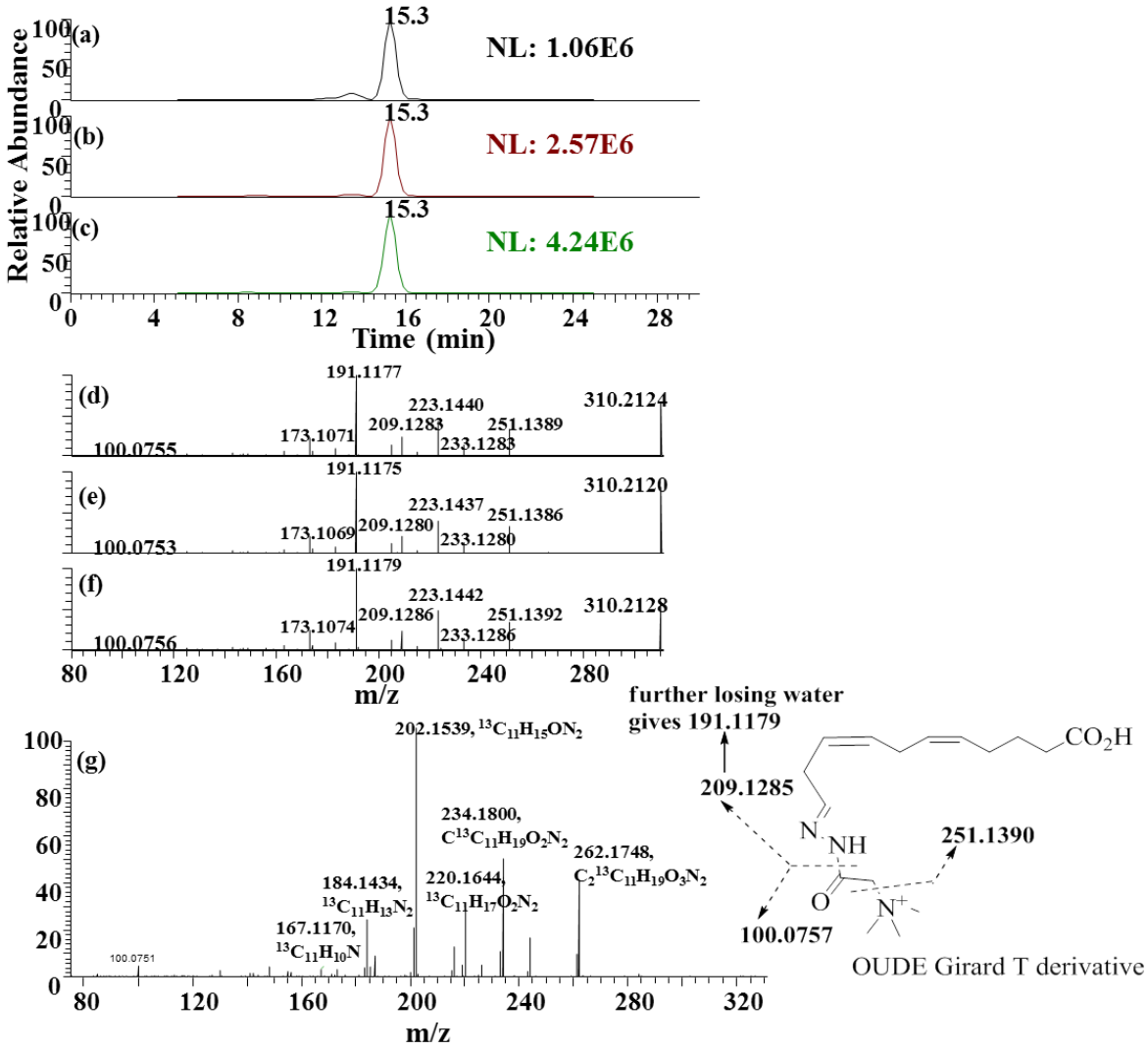

Figure 4.7. LC-MS/MS of OUDE-GT derivative and [$^{13}C_{11}$]-OUDE-GT derivative.

However, based on this evidence alone it remains unknown whether OUDE1 or OUDE2 is formed from HPETE decomposition, since these two isomers and their GT derivatives have the same elemental compositions, similar retention times, and also MS/MS fragments. Thus, OUDE was conjugated with

hydroxylamine to make the oxime derivative (to increase MS response by introducing a nitrogen atom) and then Chiralpak AD-RH column was applied to separate these isomers. Both OUDE1 and OUDE2-oxime were split into two peaks, which corresponded to *syn*- and *anti*-isomers, due to the newly formed C=N double bond. Figure 5, clearly shows that OUDE1-oxime and OUDE2-oxime are well separated on the AD-RH column. From this Figure, it is also evident that 15(S)-HPETE-derived OUDE is a mixture of OUDE1 and OUDE2 isomers.

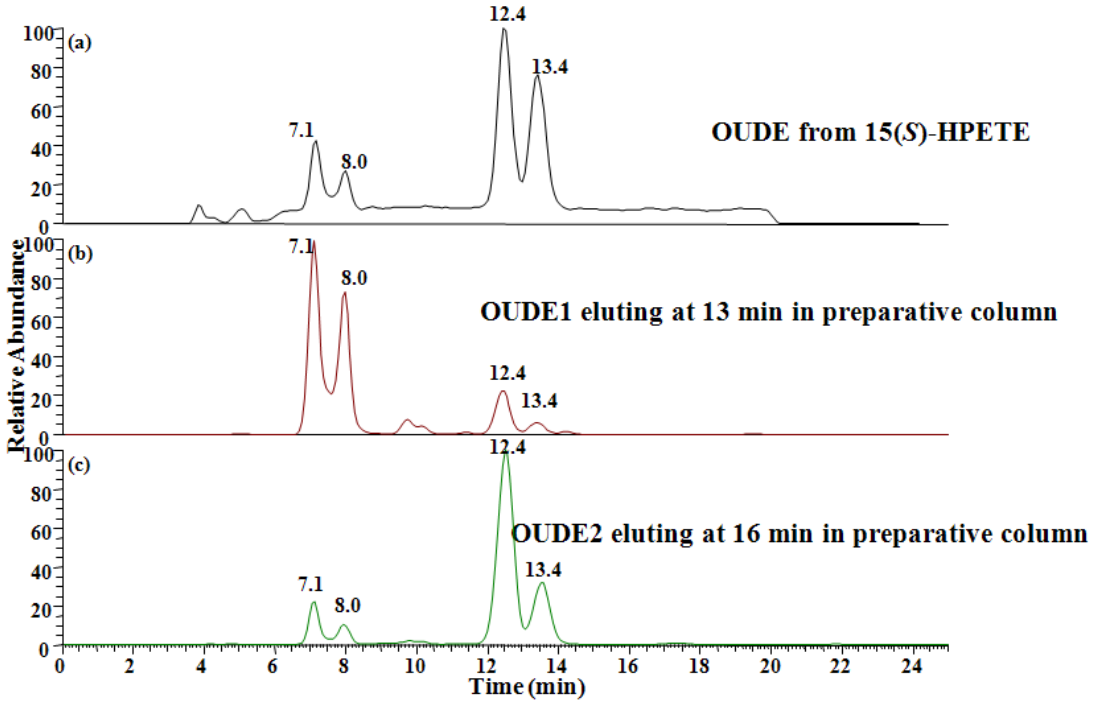

Figure 4.8. Chiral LC-MS detection of OUDE-oxime derivative from 15(*S*)-HPETE and authentic OUDE. (a) shows OUDE-oxime from 15(*S*)-HPETE decomposition, (b) shows authentic OUDE-oxime, while (c) shows OUDE-oxime with double bond translocation.

4.4.3 Chirality of HPNE-oxime derivatives formed from eicosanoids. In order to determine a potential decomposition mechanism, HPNEs generated from HPETE decomposition were converted to oxime derivatives and separated on AD-RH column. In Figure 4.9, it is evident that HPNE derived from 15-HPETE retains the original chirality at C-15 position, while HPNE from 11(*R*)-HPETE was a racemic 1 to 1 mixture. Thus, it is proposed that the 15-hydroperoxy group in 15-HPETE does not participate in the decomposition of HPETE to HPNE. In contrast, it appears that for 11(*R*)-HPETE, a beta scission occurs at C-11 (Figure 4.1).

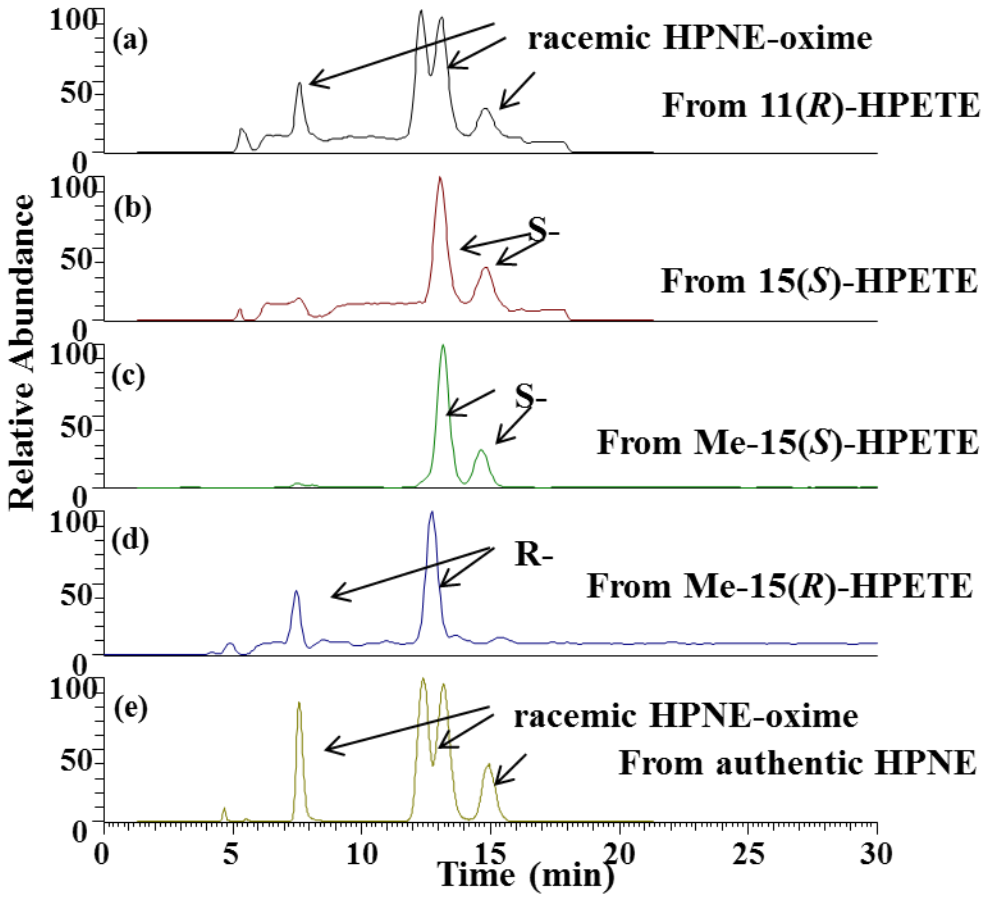

Figure 4.9. The chiral characters of HPNE formed from HPETEs. Figures a to d show the chromatography of HPNE hydroxylamine derivative (HPNE-oxime) formed from 11(*R*)-HPETE, 15(*S*)-HPETE, 15(*S*)-HPETE methyl ester and 15(*R*)-HPETE methyl ester, respectively. Figure (e) is the chromatography of racemic HPNE-oxime standard. HPNE-oxime is separated by reverse phase LC, and monitored by SRM transition m/z 188 to 154.

4.4.4 Characterization of epoxide alcohol formed from 15(*S*)-HPETE.

To confirm the hypothesis that an epoxide alcohol was a major intermediate, the 15(*S*)-HPETE reaction mixture was incubated with 0.1 N HCl, and the products were analyzed by LC-MS (Figure 4.10). The relative intensity ratio of 371.1995 to its highest isotope peak 373.1965 is 3 to 1, which agrees with the predicted ratio. This isotope distribution pattern confirms the presence of Cl and indicates the original compound contained an epoxide group. Figure 4.10(d) shows the MS^3 product ion spectrum from the MS^2 product ion, 317.2121, which is an HCl elimination product. The ion at *m/z* 193.1235 was generated through cleavage between C12 and C13, while the ion at *m/z* 235.1340 was formed by cleavage between C14 and C15, together with loss of a water molecule (Figure 4.10 d).

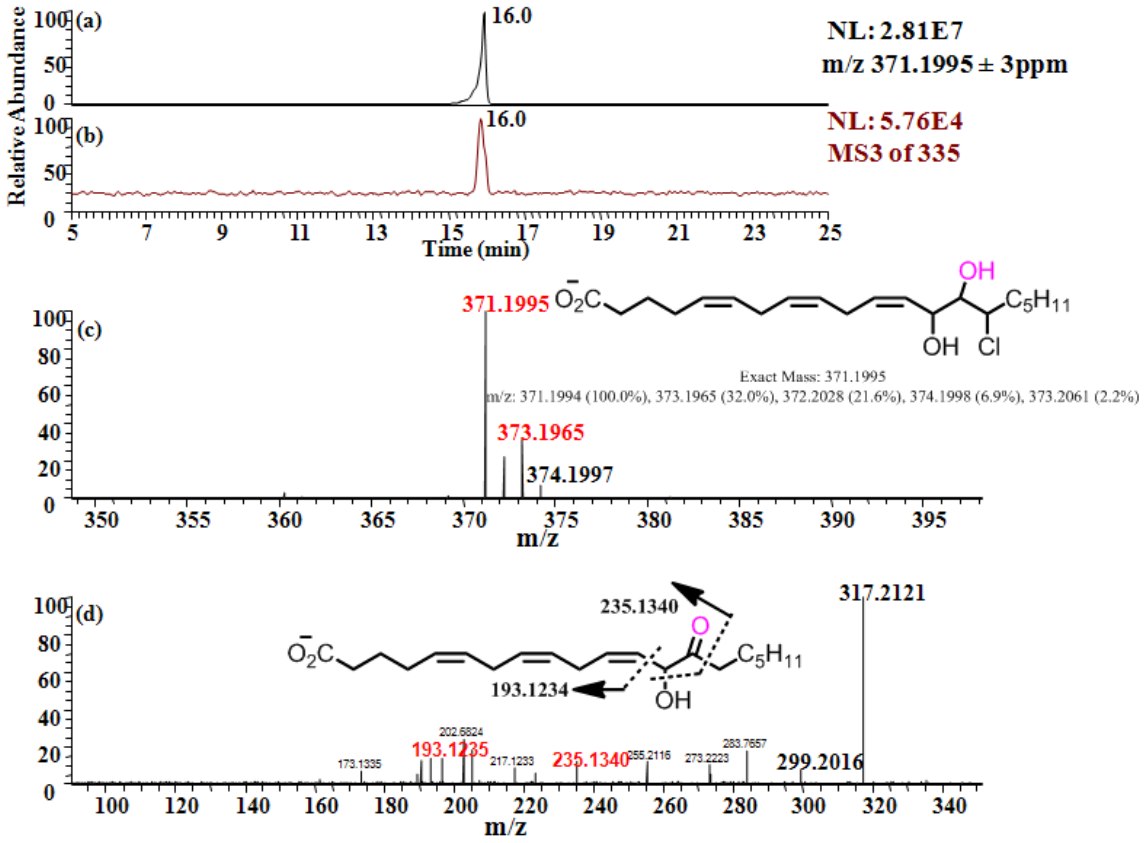

Figure 4.10. Hydrolysis of epoxide in the presence of 0.1 N HCl. Figure, (a) is the reconstructed ion of 371.1995 with 3 ppm window. The product ion spectrum of this peak is shown in (c), where 371.1995 indicates the mass assignment was correct to the fourth decimal place. The ion at *m/z* 373.1965 corresponded to the ^{37}Cl isotopomer. The lower channel (d) shows the MS^3 product ions derived from the ion at *m/z* 371.1995.

4.5 DISCUSSION:

The novel aldehyde OUDE was identified as a product from the non-enzymatic decomposition of 15-HPETE and 11(*R*)-HPETE. Two OUDE isomers were identified. OUDE2 contains an α,β–unsaturated aldehyde and so can be considered to be a carboxylate-containing analog of ONE. These two OUDE isomers differ by the location of C9-C10 double bond, so they or their GT

derivatives cannot be distinguished simply by LC-MS analysis. However, they show different NMR spectra and different retention times on Chiral AD-RH column. Although the driving force for the double bond translocation is unknown, both isomers were observed in the decomposition of 15- and 11-HPETE. This phenomenon also indicates the complexity of the products that can arise from lipid oxidation. The *bis*-allylic hydrogen atoms that are present in AA can be readily replaced by molecular oxygen while the number of double bonds contributes to the formation of complex structural isomers.

15-HPETE is the primary product of 15-LOX, and numerous studies have shown that 15-LOX is involved in oxidized LDL formation. This is based on the evidence that there is co-localization of 15-LOX and oxidized LDL (*122, 123*). It is not completely clear how 15-LOX contributes to LDL oxidation. There are several potential explanations. First, although 15-LOX is a cytosolic enzyme, it might be excreted out of cells when cells are under injured conditions. Once the LDL membrane is oxidized by 15-LOX, changing of hydrophobicity would cause a re-alignment of the original membranes. The oxidized moiety would flip up and be present on the membrane surface, where it could be recognized by the CD36 receptor (*113*). Second, oxidized LDL could be taken up by macrophage cells, and since LDL is rich in unsaturated fatty acids, such as linoleic acid and AA, which could be substrates for 15-LOX-mediated oxidation for further oxidation. There is evidence showing 15-LOX is active in the presence of lipid drops (*124*). Third, the lipids oxidized by 15-LOX might be released from cells and be recruited

by LDL. It was reported that oxidized fatty acids could be incorporated into membranes and play important biological roles (*125,126, 127*).

11-Oxo-ETE is rapidly excreted from LoVo cells (chapter 2), and so it is possible that there are also an export transporters for other oxidized lipids. Yoshimoto and colleagues suggested a potential mechanism, which involved the exchanging of cholesteryl esters of LDL with cell membranes and the relocation of 15-LOX to the LDL binding site (*128*). 11(*R*)-HPETE is the major product from the LOX-like activity of COX. Since the substrate of COX has to be free fatty acids, then it is less likely that COX will directly oxidize LDL. However, COX will generate free OUDE1 and OUDE2, which could be secreted and transported to other cells or LDL.

In summary, there is substantial evidence suggesting a relationship between oxidized lipids and immune recognition. The studies described above have shown that 15-LOX and COXs can contribute to the formation of oxidized lipids with structural similarity to immunogenic lipids. This provides a potential novel pathway by which lipids could be involved in immune recognition.

Chapter 5

Conclusion and future directions

5.1 Conclusions

COX-2 converts AA into PGG_2, 11(*R*)-HPETE, 15(*S*)-HPETE and 15(*R*)-HPETE (Chapter 3). Although there are intense studies showing that COX-2 contributes to cancer development by generating PGE_2, which is pro-inflammatory and oncogenic, the studies described above have revealed that the PGG_2 and the HPETEs can decompose to shorter chain aldehydes HNE and ONE, which could be involved in a myriad of biological processes (Chapter 3). 11(*R*)-HPETE was found to generate a racemic mixture of 4(*R,S*)-HNE, while PGG_2 and 15(*S*)-HPETE generated only 4(*S*)-HNE and 15(*R*)-HPETE generated only 4(*R*)-HNE. HNE and ONE can cause oxidative stress by GSH depletion, or alternatively, they can modify proteins and DNA, resulting in the dysregulation of protein function or causing DNA mutations. 4(*S*)-HNE was the major enantiomer identified in COX-2-expressiong LoVo cells, suggesting that its major source was it's the initially formed COX-derived product of AA oxidation, PGG_2. Earlier studies have shown that HNE can be derived from HPNE, which also serves as the precursor to ONE. This suggests that any COX-2-derived ONE also arose from PGG_2 decomposition rather than the HPETEs as had been previously suggested. No ONE dGuo adduct (H-εdGuo) was found in COX-2 expressing LoVo cells, suggesting that DNA repair was more efficient than in rodent epithelial cells or that the ONE was detoxified more rapidly. Therefore, additional human cell lines should be

examined to determine whether H-εdGuo can be detected. If human cells do have advanced DNA repair system the excised DNA-adduct may be present in urine, which would be a good biomarker for exposure to COX-2-mediated DNA-adduct formation. 15-HPETE and 11(*R*)-HPETE also generate the carboxylate-containing aldehydes, OUDE 1 and 2, which might be incorporated into membranes and function as signaling molecules, for example, the ligand of CD36 receptor (Chapter 4). Thus, not only 15-LOX is related to OxPLs formation, but also COX-2. There are many enzymes involved in the conversion of COX-2-derived AA metabolites into other eicosanoids. The ability of 15-PGDH to oxidize 11(*R*)-HETE into 11-oxo-ETE was clearly demonstrated. The resulting 11-oxo-ETE I rapidly secreted from cells presumably by the action of membrane transporters, or is further transformed by GST/GSH or unknown reductases (Chapter 2). 11-Oxo-ETE might play an important role in inhibiting endothelial cell proliferation. Additional studies will be required in order to elucidate the anti-proliferative effect of 11-oxo-ETE. Considering the structural similarity of 11-oxo-ETE to other oxidized lipid products, it might either bind to PPARγ and activate PPARγ regulated gene transcription or bind the cysteine residue of the NF-κB DNA binding domain and inhibit NF-κB activity. Such future mechanistic studies would further our understanding of how the COX-2/15-PGDH pathway is involved in the regulation of tumorogenesis. Clearly, the physiological levels of these AA metabolites are controlled by multiple pathways, and the changing of any of these pathways would cause a shift in the eicosanoid levels, and initiate a series of biological consequences. The studies described

above have provided additional insight into how such changes could impact on pathophysiological processes.

LC-MS techniques were critical for the studies on AA metabolites, because of the high sensitivity and specificity that could be obtained when compared with other techniques, such as LC-UV or LC-NMR. Moreover, it was possible to analyze a broad spectrum of metabolites because they did not have to possess UV activity. Most of the metabolites could be analyzed by LC-MS, chemical derivatization was used in some cases to increase the MS response. Specific examples of derivatives that were used included PFB, GT, and oximes (Chapters 2 and 3). Moreover, LC coupled with high resolution MS further increased the detection specificity, since most high resolution MS (HRMS) can give mass accuracy to the third or fourth decimal place (Chapter 4), which facilitated the determination of a compounds elemental composition and structure elucidation. In addition, another advantage of LC-MS is that it could analyze crude samples with minimal sample purification procedures, although a de-salting process (SPE method) was required in order to avoid complex adduct formation between the analyte and different cations such as sodium, potassium or ammonium.

5.2 Future directions

Considering the complexity of AA metabolism, the major limit of current methodology is that it focuses on limited numbers of metabolites within a specific cell line. Therefore, it is difficult to conclude whether these targets are the major metabolites and decide which ones are undergoing the most

significant changes when comparisons are made between different treatments. The growth of metabolism software and metabolite databases, together with HRMS, will make it possible to begin addressing these issues (*129, 130*). Newly launched mass spectrometry platforms, such as LTQ-Orbitrap, TripleTOF 5600, and Q-exactive, all provide high resolution capacity, which facilitate good mass accuracy (*131, 132, 133*). The data from different cell treatments or from different population after analyzed by HRMS can be loaded to a software package such as XCMS or SIEVE in order to determine the most significant changes. Initially the software aligns the chromatograms and then and after alignment of the LC chromatography, the software will extract peaks based on retention time and *m/z*. It will then provide the relative levels of different metabolites initially identified by comparing m/z information to the existing database, such as Metlin, chemical spider, and lipidmaps (*134, 135, 136*). However, the small molecule metabolite databases are far from completion, and compared to proteomic databases, it is more complex to assign specific structure. This is due to the enormous diversity of structures that can be encountered with small molecule metabolites (<1500 Da). Thus, more basic discovery research will be required in order to make the databases more complete.

The analysis of small molecule metabolites based on HRMS is rarely enough to provide accurate quantitation and complete specificity, since no single tool is currently available is applicable to every experimental design. Besides LC-MS, NMR is also crucial for unknown metabolite structure elucidation. The characterization of OUDE isomers in chapter 4 is a good example. However,

NMR does have a major limitation it lacks the sensitivity to analyze trace amounts of metabolites.

Gene and protein expression changes will modulate metabolite levels, and in complex feedback relationships, fine tuning of metabolites will also affect genes and proteins through direct modifications or multiple-step signal transductions. Mapping the interaction between metabolic genes, enzymes, and small molecule metabolites is the ultimate goal of metabolism study. The combination of genomics, proteomics, and metabolomics tools will help to understand the multiple layers of regulatory mechanisms governing cellular signaling, and will also help to uncover more disease related pathways or targets (*137, 138, 139*). As described in chapter 1, aspirin is an important drug, not only because of its anti-inflammatory effect, but also because its potential anti-cancer benefit. It is well know that aspirin inhibit PG formation through acetylation of COX-1 and COX-2. It is believed that there are other possible pathways, other than inhibition of PGs, which are also regulated by aspirin to inhibit cancer development (*140-142*). The acetylation of other proteins or enzymes by aspirin might affect the formation of other metabolites.. Ultra performance liquid chromatography (UPLC) coupled with high resolution MS will facilitate the analysis of such metabolites in an accurate yet efficient way, which will be highly complementary to the proteomics analysis of acetylated proteins.

In addtion, considering the incredible complexity of biological system, the variations of metabolite biosynthesis will also depend on the cell types or

tissues, as well as the species being studies. Thus, simple comparison of two samples in one dimension of biological complexity is less meaningful without taking other biological variations into consideration. To draw a picture of metabolites level in different tissues or species or human subjects will require the teamwork from different research groups. A recently published integrated colon cancer genomic study is a good example showing large variations from different sample types and the teamwork enables the researchers get the genomics information from different types of colon cancer (*143*). By systemic study, it was possible to identify the most frequent gene mutations from different tumors. This information can also provide important guidance for the analysis of small molecule metabolites from colon cancer, as they highlight certain pathways for further study. However, the factors causing DNA mutations are not well-understood yet. Thus, our findings of new bioactive aldehydes generated from COX-2 might contribute to DNA damage, even though it has not been yet been possible to fully evaluate the importance of COX-2-derived AA metabolism. Therefore, it might be worth building a database for DNA adducts, so that different research groups could develop screening methods for DNA-adduct detection from different types of samples. In this way, it would be possible to connect the major DNA adducts to sample types, which would in turn would provide a better understanding of the relationship between the pathways causing DNA-adduct formation and the resulting DNA mutations. This would ultimately provide better targets for chemoprevention based on specific sample types.

References:

(1) Stenson, W. F.; Parker, C. W. **(1979)** Metabolism of arachidonic acid in ionophore-stimulated neutrophils. Esterification of a hydroxylated metabolite into phospholipids. *J. Clin. Invest. 64*, 1457-1465.

(2) Wayman, N. S.; Hattori, Y.; McDonald, M. C.; Mota-Filipe, H.; Cuzzocrea, S.; Pisano, B.; Chatterjee, P. K.; Thiemermann, C. **(2002)** Ligands of the peroxisome proliferator-activated receptors (PPAR-gamma and PPAR-alpha) reduce myocardial infarct size. *FASEB J. 16*, 1027-1040.

(3) Zingarelli, B.; Sheehan, M.; Hake, P. W.; O'Connor, M.; Denenberg, A.; Cook, J. A. **(2003)** Peroxisome proliferator activator receptor-gamma ligands, 15-deoxy-Delta(12,14)-prostaglandin J2 and ciglitazone, reduce systemic inflammation in polymicrobial sepsis by modulation of signal transduction pathways. *J. Immunol. 171*, 6827-6837.

(4) Jiang, C.; Ting, A. T.; Seed, B. **(1998)** PPAR-gamma agonists inhibit production of monocyte inflammatory cytokines. *Nature 391*, 82-86.

(5) Chun, K. S.; Lao, H. C.; Langenbach, R. **(2010)** The prostaglandin E2 receptor, EP2, stimulates keratinocyte proliferation in mouse skin by G protein-dependent and {beta}-arrestin1-dependent signaling pathways. *J. Biol. Chem. 285*, 39672-39681.

(6) Clark, J. D.; Lin, L. L.; Kriz, R. W.; Ramesha, C. S.; Sultzman, L. A.; Lin, A. Y.; Milona, N.; Knopf, J. L. **(1991)** A novel arachidonic acid-selective cytosolic PLA2 contains a Ca(2+)-dependent translocation domain with homology to PKC and GAP. *Cell 65*, 1043-1051.

(7) Kennerly, D. A.; Sullivan, T. J.; Sylwester, P.; Parker, C. W. **(1979)** Diacylglycerol metabolism in mast cells: a potential role in membrane fusion and arachidonic acid release. *J. Exp. Med. 150*, 1039-1044.

(8) Nomura, D. K.; Morrison, B. E.; Blankman, J. L.; Long, J. Z.; Kinsey, S. G.; Marcondes, M. C.; Ward, A. M.; Hahn, Y. K.; Lichtman, A. H.; Conti, B.; Cravatt, B. F. **(2011)** Endocannabinoid hydrolysis generates brain prostaglandins that promote neuroinflammation. *Science 334*, 809-813.

(9) Ned A. Porter, Laura S. Lehman, Bruce A. Weber, and Karl J. Smith **(1981)** Unified Mechanism for Polyunsaturated Fatty Acid Autoxidation Competition of Peroxy Radical Hydrogen Atom Abstraction, Beta Scission, and Cyclization. *Journal of american chemical society 103,* 6447-6455.

(10) Gao, L.; Zackert, W. E.; Hasford, J. J.; Danekis, M. E.; Milne, G. L.; Remmert, C.; Reese, J.; Yin, H.; Tai, H. H.; Dey, S. K.; Porter, N. A.; Morrow, J. D. **(2003)** Formation of prostaglandins E2 and D2 via the isoprostane pathway: a mechanism for the generation of bioactive prostaglandins independent of cyclooxygenase. *J. Biol. Chem. 278*, 28479-28489.

(11) Fam, S. S.; Morrow, J. D. **(2003)** The isoprostanes: unique products of arachidonic acid oxidation-a review. *Curr. Med. Chem. 10*, 1723-1740.

(12) Dietrich, M.; Block, G.; Benowitz, N. L.; Morrow, J. D.; Hudes, M.; Jacob, P.,3rd; Norkus, E. P.; Packer, L. **(2003)** Vitamin C supplementation decreases oxidative stress biomarker f2-isoprostanes in plasma of nonsmokers exposed to environmental tobacco smoke. *Nutr. Cancer 45*, 176-184.

(13)Hamberg,M.; Samuelsson, B. **(1974)**Prostaglandin Endoperoxides.Novel Transformations of Arachidonic acid in Human Platelets. *71*, 3400-3404.

(14) Adam, O.; Beringer, C.; Kless, T.; Lemmen, C.; Adam, A.; Wiseman, M.; Adam, P.; Klimmek, R.; Forth, W. **(2003)** Anti-inflammatory effects of a low arachidonic acid diet and fish oil in patients with rheumatoid arthritis. *Rheumatol. Int. 23*, 27-36.

(15) Simmons, D. L.; Botting, R. M.; Hla, T. **(2004)** Cyclooxygenase isozymes: the biology of prostaglandin synthesis and inhibition. *Pharmacol. Rev. 56*, 387-437

(16) Bai, H. W.; Zhu, B. T. **(2008)** Strong activation of cyclooxygenase I and II catalytic activity by dietary bioflavonoids. *J. Lipid Res. 49*, 2557-2570.

(17) Song, I.; Ball, T. M.; Smith, W. L. **(2001)** Different suicide inactivation processes for the peroxidase and cyclooxygenase activities of prostaglandin endoperoxide H synthase-1. *Biochem. Biophys. Res. Commun. 289*, 869-875.

(18) Fu, J. Y.; Masferrer, J. L.; Seibert, K.; Raz, A.; Needleman, P. **(1990)** The induction and suppression of prostaglandin H2 synthase (cyclooxygenase) in human monocytes. *J. Biol. Chem. 265*, 16737-16740.

(19) Xie, W. L.; Chipman, J. G.; Robertson, D. L.; Erikson, R. L.; Simmons, D. L. **(1991)** Expression of a mitogen-responsive gene encoding prostaglandin synthase is regulated by mRNA splicing. *Proc. Natl. Acad. Sci. U. S. A. 88*, 2692-2696.

(20) Kujubu, D. A.; Fletcher, B. S.; Varnum, B. C.; Lim, R. W.; Herschman, H. R. **(1991)** TIS10, a phorbol ester tumor promoter-inducible mRNA from Swiss 3T3 cells, encodes a novel prostaglandin synthase/cyclooxygenase homologue. *J. Biol. Chem. 266*, 12866-12872.

(21) Groeger, A. L.; Cipollina, C.; Cole, M. P.; Woodcock, S. R.; Bonacci, G.; Rudolph, T. K.; Rudolph, V.; Freeman, B. A.; Schopfer, F. J. **(2010)** Cyclooxygenase-2 generates anti-inflammatory mediators from omega-3 fatty acids. *Nat. Chem. Biol. 6*, 433-441.

(22) DeWitt, D. L. **(1999)** Cox-2-selective inhibitors: the new super aspirins. *Mol. Pharmacol. 55*, 625-631.

(23) Patrono, C. **(1994)** Aspirin as an antiplatelet drug. *N. Engl. J. Med. 330*, 1287-1294.

(24) Paganini-Hill, A.; Hsu, G.; Ross, R. K.; Henderson, B. E. **(1992)** Aspirin use and reduced risk of fatal colon cancer. *N. Engl. J. Med. 326*, 1290; author reply 1290-1.

(25) Rothwell, P. M.; Wilson, M.; Elwin, C. E.; Norrving, B.; Algra, A.; Warlow, C. P.; Meade, T. W. **(2010)** Long-term effect of aspirin on colorectal cancer incidence and mortality: 20-year follow-up of five randomised trials. *Lancet 376*, 1741-1750.

(26) Uppal, S.; Diggle, C. P.; Carr, I. M.; Fishwick, C. W.; Ahmed, M.; Ibrahim, G. H.; Helliwell, P. S.; Latos-Bielenska, A.; Phillips, S. E.; Markham, A. F.; Bennett, C. P.; Bonthron, D. T. **(2008)** Mutations in 15-hydroxyprostaglandin dehydrogenase cause primary hypertrophic osteoarthropathy. *Nat. Genet. 40*, 789-793.

(27) Lee, S. C.; Levine, L. **(1975)** Prostaglandin metabolism. II. Identification of two 15-hydroxyprostaglandin dehydrogenase types. *J. Biol. Chem. 250*, 548-552.

(28) Agins, A. P.; Delhagen, J. E. **(1987)** Metabolism of prostaglandin E2 by human HL-60 leukemia cells. *Agents Actions 21*, 400-402.

(29) Backlund, M. G.; Mann, J. R.; Holla, V. R.; Buchanan, F. G.; Tai, H. H.; Musiek, E. S.; Milne, G. L.; Katkuri, S.; DuBois, R. N. **(2005)** 15-Hydroxyprostaglandin dehydrogenase is down-regulated in colorectal cancer. *J. Biol. Chem. 280*, 3217-3223.

(30) Eruslanov, E.; Kaliberov, S.; Daurkin, I.; Kaliberova, L.; Buchsbaum, D.; Vieweg, J.; Kusmartsev, S. **(2009)** Altered expression of 15-hydroxyprostaglandin dehydrogenase in tumor-infiltrated CD11b myeloid cells: a mechanism for immune evasion in cancer. *J. Immunol. 182*, 7548-7557.

(31) Yan, M., et al **(2009)** 15-Hydroxyprostaglandin dehydrogenase inactivation as a mechanism of resistance to celecoxib chemoprevention of colon tumors. *Proc. Natl. Acad. Sci. U. S. A. 106*, 9409-9413.

(32) Esterbauer, H.; Schaur, R. J.; Zollner, H. **(1991)** Chemistry and biochemistry of 4-hydroxynonenal, malonaldehyde and related aldehydes. *Free Radic. Biol. Med. 11*, 81-128.

(33) Hock, H. and Schrader, O., *Angew. Chem.,* **1936**, *49*, 595.

(34) *Comprehensive Organic Name Reactions and Reagents,* by Zerong Wang, 2010, 1439

(35) Wilcox, A. L.; Marnett, L. J. **(1993)** Polyunsaturated fatty acid alkoxyl radicals exist as carbon-centered epoxyallylic radicals: a key step in hydroperoxide-amplified lipid peroxidation. *Chem. Res. Toxicol. 6*, 413-416.

(36) Jian, W.; Lee, S. H.; Arora, J. S.; Silva Elipe, M. V.; Blair, I. A. **(2005)** Unexpected formation of etheno-2'-deoxyguanosine adducts from 5(S)-hydroperoxyeicosatetraenoic acid: evidence for a bis-hydroperoxide intermediate. *Chem. Res. Toxicol. 18*, 599-610.

(37) Schneider, C.; Porter, N. A.; Brash, A. R. **(2008)** Routes to 4-hydroxynonenal: fundamental issues in the mechanisms of lipid peroxidation. *J. Biol. Chem. 283*, 15539-15543.

(38) Schneider, C.; Boeglin, W. E.; Yin, H.; Porter, N. A.; Brash, A. R. **(2008)** Intermolecular peroxyl radical reactions during autoxidation of hydroxy and hydroperoxy arachidonic acids generate a novel series of epoxidized products. *Chem. Res. Toxicol. 21*, 895-903.

(39) Suzuki, D.; Miyata, T.; Saotome, N.; Horie, K.; Inagi, R.; Yasuda, Y.; Uchida, K.; Izuhara, Y.; Yagame, M.; Sakai, H.; Kurokawa, K. **(1999)** Immunohistochemical evidence for an increased oxidative stress and carbonyl modification of proteins in diabetic glomerular lesions. *J. Am. Soc. Nephrol. 10*, 822-832.

(40) Kumagai, T.; Nakamura, Y.; Osawa, T.; Uchida, K. **(2002)** Role of p38 mitogen-activated protein kinase in the 4-hydroxy-2-nonenal-induced cyclooxygenase-2 expression. *Arch. Biochem. Biophys. 397*, 240-245.

(41) Blair, I. A. **(2001)** Lipid hydroperoxide-mediated DNA damage. *Exp. Gerontol. 36*, 1473-1481.

(42) Blair, I. A. **(2010)** Analysis of endogenous glutathione-adducts and their metabolites. *Biomed. Chromatogr. 24*, 29-38.

(43) Lee, S. H., Rangiah, K., Williams, M. V., Wehr, A. Y., Dubois, R. N., and Blair, I. A. (2007) Cyclooxygenase-2-mediated metabolism of arachidonic acid to 15-oxo-eicosatetraenoic acid by rat intestinal epithelial cells. *Chem. Res. Toxicol. 20*, 665-1675.

(44) Ouyang, W., Zhang, D., Ma, Q., Li, J., and Huang, C. (2007) Cyclooxygenase-2 induction by arsenite through the IKKbeta/NFkappaB pathway exerts an antiapoptotic effect in mouse epidermal Cl41 cells. *Environ. Health Perspect. 115*, 513-518.

(45) Matsumura, F. (2009) The significance of the nongenomic pathway in mediating inflammatory signaling of the dioxin-activated Ah receptor to cause toxic effects. *Biochem. Pharmacol. 77*, 608-626.

(46) Ouyang, W., Ma, Q., Li, J., Zhang, D., Ding, J., Huang, Y., Xing, M. M., and Huang, C. (2007) Benzo[a]pyrene diol-epoxide (B[a]PDE) upregulates COX-2 expression through MAPKs/AP-1 and IKKbeta/NF-kappaB in mouse epidermal Cl41 cells. *Mol. Carcinog. 46*, 32-41.

(47) Huang, R. Y., and Chen, G. G. (2011) Cigarette smoking, cyclooxygenase-2 pathway and cancer. *Biochim. Biophys. Acta 1815*, 158-169.

(48) Wang, D., and Dubois, R. N. (2010) The role of COX-2 in intestinal inflammation and colorectal cancer. *Oncogene 29*, 781-788.

(49) Tai, H. H., Tong, M., and Ding, Y. (2007) 15-hydroxyprostaglandin dehydrogenase (15-PGDH) and lung cancer. *Prostaglandins Other Lipid Mediat. 83*, 203-208.

(50) Hughes, D., Otani, T., Yang, P., Newman, R. A., Yantiss, R. K., Altorki, N. K., Port, J. L., Yan, M., Markowitz, S. D., Mazumdar, M., Tai, H. H., Subbaramaiah, K., and Dannenberg, A. J. (2008) NAD+-dependent 15-hydroxyprostaglandin dehydrogenase regulates levels of bioactive lipids in non-small cell lung cancer. *Cancer Prev. Res. (Phila Pa) 1*, 241-249.

(51) Chou, W. L., Chuang, L. M., Chou, C. C., Wang, A. H., Lawson, J. A., FitzGerald, G. A., and Chang, Z. F. (2007) Identification of a novel prostaglandin reductase reveals the involvement of prostaglandin E2 catabolism in regulation of peroxisome proliferator-activated receptor gamma activation. *J. Biol. Chem. 282*, 18162-18172.

(52) Backlund, M. G., Mann, J. R., Holla, V. R., Buchanan, F. G., Tai, H. H., Musiek, E. S., Milne, G. L., Katkuri, S., and Dubois, R. N. (2005) 15-Hydroxyprostaglandin dehydrogenase is down-regulated in colorectal cancer. *J. Biol. Chem. 280*, 3217-3223.

(53) Celis, J. E., Gromov, P., Cabezon, T., Moreira, J. M., Friis, E., Jirstrom, K., Llombart-Bosch, A., Timmermans-Wielenga, V., Rank, F., and Gromova, I. (2008) 15-prostaglandin dehydrogenase expression alone or in combination with ACSM1 defines a subgroup of the apocrine molecular subtype of breast carcinoma. *Mol. Cell Proteomics. 7*, 1795-1809.

(54) Pham, H., Chen, M., Li, A., King, J., Angst, E., Dawson, D. W., Park, J., Reber, H. A., Hines, O. J., and Eibl, G. (2010) Loss of 15-hydroxyprostaglandin dehydrogenase increases prostaglandin E2 in pancreatic tumors. *Pancreas 39*, 332-339.

(55) Thiel, A., Ganesan, A., Mrena, J., Junnila, S., Nykanen, A., Hemmes, A., Tai, H. H., Monni, O., Kokkola, A., Haglund, C., Petrova, T. V., and Ristimaki, A. (2009) 15-hydroxyprostaglandin dehydrogenase is down-regulated in gastric cancer. *Clin. Cancer Res. 15*, 4572-4580.

(56) Tseng-Rogenski, S., Gee, J., Ignatoski, K. W., Kunju, L. P., Bucheit, A., Kintner, H. J., Morris, D., Tallman, C., Evron, J., Wood, C. G., Grossman, H.

B., Lee, C. T., and Liebert, M. (2010) Loss of 15-hydroxyprostaglandin dehydrogenase expression contributes to bladder cancer progression. *Am. J. Pathol. 176*, 1462-1468.

(57) Markowitz, S. D., and Bertagnolli, M. M. (2009) Molecular origins of cancer: Molecular basis of colorectal cancer. *N. Engl. J. Med. 361*, 2449-2460.

(58) Rangachari, P. K., and Betti, P. A. (1993) Biological activity of metabolites of PGD2 on canine proximal colon. *Am. J. Physiol 264*, G886-G894.

(59) Fitzpatrick, F. A., and Wynalda, M. A. (1983) Albumin-catalyzed metabolism of prostaglandin D2. Identification of products formed in vitro. *J. Biol. Chem. 258*, 11713-11718.

(60) Forman, B. M., Tontonoz, P., Chen, J., Brun, R. P., Spiegelman, B. M., and Evans, R. M. (1995) 15-Deoxy-delta 12, 14-prostaglandin J2 is a ligand for the adipocyte determination factor PPAR gamma. *Cell 83*, 803-812.

(61) Xin, X., Yang, S., Kowalski, J., and Gerritsen, M. E. (1999) Peroxisome proliferator-activated receptor gamma ligands are potent inhibitors of angiogenesis in vitro and in vivo. *J. Biol. Chem. 274*, 9116-9121.

(62) Bishop-Bailey, D., and Hla, T. (1999) Endothelial cell apoptosis induced by the peroxisome proliferator-activated receptor (PPAR) ligand 15-deoxy-Delta12, 14-prostaglandin J2. *J. Biol. Chem. 274*, 17042-17048.

(63) Straus, D. S., Pascual, G., Li, M., Welch, J. S., Ricote, M., Hsiang, C. H., Sengchanthalangsy, L. L., Ghosh, G., and Glass, C. K. (2000) 15-deoxy-delta 12,14-prostaglandin J2 inhibits multiple steps in the NF-kappa B signaling pathway. *Proc. Natl. Acad. Sci. USA 97*, 4844-4849.

(64) Scher, J. U., and Pillinger, M. H. (2009) The anti-inflammatory effects of prostaglandins. *J. Investig. Med. 57*, 703-708.

(65) Ho, T. C., Chen, S. L., Yang, Y. C., Chen, C. Y., Feng, F. P., Hsieh, J. W., Cheng, H. C., and Tsao, Y. P. (2008) 15-deoxy-Delta(12,14)-

prostaglandin J2 induces vascular endothelial cell apoptosis through the sequential activation of MAPKS and p53. *J. Biol. Chem. 283*, 30273-30288.

(66) Lee, S. H., Williams, M. V., Dubois, R. N., and Blair, I. A. (2005) Cyclooxygenase-2-mediated DNA damage. *J. Biol. Chem. 280*, 28337-28346.

(67) Blair, I. A. (2008) DNA-adducts with lipid peroxidation products. *J. Biol. Chem. 283*, 15545-15549.

(68) Wei, C., Zhu, P., Shah, S. J., and Blair, I. A. (2009) 15-Oxo-Eicosatetraenoic Acid, a Metabolite of Macrophage 15-Hydroxyprostaglandin Dehydrogenase that Inhibits Endothelial Cell Proliferation. *Mol. Pharm. 76*, 516-529.

(69) Ide, T., Egan, K., Bell-Parikh, L. C., and FitzGerald, G. A. (2003) Activation of nuclear receptors by prostaglandins. *Thromb. Res. 110*, 311-315.

(70) Dixon, D. A., Tolley, N. D., King, P. H., Nabors, L. B., McIntyre, T. M., Zimmerman, G. A., and Prescott, S. M. (2001) Altered expression of the mRNA stability factor HuR promotes cyclooxygenase-2 expression in colon cancer cells. *J. Clin. Invest 108*, 1657-1665.

(71) Shao, J., Sheng, H., Inoue, H., Morrow, J. D., and Dubois, R. N. (2000) Regulation of constitutive cyclooxygenase-2 expression in colon carcinoma cells. *J. Biol. Chem. 275*, 33951-33956.

(72) Lee, S. H., and Blair, I. A. (2007) Targeted chiral lipidomics analysis by liquid chromatography electron capture atmospheric pressure chemical ionization mass spectrometry (LC-ECAPCI/MS). *Methods Enzymol. 433*, 159-174.

(73) Mesaros, C., Lee, S. H., and Blair, I. A. (2009) Targeted quantitative analysis of eicosanoid lipids in biological samples using liquid chromatography-tandem mass spectrometry. *J. Chromatogr. B 877*, 2736-2745.

(74) Meijerman, I., Beijnen, J. H., and Schellens, J. H. (2008) Combined action and regulation of phase II enzymes and multidrug resistance proteins in multidrug resistance in cancer. *Cancer Treat. Rev. 34*, 505-520.

(75) Holla, V. R., Backlund, M. G., Yang, P., Newman, R. A., and Dubois, R. N. (2008) Regulation of prostaglandin transporters in colorectal neoplasia. *Cancer Prev. Res. (Phila Pa) 1*, 93-99.

(76) Waku, T., Shiraki, T., Oyama, T., Fujimoto, Y., Maebara, K., Kamiya, N., Jingami, H., and Morikawa, K. (2009) Structural insight into PPARgamma activation through covalent modification with endogenous fatty acids. *J. Mol. Biol. 385*, 188-199.

(77) Wang, D., and Dubois, R. N. (2008) Peroxisome proliferator-activated receptors and progression of colorectal cancer. *PPAR. Res. 2008*, 931074.

(78) Ciucci, A., Gianferretti, P., Piva, R., Guyot, T., Snape, T. J., Roberts, S. M., and Santoro, M. G. (2006) Induction of apoptosis in estrogen receptor-negative breast cancer cells by natural and synthetic cyclopentenones: role of the IkappaB kinase/nuclear factor-kappaB pathway. *Mol. Pharmacol. 70*, 1812-1821.

(79) Piva, R., Gianferretti, P., Ciucci, A., Taulli, R., Belardo, G., and Santoro, M. G. (2005) 15-Deoxy-delta 12,14-prostaglandin J2 induces apoptosis in human malignant B cells: an effect associated with inhibition of NF-kappa B activity and down-regulation of antiapoptotic proteins. *Blood 105*, 1750-1758.

(80) Grant, G. E., Gravel, S., Guay, J., Patel, P., Mazer, B. D., Rokach, J., and Powell, W. S. (2011) 5-oxo-ETE is a major oxidative stress-induced arachidonate metabolite in B lymphocytes. *Free Radic. Biol. Med. 50*, 1297-1304.

(81) O'Flaherty, J. T., Cordes, J. F., Lee, S. L., Samuel, M., and Thomas, M. J. (1994) Chemical and biological characterization of oxo-eicosatetraenoic acids. *Biochim. Biophys. Acta 1201*, 505-515.

(82) Grant, G. E., Rokach, J., and Powell, W. S. (2009) 5-Oxo-ETE and the OXE receptor. *Prostaglandins Other Lipid Mediat. 89*, 98-104.

(83) Waddington, E., Sienuarine, K., Puddey, I., and Croft, K. (2001) Identification and quantitation of unique fatty acid oxidation products in human atherosclerotic plaque using high-performance liquid chromatography. *Anal. Biochem. 292*, 234-244.

(84) Mattson, M. P. **(2009)** Roles of the lipid peroxidation product 4-hydroxynonenal in obesity, the metabolic syndrome, and associated vascular and neurodegenerative disorders. *Exp. Gerontol. 44*, 625-633.

(85) Perluigi, M.; Coccia, R.; Butterfield, A. **(2011)** Hne, a Reactive Product of Lipid Peroxidation and Neurodegenerative Diseases: a Toxic Combination Illuminated by Redox Proteomics Studies. *Antioxid. Redox Signal.* .

(86) Butterfield, D. A.; Reed, T.; Sultana, R. **(2011)** Roles of 3-nitrotyrosine- and 4- hydroxynonenal-modified brain proteins in the progression and pathogenesis of Alzheimer's disease. *Free Radic. Res. 45*, 59-72.

(87) Balogh, L. M.; Le Trong, I.; Kripps, K. A.; Shireman, L. M.; Stenkamp, R. E.; Zhang, W.; Mannervik, B.; Atkins, W. M. **(2010)** Substrate specificity combined with stereopromiscuity in glutathione transferase A4-4-dependent metabolism of 4-hydroxynonenal. *Biochemistry 49*, 1541-1548.

(88) Honzatko, A.; Brichac, J.; Picklo, M. J. **(2007)** Quantification of trans-4-hydroxy-2-nonenal enantiomers and metabolites by LC-ESI-MS/MS. *J. Chromatogr. B. Analyt Technol. Biomed. Life. Sci. . 857*, 115-122.

(89) Schneider, C.; Porter, N. A.; Brash, A. R. **(2004)** Autoxidative transformation of chiral omega6 hydroxy linoleic and arachidonic acids to chiral 4-hydroxy-2E-nonenal. *Chem. Res. Toxicol. 17*, 937-941.

(90) Wakita, C.; Honda, K.; Shibata, T.; Akagawa, M.; Uchida, K. **(2011)** A method for detection of 4-hydroxy-2-nonenal adducts in proteins. *Free Radic. Biol. Med. 51*, 1-4.

(91) Hashimoto, M.; Sibata, T.; Wasada, H.; Toyokuni, S.; Uchida, K. **(2003)** Structural basis of protein-bound endogenous aldehydes. Chemical and immunochemical characterizations of configurational isomers of a 4-hydroxy-2-nonenal-histidine adduct. *J. Biol. Chem. 278*, 5044-5051.

(92) Wakita, C.; Maeshima, T.; Yamazaki, A.; Shibata, T.; Ito, S.; Akagawa, M.; Ojika, M.; Yodoi, J.; Uchida, K. **(2009)** Stereochemical configuration of 4-hydroxy-2-nonenal-cysteine adducts and their stereoselective formation in a redox-regulated protein. *J. Biol. Chem. 284*, 28810-28822.

(93) Brichac, J.; Ho, K. K.; Honzatko, A.; Wang, R.; Lu, X.; Weiner, H.; Picklo MJ, S. **(2007)** Enantioselective oxidation of trans-4-hydroxy-2-nonenal is aldehyde dehydrogenase isozyme and Mg2+ dependent. *Chem. Res. Toxicol. 20*, 887-895.

(94) Honzatko, A.; Brichac, J.; Murphy, T. C.; Reberg, A.; Kubatova, A.; Smoliakova, I. P.; Picklo MJ, S. **(2005)** Enantioselective metabolism of trans-4-hydroxy-2-nonenal by brain mitochondria. *Free Radic. Biol. Med. 39*, 913-924.

(95) Liu, X.; Zhang, S.; Arora, J. S.; Snyder, N. W.; Shah, S. J.; Blair, I. A. **(2011)** 11-Oxoeicosatetraenoic acid is a cyclooxygenase-2/15-

hydroxyprostaglandin dehydrogenase-derived antiproliferative eicosanoid. *Chem. Res. Toxicol. 24*, 2227-2236.

(96) Lee, S. H.; Blair, I. A. **(2000)** Characterization of 4-oxo-2-nonenal as a novel product of lipid peroxidation. *Chem. Res. Toxicol. 13*, 698-702.

(97) Lee, S. H.; Oe, T.; Blair, I. A. **(2001)** Vitamin C-induced decomposition of lipid hydroperoxides to endogenous genotoxins. *Science 292*, 2083-2086.

(98) Nair, J.; Gansauge, F.; Beger, H.; Dolara, P.; Winde, G.; Bartsch, H. **(2006)** Increased etheno-DNA adducts in affected tissues of patients suffering from Crohn's disease, ulcerative colitis, and chronic pancreatitis. *Antioxid. Redox Signal. 8*, 1003-1010.

(99) Otteneder, M. B.; Knutson, C. G.; Daniels, J. S.; Hashim, M.; Crews, B. C.; Remmel, R. P.; Wang, H.; Rizzo, C.; Marnett, L. J. **(2006)** In vivo oxidative metabolism of a major peroxidation-derived DNA adduct, M1dG. *Proc. Natl. Acad. Sci. U. S. A. 103*, 6665-6669.

(100) Pang, B.; Zhou, X.; Yu, H.; Dong, M.; Taghizadeh, K.; Wishnok, J. S.; Tannenbaum, S. R.; Dedon, P. C. **(2007)** Lipid peroxidation dominates the chemistry of DNA adduct formation in a mouse model of inflammation. *Carcinogenesis 28*, 1807-1813.

(101) Taghizadeh, K.; McFaline, J. L.; Pang, B.; Sullivan, M.; Dong, M.; Plummer, E.; Dedon, P. C. **(2008)** Quantification of DNA damage products resulting from deamination, oxidation and reaction with products of lipid

peroxidation by liquid chromatography isotope dilution tandem mass spectrometry. *Nat. Protoc. 3*, 1287-1298.

(102) Federico A, Morgillo F, Tuccillo C, Ciardiello F & Loguercio C. **(2007)** chronic inflammation and oxidative stress in human carcinogenesis. *International Journal of Cancer 121*, 2381.

(103) Douglas Hanahan* and Robert A. Weinberg **(2000)** The Hallmarks of Cancer. *Cell 100*, 57.

(104) Chang, M. S.; Boeglin, W. E.; Guengerich, F. P.; Brash, A. R. **(1996)** Cytochrome P450-dependent transformations of 15R- and 15S-hydroperoxyeicosatetraenoic acids: stereoselective formation of epoxy alcohol products. *Biochemistry 35*, 464-471.

(105) E. J. Corey, John O. Albright, Alan E. Barton, Shunichi Hashimoto **(1980)** Chemical and enzymic syntheses of 5-HPETE, a key biological precursor of slow-reacting substance of anaphylaxis(SRS), 5-HETE. *Journal of american chemical society 102*, 1435.

(106) Adeniji AO, Twenter BM, Byrns MC, Jin Y, Chen M, Winkler JD, Penning TM **(2012)** Development of Potent and Selective Inhibitors of Aldo-Keto Reductase 1C3 (Type 5 17β-Hydroxysteroid Dehydrogenase) Based on N-Phenyl-Aminobenzoates and Their Structure-Activity Relationships. *Journal of medicinal chemistry* .

(107) Wang, H.; Kozekov, I. D.; Harris, T. M.; Rizzo, C. J. **(2003)** Site-specific synthesis and reactivity of oligonucleotides containing

stereochemically defined 1,N2-deoxyguanosine adducts of the lipid peroxidation product trans-4-hydroxynonenal. *J. Am. Chem. Soc. 125*, 5687-5700.

(108) Voulgaridou, G. P.; Anestopoulos, I.; Franco, R.; Panayiotidis, M. I.; Pappa, A. **(2011)** DNA damage induced by endogenous aldehydes: current state of knowledge. *Mutat. Res. 711*, 13-27.

(109) Kuhn, H.; Belkner, J.; Wiesner, R.; Brash, A. R. **(1990)** Oxygenation of biological membranes by the pure reticulocyte lipoxygenase. *J. Biol. Chem. 265*, 18351-18361.

(110) Niehaus, W. G.,Jr; Samuelsson, B. **(1968)** Formation of malonaldehyde from phospholipid arachidonate during microsomal lipid peroxidation. *Eur. J. Biochem. 6*, 126-130.

(111) Pryor, W. A.; Porter, N. A. **(1990)** Suggested mechanisms for the production of 4-hydroxy-2-nonenal from the autoxidation of polyunsaturated fatty acids. *Free Radic. Biol. Med. 8*, 541-543.

(112) Podrez EA, Byzova TV, Febbraio M, Salomon RG, Ma Y, Valiyaveettil M, Poliakov E, Sun M, Finton PJ, Curtis BR, Chen J, Zhang R, Silverstein RL, Hazen SL. **(2007)** platelet CD36 links hyperlipidemia, oxidant stress and a prothrombotic phenotype. *Nature medicine 13*, 1086-1095.

(113) Podrez, E. A.; Poliakov, E.; Shen, Z.; Zhang, R.; Deng, Y.; Sun, M.; Finton, P. J.; Shan, L.; Febbraio, M.; Hajjar, D. P.; Silverstein, R. L.; Hoff, H. F.; Salomon, R. G.; Hazen, S. L. **(2002)** A novel family of atherogenic

oxidized phospholipids promotes macrophage foam cell formation via the scavenger receptor CD36 and is enriched in atherosclerotic lesions. *J. Biol. Chem. 277*, 38517-38523.

(114) Hazen, S. L. **(2008)** Oxidized phospholipids as endogenous pattern recognition ligands in innate immunity. *J. Biol. Chem. 283*, 15527-15531.

(115) Chen, X; Zhang, W.; Laird, J.; Hazen, S.L.; and Salomon R.G. **(2008)** Polyunsaturated phospholipids promote the oxidation and fragmentation of g-hydroxyalkenals: formation and reactions of oxidatively truncated ether phospholipids. *J. Lipid Res. 49*, 832-846.

(116) Greenberg, M. E.; Li, X. M.; Gugiu, B. G.; Gu, X.; Qin, J.; Salomon, R. G.; Hazen, S. L. **(2008)** The lipid whisker model of the structure of oxidized cell membranes. *J. Biol. Chem. 283*, 2385-2396.

(117) Berliner, J.A.; Leitinger, N.; and Tsimikas S. **(2009)** The role of oxidized phospholipids in atherosclerosis. *J. Lipid Res.* S207-S212.

(118) Leonarduzzi, G.; Gamba, P.; Gargiulo, S.; Biasi, F.; Poli, G. **(2012)** Inflammation-related gene expression by lipid oxidation-derived products in the progression of atherosclerosis. *Free Radic. Biol. Med. 52*, 19-34.

(119) Silverman, E. S.; Drazen, J. M. (1999) The biology of 5-lipoxygenase: function, structure, and regulatory mechanisms. Proc. Assoc. Am. Physicians 111, 525-536. (120) Dwyer, J. H.; Allayee, H.; Dwyer, K. M.; Fan, J.; Wu, H.; Mar, R.; Lusis, A. J.; Mehrabian, M. **(2004)** Arachidonate 5-lipoxygenase promoter genotype, dietary arachidonic acid, and atherosclerosis. *N. Engl. J.*

Med. 350, 29-37.

(121) Prakash, C.; Saleh, S.; Taber, D. F.; Blair, I. A. **(1989)** Synthesis of trideuterated O-alkyl platelet activating factor and lyso derivatives. *Lipids 24*, 786-792.

(122) Yla-Herttuala, S.; Rosenfeld, M. E.; Parthasarathy, S.; Glass, C. K.; Sigal, E.; Witztum, J. L.; Steinberg, D. **(1990)** Colocalization of 15-lipoxygenase mRNA and protein with epitopes of oxidized low density lipoprotein in macrophage-rich areas of atherosclerotic lesions. *Proc. Natl. Acad. Sci. U. S. A. 87*, 6959-6963.

(123) Miller, Y. I.; Choi, S. H.; Wiesner, P.; Fang, L.; Harkewicz, R.; Hartvigsen, K.; Boullier, A.; Gonen, A.; Diehl, C. J.; Que, X.; Montano, E.; Shaw, P. X.; Tsimikas, S.; Binder, C. J.; Witztum, J. L. **(2011)** Oxidation-specific epitopes are danger-associated molecular patterns recognized by pattern recognition receptors of innate immunity. *Circ. Res. 108*, 235-248.

(124) Weibel, G. L.; Joshi, M. R.; Wei, C.; Bates, S. R.; Blair, I. A.; Rothblat, G. H. **(2009)** 15(S)-Lipoxygenase-1 associates with neutral lipid droplets in macrophage foam cells: evidence of lipid droplet metabolism. *J. Lipid Res. 50*, 2371-2376.

(125) Stenson, W. F.; Parker, C. W. **(1979)** Metabolism of arachidonic acid in ionophore-stimulated neutrophils. Esterification of a hydroxylated metabolite into phospholipids. *J. Clin. Invest. 64*, 145

(126) Bonser, R. W.; Siegel, M. I.; Chung, S. M.; McConnell, R. T.;

Cuatrecasas, P. **(1981)** Esterification of an endogenously synthesized lipoxygenase product into granulocyte cellular lipids. *Biochemistry 20*, 5297-5301.

(127) Seimon, T. A.; Nadolski, M. J.; Liao, X.; Magallon, J.; Nguyen, M.; Feric, N. T.; Koschinsky, M. L.; Harkewicz, R.; Witztum, J. L.; Tsimikas, S.; Golenbock, D.; Moore, K. J.; Tabas, I. **(2010)** Atherogenic lipids and lipoproteins trigger CD36-TLR2-dependent apoptosis in macrophages undergoing endoplasmic reticulum stress. *Cell. Metab. 12*, 467-482.

(128) Takahashi, Y.; Zhu, H.; Xu, W.; Murakami, T.; Iwasaki, T.; Hattori, H.; Yoshimoto, T. **(2005)** Selective uptake and efflux of cholesteryl linoleate in LDL by macrophages expressing 12/15-lipoxygenase. *Biochem. Biophys. Res. Commun. 338*, 128-135.

(129) Cui, Q.; Lewis, I. A.; Hegeman, A. D.; Anderson, M. E.; Li, J.; Schulte, C. F.; Westler, W. M.; Eghbalnia, H. R.; Sussman, M. R.; Markley, J. L. (2008) Metabolite identification via the Madison Metabolomics Consortium Database. *Nat. Biotechnol. 26*, 162-164.

(130) Patti, G. J.; Yanes, O.; Siuzdak, G. (2012) Innovation: Metabolomics: the apogee of the omics trilogy. *Nat. Rev. Mol. Cell Biol. 13*, 263-269.

(131) Makarov, A.; Denisov, E.; Lange, O.; Horning, S. **(2006)** Dynamic range of mass accuracy in LTQ Orbitrap hybrid mass spectrometer. *J. Am. Soc. Mass Spectrom. 17*, 977-982.

(132) Michalski, A.; Damoc, E.; Hauschild, J. P.; Lange, O.; Wieghaus, A.; Makarov, A.; Nagaraj, N.; Cox, J.; Mann, M.; Horning, S. **(2011)** Mass spectrometry-based proteomics using Q Exactive, a high-performance benchtop quadrupole Orbitrap mass spectrometer. *Mol. Cell. Proteomics 10*, M111.011015.

(133) Andrews, G. L.; Simons, B. L.; Young, J. B.; Hawkridge, A. M.; Muddiman, D. C. **(2011)** Metabolomic approach based on liquid chromatography coupled to high resolution mass Performance characteristics of a new hybrid quadrupole time-of-flight tandem mass spectrometer (TripleTOF 5600). *Anal. Chem. 83*, 5442-5446.

(134) Regal, P.; Anizan, S.; Antignac, J. P.; Le Bizec, B.; Cepeda, A.; Fente, C. **(2011)** Metabolomic approach based on liquid chromatography coupled to high resolution mass spectrometry to screen for the illegal use of estradiol and progesterone in cattle. *Anal. Chim. Acta 700*, 16-25.

(135) Smith, C. A.; Want, E. J.; O'Maille, G.; Abagyan, R.; Siuzdak, G. **(2006)** XCMS processing mass spectrometry data for metabolite profiling using nonlinear peak alignment, matching, and identification. *Anal. Chem. 78*, 779-787.

(136) Zhu, W.; Smith, J. W.; Huang, C. M. **(2010)** Mass spectrometry-based label-free quantitative proteomics. *J. Biomed. Biotechnol. 2010,* 840518

(137) Fiehn, O. **(2002)** Metabolomics--the link between genotypes and phenotypes. *Plant Mol. Biol. 48*, 155-171.

(138) Bino, R. J.; Hall, R. D.; Fiehn, O.; Kopka, J.; Saito, K.; Draper, J.; Nikolau, B. J.; Mendes, P.; Roessner-Tunali, U.; Beale, M. H.; Trethewey, R. N.; Lange, B. M.; Wurtele, E. S.; Sumner, L. W. **(2004)** Potential of metabolomics as a functional genomics tool. *Trends Plant Sci. 9*, 418-425.

(139) Buescher, J. M., et al **(2012)** Global network reorganization during dynamic adaptations of Bacillus subtilis metabolism. *Science 335*, 1099-1103.

(140) Pinckard, R. N.; Hawkins, D.; Farr, R. S. **(1968)** In vitro acetylation of plasma proteins, enzymes and DNA by aspirin. *Nature 219*, 68-69.

(141) Alfonso, L. F.; Srivenugopal, K. S.; Bhat, G. J. **(2009)** Does aspirin acetylate multiple cellular proteins? (Review). *Mol. Med. Report 2*, 533-537.

(142) Marimuthu, S.; Chivukula, R. S.; Alfonso, L. F.; Moridani, M.; Hagen, F. K.; Bhat, G. J. **(2011)** Aspirin acetylates multiple cellular proteins in HCT-116 colon cancer cells: Identification of novel targets. *Int. J. Oncol. 39*, 1273-1283.

(143) Cancer Genome Atlas Network **(2012)** Comprehensive molecular characterization of human colon and rectal cancer. *Nature 487*, 330-337.